Strong Gravitational Lensing:

Effects of Substructure

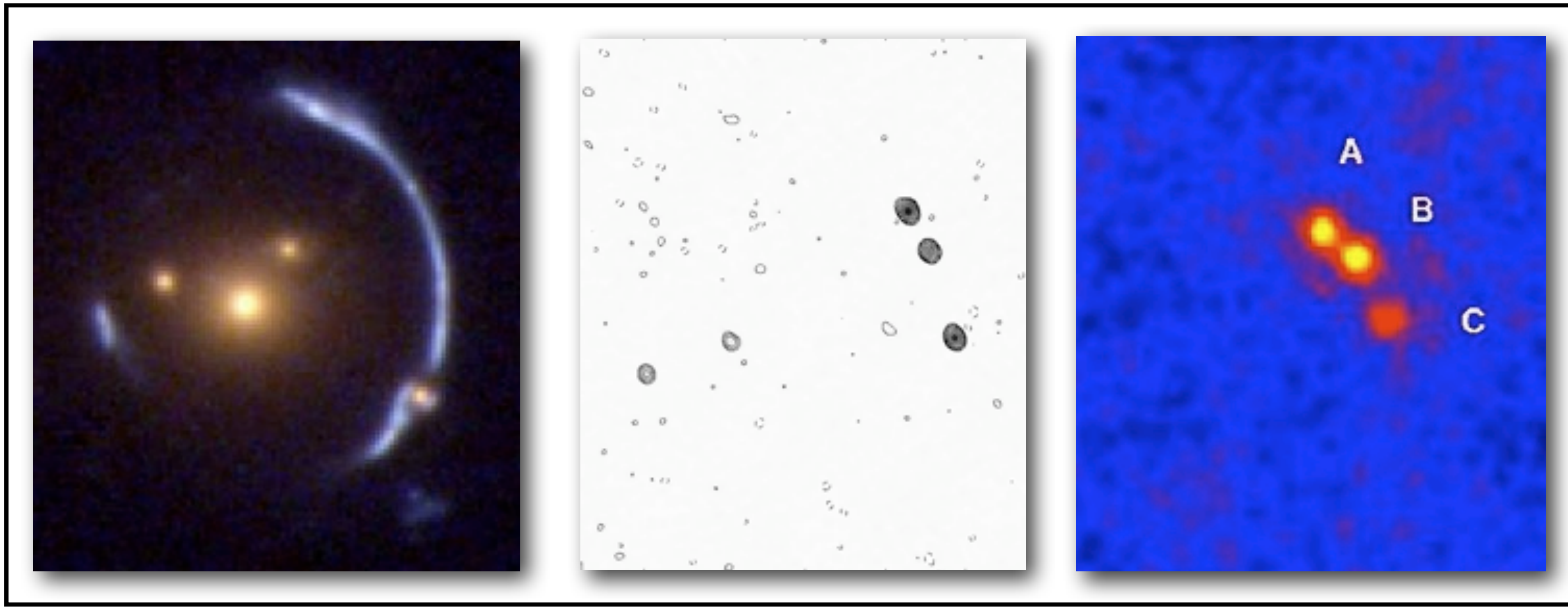

Léon Koopmans
(Kapteyn Astronomical Institute)

Outline

Lecture #1 - Theory:

Flux/Surface-brightness anomalies.

Lecture #2 - Observations

Examples of anomalies due to luminous and dark substructures.

Lecture #3 - Modeling

How to use anomalies to infer properties about substructure(s).

Before continuing: I will discuss these two phenomena

Flux-ratio anomaly

Perturbations to a smooth lens mass model

Surface-brightness anomaly

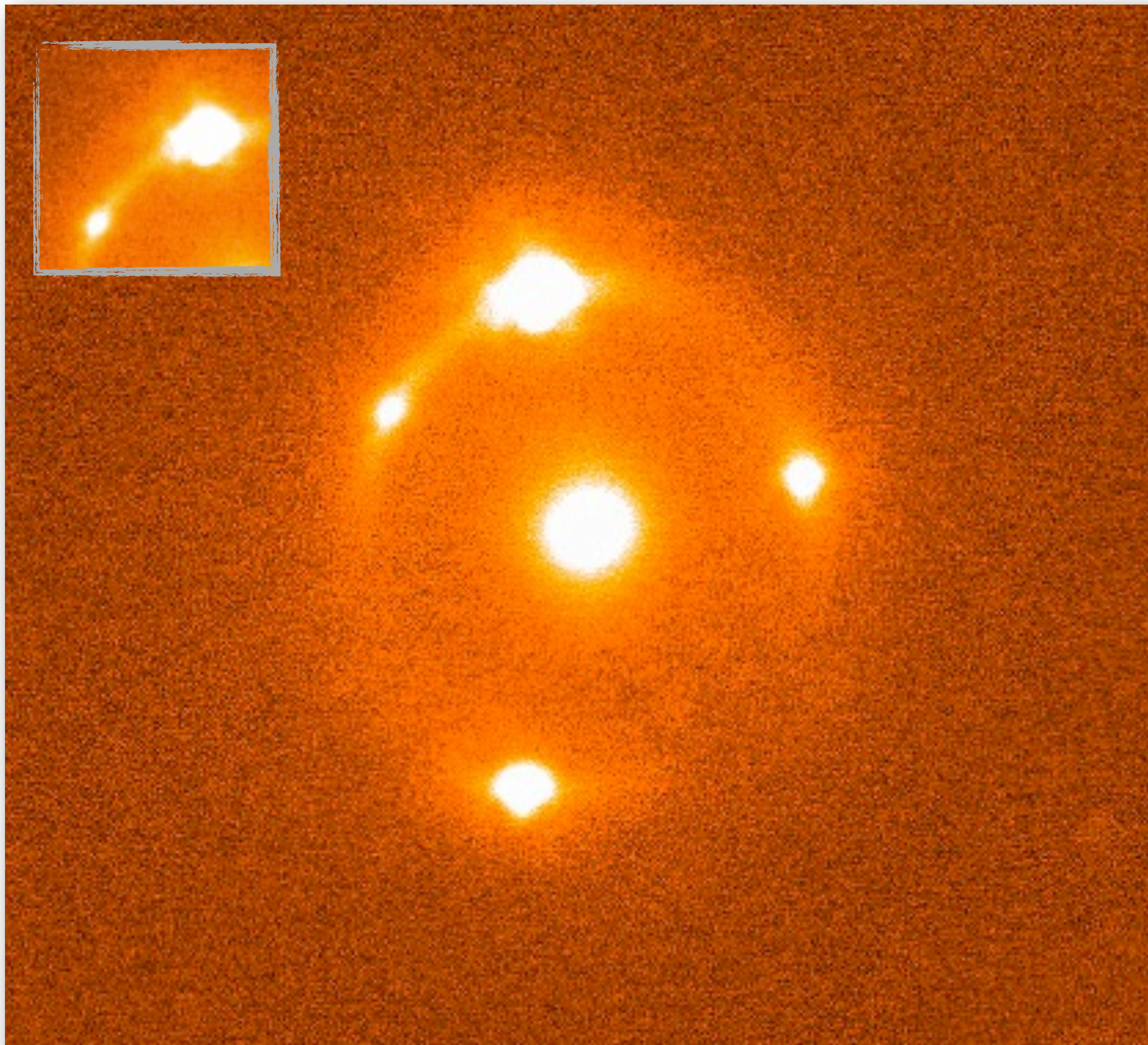

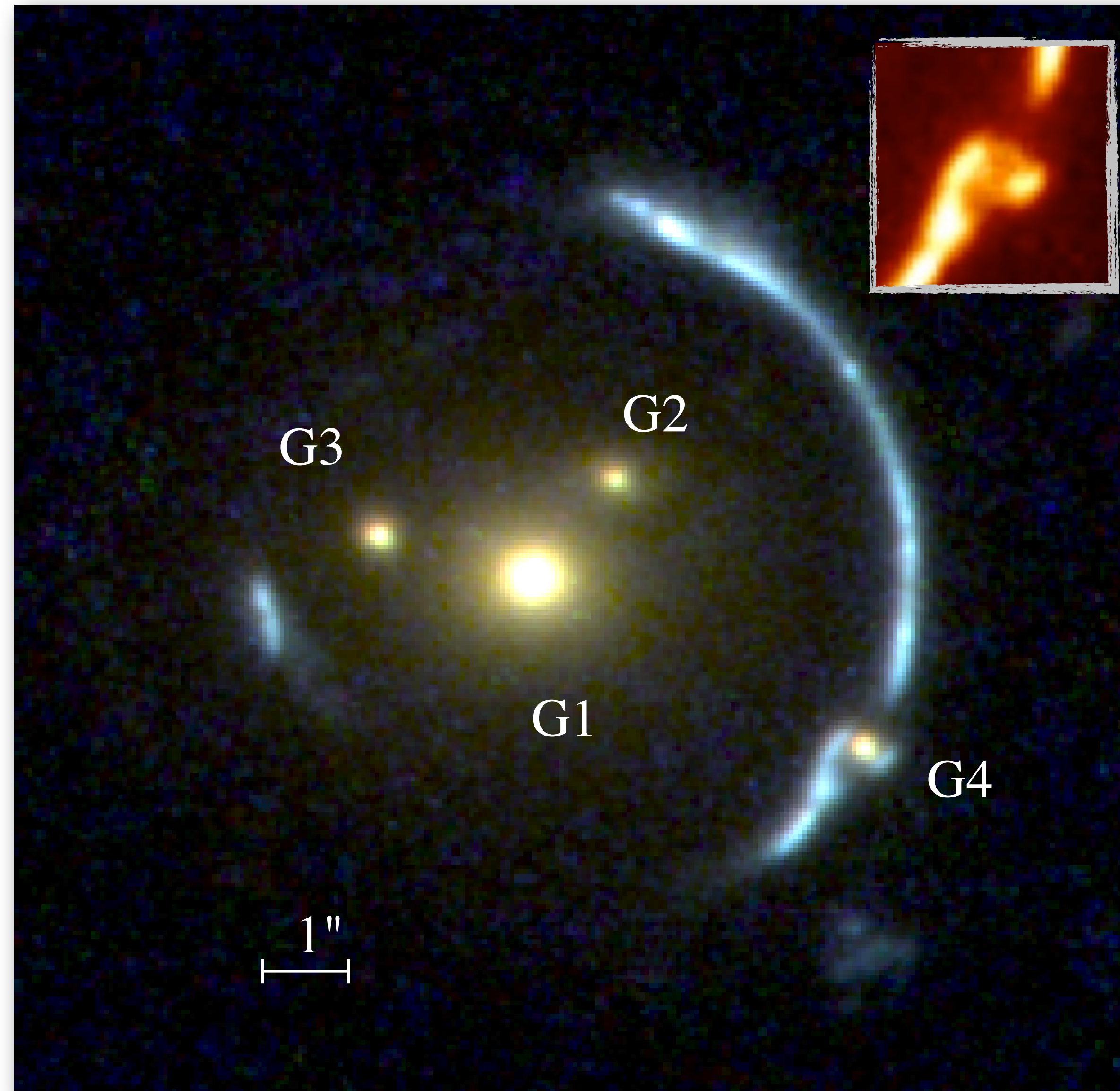

Compact sources
Only their flux can be measured

Extended sources
Image surface-brightness can be measured

Observed (compact) sources: CLASS

Compact (AGN-source) gravitational lenses discovered in the Cosmic Lens All Sky Survey (Browne et al. 2003)

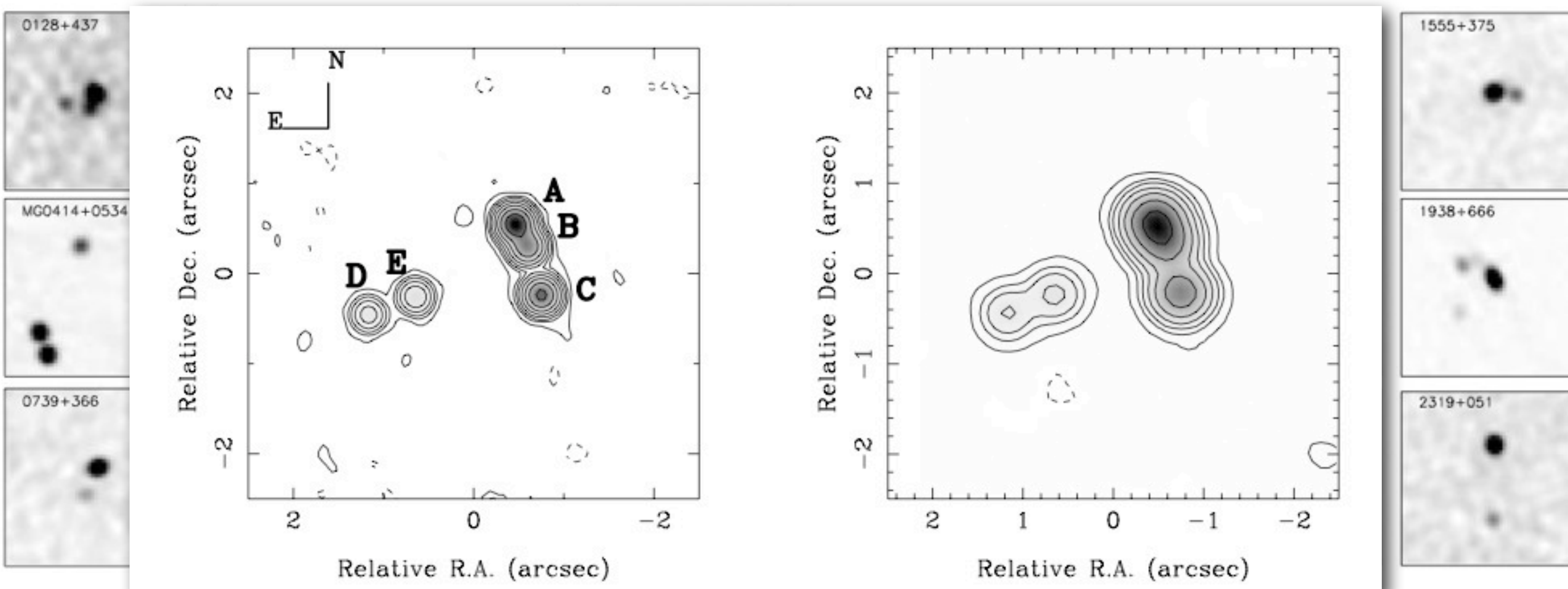

Some of these lenses are claimed to be anomalous (Dalal & Kochanek 2002)

Observed (extended) sources: SLACS

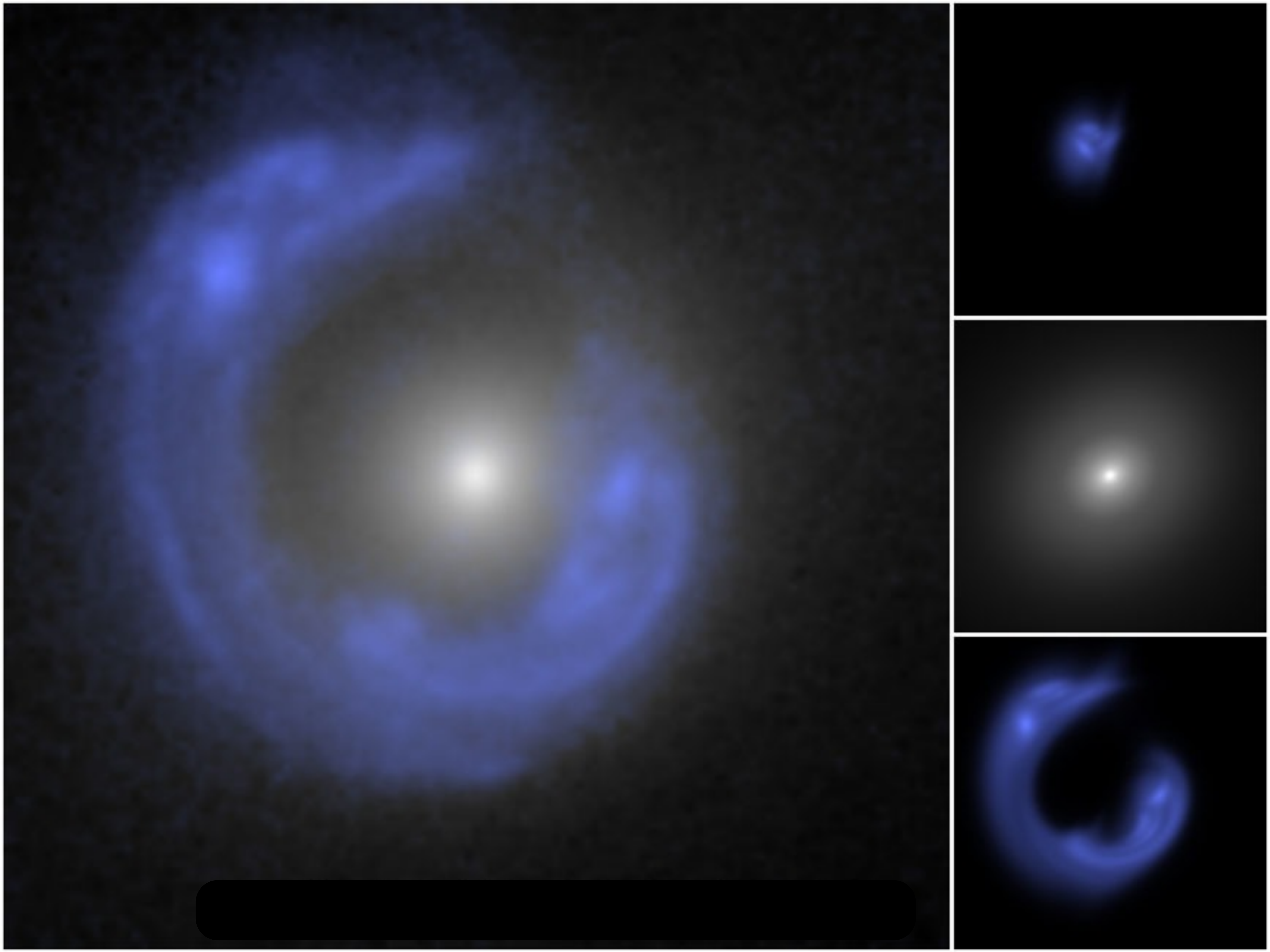

Theory

Strong Lensing Geometry

Gravitational Lensing is Geometric Optics in Curved Space-Time

$$\boxed{\vec{y} = \vec{x} - \vec{\alpha}(\vec{x})}$$

Gravitational lensing maps points in the source plane on to (multiple) points on the images plane through light-rays that follow geodesics. Surface brightness is conserved. In terms of Fermat's principle: light-rays follow stationary (min/max/saddle) paths in their travel time, including both geometric/Shapiro delays.

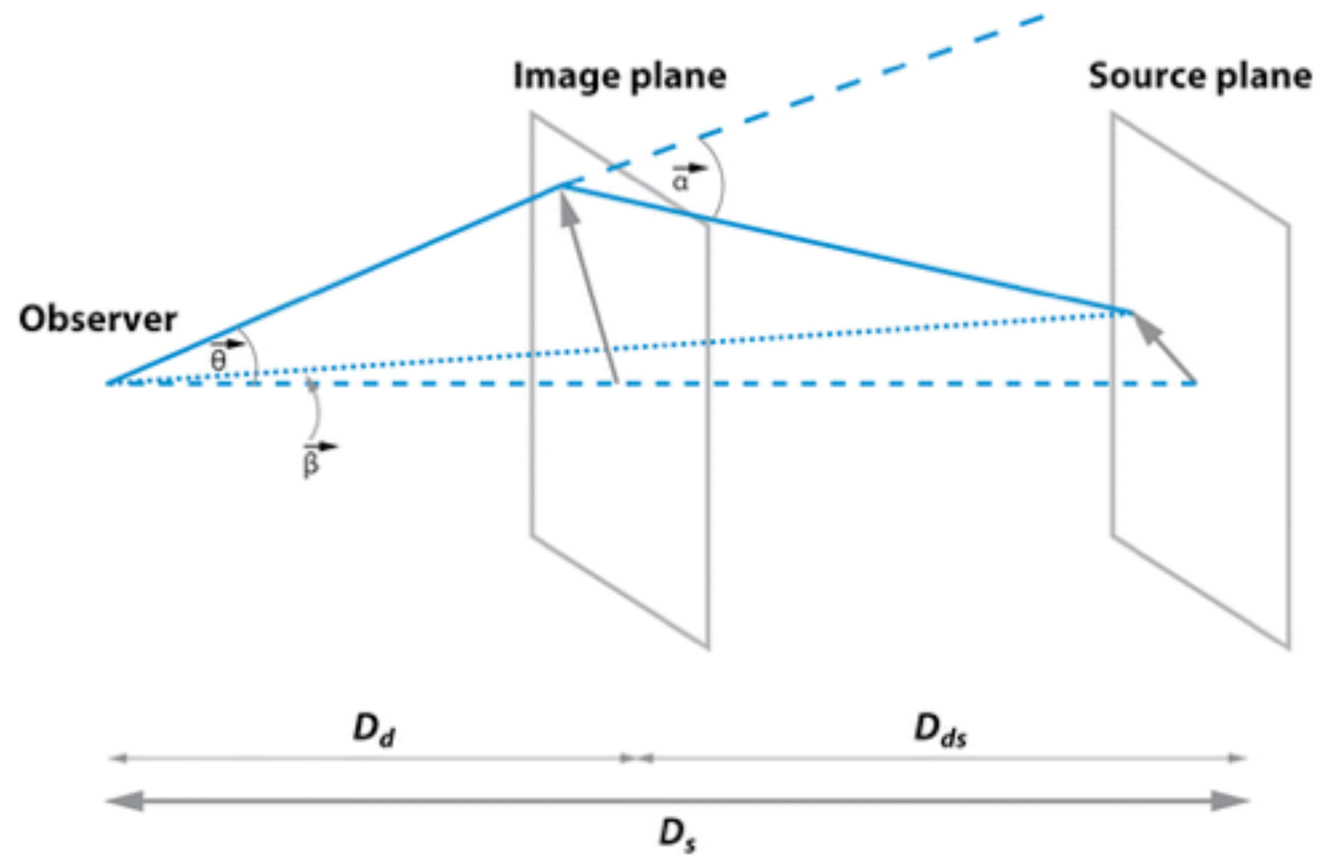

Studies of the lens or source require one to invert this mapping and derive both the source brightness distribution and the lens potential.

Typical Multiple-image Configurations

What these lines are will be explained later

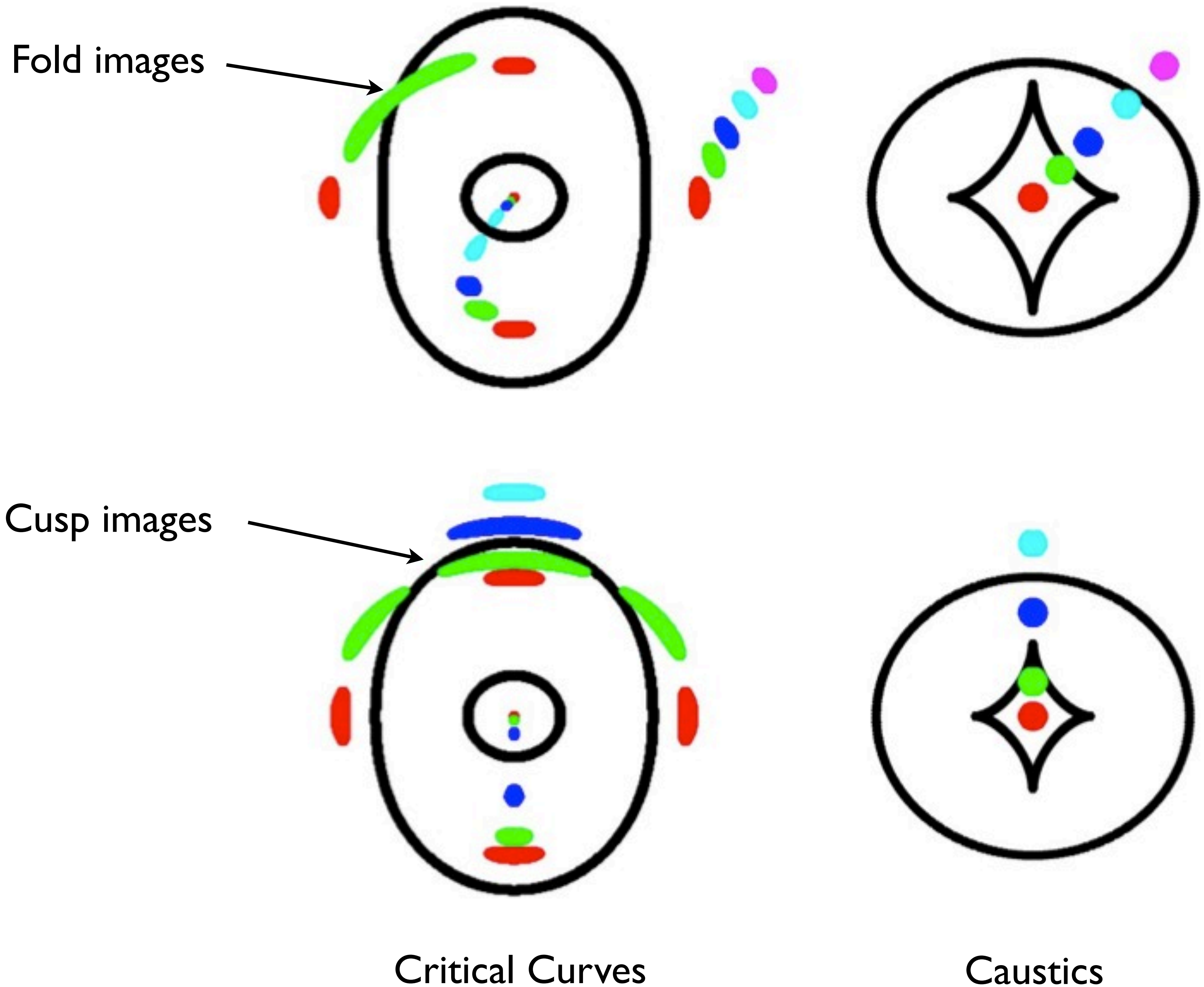

Image Distortions

The lens equation that relates the image positions to a (unknown) source position is given - in dimensionless form - by (see lectures by Wambsganss/Bacon):

$$\vec{y} = \vec{x} - \vec{\alpha}(\vec{x})$$

where the reduced deflection angle is related to the 2D lens potential (the latter is derived from the 2D Poisson equation applied to the surface density of the lens)

$$\vec{\alpha}(\vec{x}) = \vec{\nabla}\psi(\vec{x})$$

In case of a small perturbation one can modify this relation as follows and then linearize/Taylor-expand all subsequent derivations (if needed).

$$\vec{\alpha}(\vec{x}) + \boxed{\delta\vec{\alpha}(\vec{x})} = \nabla(\psi(\vec{x}) + \boxed{\delta\psi(\vec{x})})$$

In these lectures, we study the theory, observational effects and modeling of small (in mass, not in effect!) perturbations to the lens potential

Image Distortions

Since surface brightness is conserved in gravitational lensing (Liouville's theorem) one finds for an unperturbed (smooth) lens:

$$\boxed{S_x(\vec{x}) = S_y(\vec{y}) = S_y(\vec{x} - \vec{\alpha}(\vec{x}))}$$

where S_y is the surface brightness distribution of the source and S_x that of the lensed images.

Imagine now that the source is a Dirac delta function with flux F_0:

$$\mathrm{S}_y(\vec{y}) = F_0 \times \delta(\vec{y} - \vec{y}_0)$$

Let's choose for simplicity the coordinates such that y_0=(0,0). In that case

$$\mathrm{S}_x(\vec{x}) = F_0 \times \delta(\vec{x} - \vec{\alpha}(\vec{x}))$$

Image Distortions

Since the lens equation can have multiple solutions, multiple (distorted) images will appear in the image plane.

Since the images are infinitesimally small, the sum of the fluxes of the images are:

$$\mathrm{F}_{\mathrm{img}} = F_0 \times \int\int \delta(\vec{x} - \vec{\alpha}(\vec{x}))d\vec{x} = F_0 \times \sum_i \frac{1}{|A(\vec{x}_i)|}$$

The sum is made over all images *i* and the matrix (see also lectures Wambganss)

$$\boxed{A = \frac{\partial(\vec{x} - \vec{\alpha}(\vec{x}))}{\partial\vec{x}} = \begin{pmatrix} 1\text{-}\psi_{11} & \text{-}\psi_{12} \\ \text{-}\psi_{21} & 1\text{-}\psi_{22} \end{pmatrix}}$$

This Jacobian matrix indicates the distortion of an infinitesimally small source when projected on the image plane and causes the integrated flux of the image to be modified (either decrease or increase: (de)magnified).

Image Distortions

This Jacobian matrix can be related (Sach 1961) to the mass of lens (and field) that a distorts a ray-bundle while passing through the lens (traveling on geodetics).

Using the dimensionless Poisson equation in 2D, we can define the dimensionless surface density (i.e. convergence) in critical units using ψ,

$$\boxed{\kappa = \frac{1}{2}\left(\psi_{11} + \psi_{22}\right) \quad \text{or} \quad \nabla^2\psi = 2\kappa}$$

In addition we can define two shear components as function of the potential as well

$$\boxed{\gamma_1 = \frac{1}{2}\left(\psi_{11} - \psi_{22}\right) \quad \text{and} \quad \gamma_2 = \psi_{12} = \psi_{21}}$$

Image Distortions

The Jacobian matrix A, of the lens equation, tells us how a ray-bundle is (de)magnified and distorted by the surface-mass density (convergence) inside the ray-bundle and the shear coming from mass outside the bundle, as rays move along geodesics.

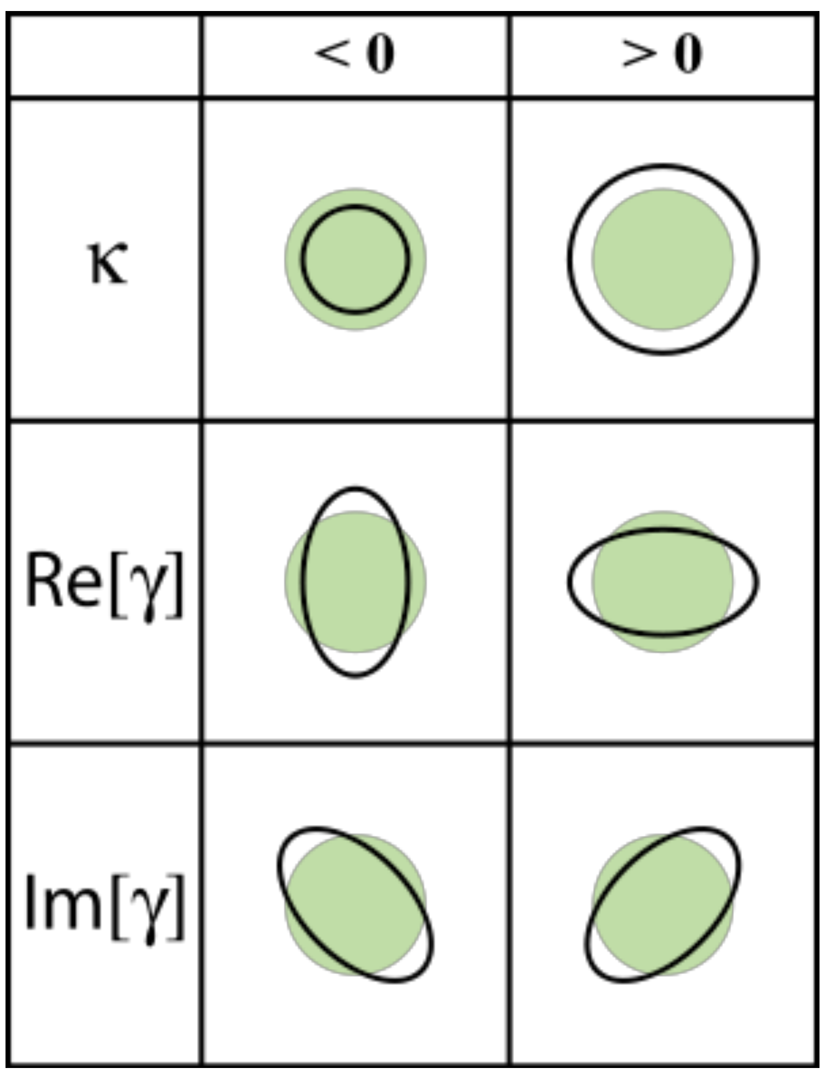

$$\boxed{A = \begin{pmatrix} 1-\kappa-\gamma_1 & -\gamma_2 \\ -\gamma_2 & 1-\kappa+\gamma_1 \end{pmatrix}}$$

$$\kappa(\vec{x}) = \frac{\Sigma(\vec{x})}{\Sigma_{\mathrm{crit}}} \qquad \gamma(\vec{x}) = \gamma_1(\vec{x}) + i\gamma_2(\vec{x})$$

$$\boxed{\mu(\vec{x}) = \frac{1}{\det[A(\vec{x})]}}$$

(de)magnification of an infinitesimally small source. The sign of μ is the parity.

Perturbations to the Lens Equation

Imagine now that the lens plane contains a small perturbation $\delta\psi$ to a smooth lens potential ψ.

This causes light-rays that an observer sees to come from a different position in the source plane compared to the smooth-only lens model. Hence a different surface brightness is seen and a different source shape compared to the smooth model.

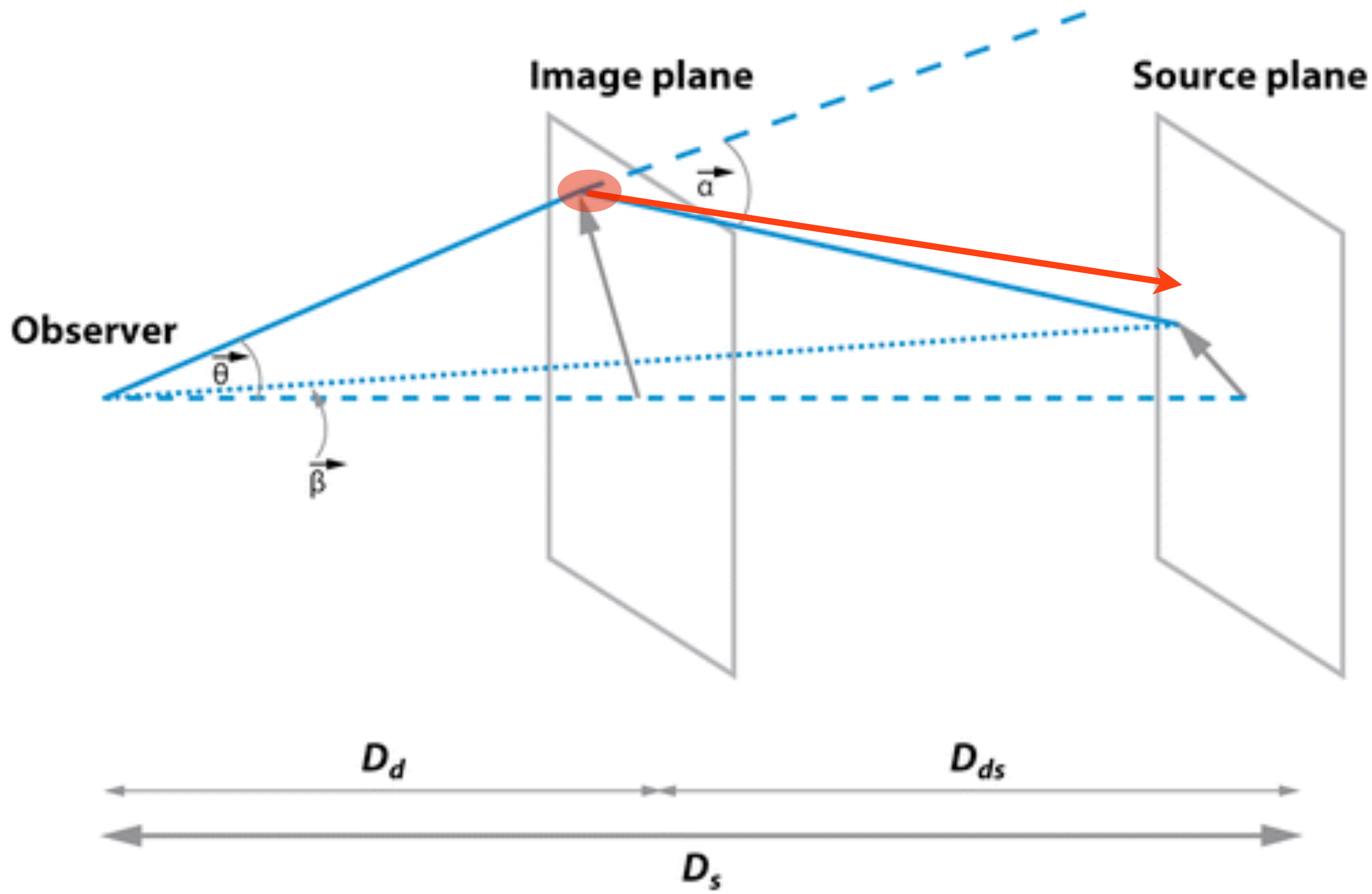

Flux-ratio Anomalies

A difference in the *flux*-ratio between compact (point-like) images from that expected from a smooth lens model.

Perturbations to the Lens Potential

A small perturbation to the lens leads to a change to the magnification matrix:

$$\delta A' = \begin{pmatrix} \text{-}\ \delta\kappa - \delta\gamma_1 & \text{-}\ \delta\gamma_2 \\ \text{-}\ \delta\gamma_2 & \text{-}\delta\kappa + \delta\gamma_2 \end{pmatrix}$$

Before adding, we transform the coordinates (locally to the image) such that A becomes diagonal (no loss of generality), with the eigenvalues of A on the diagonal,

$$A' = \begin{pmatrix} 1\ \text{-}\ \kappa - \gamma & 0 \\ 0 & 1\ \text{-}\ \kappa + \gamma \end{pmatrix} \qquad \gamma^2 = \gamma_1^2 + \gamma_2^2$$

Now we (i) add A' and δA, (ii) evaluating again their eigenvalues, (iii) Taylor-expand to first order in the perturbation, assuming the perturbations are small, and (iv) transform this to the frame (") of eigenvectors.

Perturbations to the Lens Potential

We then get:

$$A'' \approx \begin{pmatrix} 1 \text{ - } \kappa - \delta\kappa - \gamma - \delta\gamma_1 & 0 \\ 0 & 1 \text{ - } \kappa - \delta\kappa + \gamma + \delta\gamma_2 \end{pmatrix}$$

The diagonal shows the eigenvalues of the perturbed matrix, in its locally transformed eigenvector frame.

Now note that the magnification is μ=1/det(A'') or

$$\mu = \frac{1}{(1 - \kappa - \delta\kappa - \gamma - \delta\gamma_1)(1 - \kappa - \delta\kappa + \gamma + \delta\gamma_2)}$$

Let us examine where this magnification is most affected by the perturbation. For that we need to digress a little in to catastrophe theory.

Catastrophe Theory 101

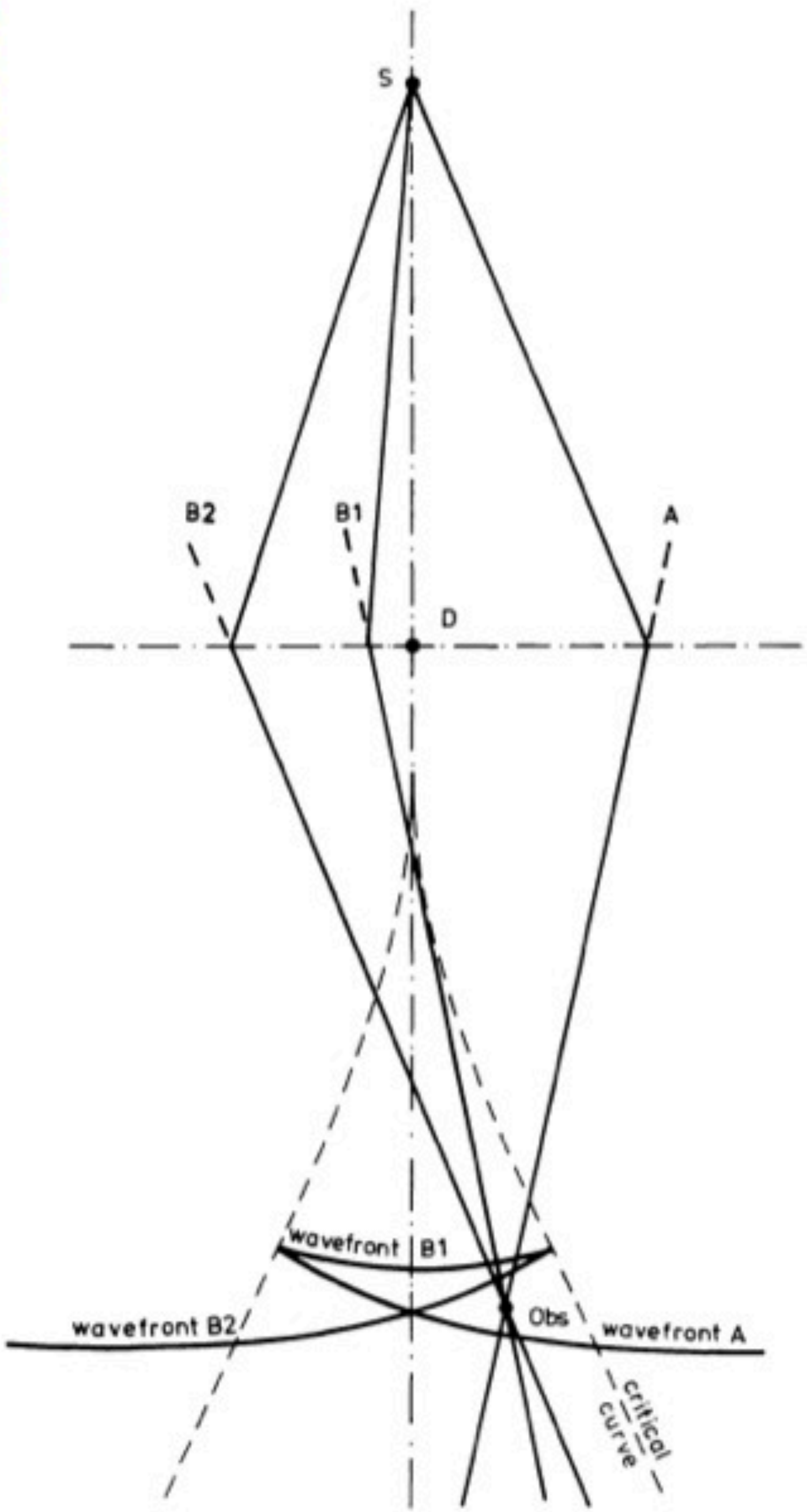

Kayser & Refsdal 1983

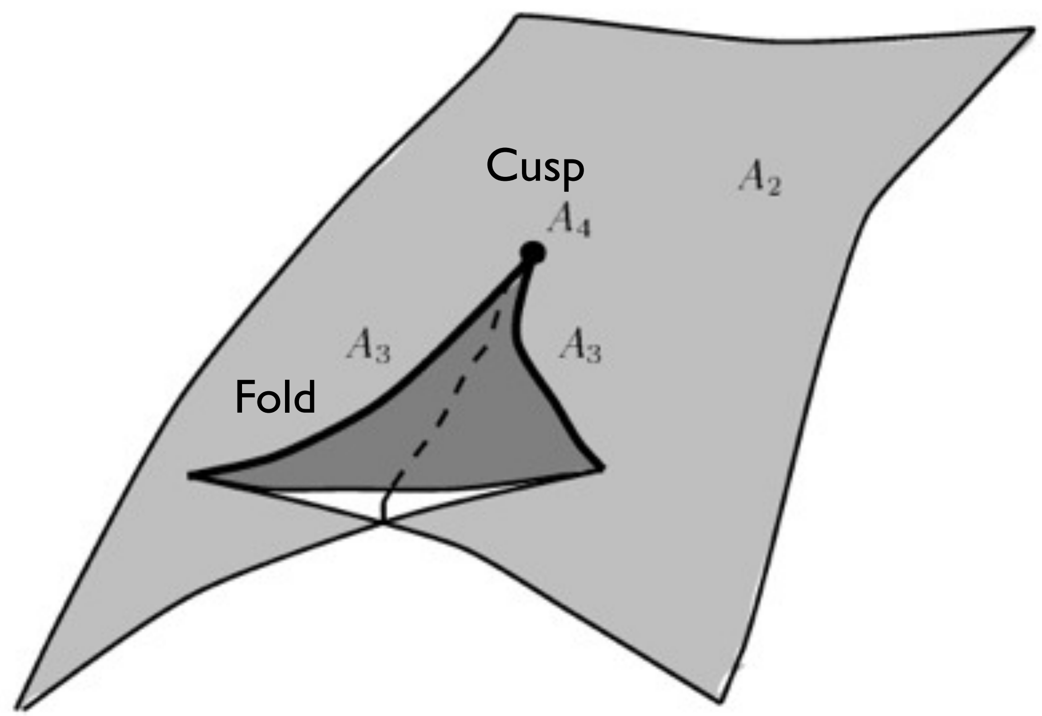

Caustics are due the folding of a single wavefront moving in curved space-time, caused by a mass distribution (say a lens).

Multiple images are equivalent to to seeing the same but folded and distorted wavefront multiple times (but delayed!). When this happens cusps, folds, etc. can form.

Catastrophe Theory 101

In gravitational lensing theory we have:

Critical curves: All closed curves with det(A) = 0 (i.e. $\mu=\infty$).
Caustics: Maps of critical curves on to the source plane.
(related to image multiplicity

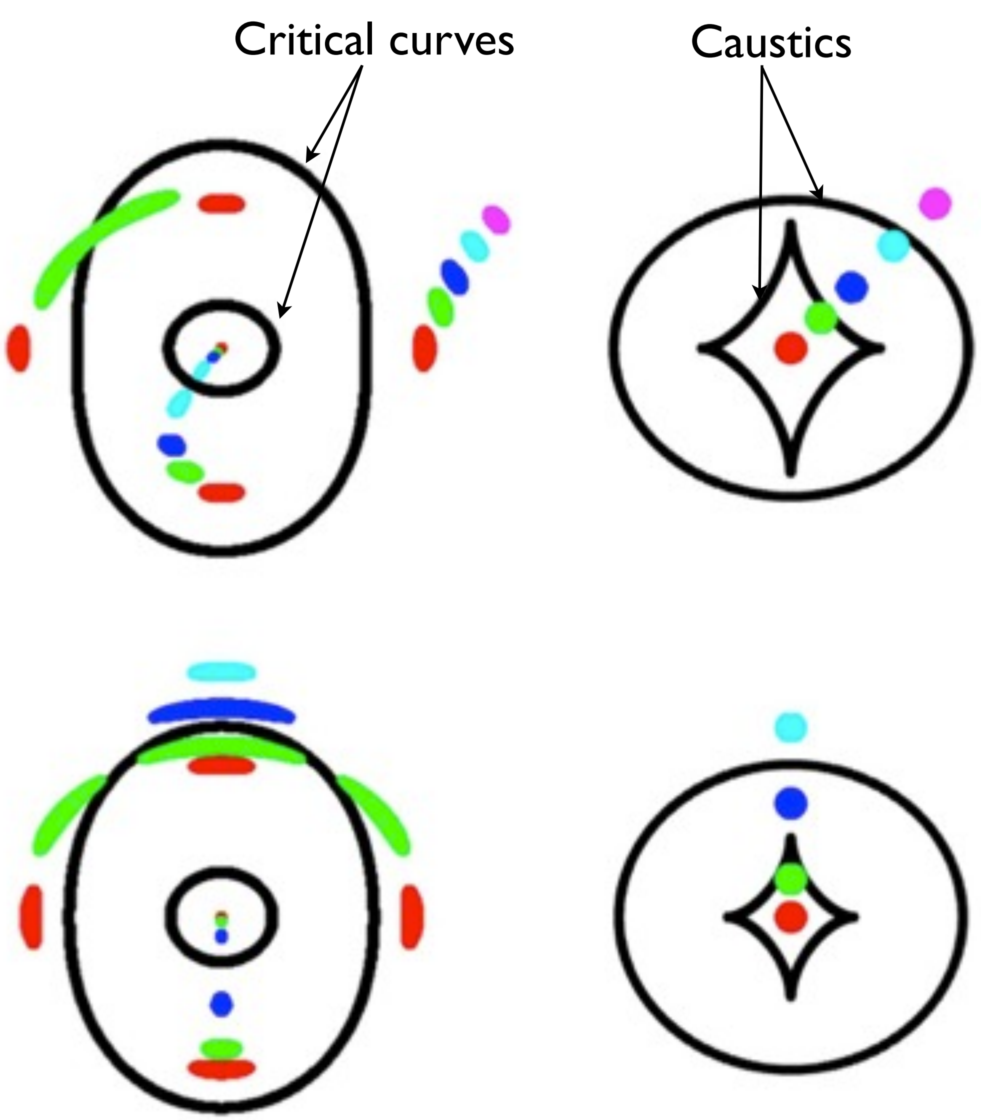

The Fermat-potential related to these critical curves/caustic have generic forms that have special properties:

	x	(non-critical)
	$\pm x_1^2 \pm \ldots \pm x_n^2$	(Morse)
smooth lenses	$x^3 + ax + (M)$	(fold)
	$\pm(x^4 + ax^2 + bx) + (M)$	(cusp)
+perturbations	$x^5 + ax^3 + bx^2 + cx + (M)$	(swallowtail)
	$\pm(x^6 + ax^4 + bx^3 + cx^2 + dx) + (M)$	(butterfly)
	$x^7 + ax^5 + bx^4 + cx^3 + dx^2 + ex + (M)$	(wigwam)
	$x^2y - y^3 + ax^2 + by + cx + (N)$	(elliptic umbilic)
	$x^2y + y^3 + ax^2 + by + cx + (N)$	(hyperbolic umbilic)
	$\pm(x^2y + y^4 + ax^2 + by^2 + cx + dy) + (N)$	(parabolic umbilic)
	$x^2y - y^5 + ay^3 + by^2 + cx^2 + dx + ey + (N)$	(second elliptic umbilic)
	$x^2y + y^5 + ay^3 + by^2 + cx^2 + dx + ey + (N)$	(second hyperbolic umbilic)
	$\pm(x^3 + y^4 + axy^2 + by^2 + cxy + dx + ey) + (N)$	(symbolic umbilic)

Catastrophe Theory: Description of Images Near Critical Curves

Lens equation: $\vec{y} = \vec{x} - \vec{\alpha}(\vec{x})$

Deflection Angle: $\vec{\alpha}(\vec{x}) = \vec{\nabla}\psi(\vec{x})$

Fermat Potential: $\phi = \frac{1}{2}(\vec{x} - \vec{y})^2 - \psi(\vec{x})$

Images form at extrema: $\vec{\nabla}\phi = 0$

See also lecture by Bacon describing Fermat's principle

Fold Images

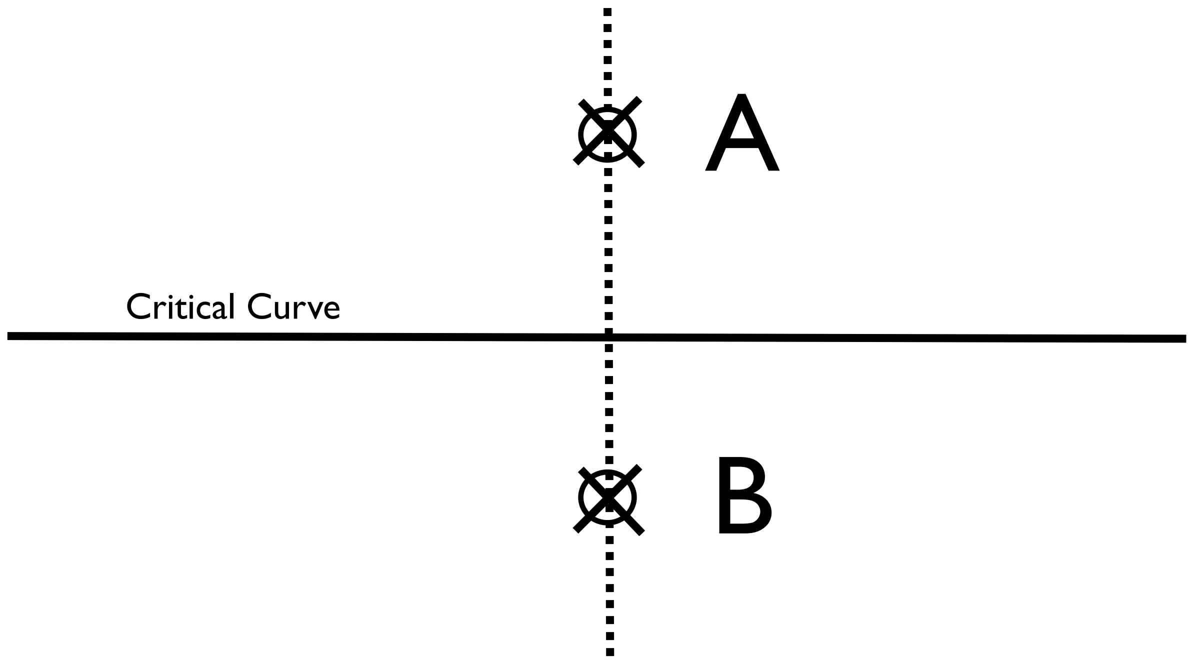

Fermat potential: $$\boxed{\phi \approx y_1 x_1 + y_2 x_2 - \frac{1}{2} x_1^2 - \frac{1}{3} x_2^3}$$

Lensed Images:

$$\partial\phi/\partial x_1 = y_1 - x_1 = 0 \qquad x_1 = y_1$$

$$\partial\phi/\partial x_2 = y_2 - x_2^2 = 0 \qquad x_2 = \pm\sqrt{y_2}$$

Fold Images

$$\partial^2\phi/\partial x_1^2 = -1$$

$$\partial^2\phi/\partial x_2^2 = -2x_2$$

$$\partial^2\phi/\partial x_2\partial x_1 = 0$$

Magnification of the lensed images become

$$\mu = [(1-\phi_{,11})(1-\phi_{,22}) - \phi_{,12}^2]^{-1} = \frac{1}{2x_2} \quad \text{or} \quad \mu = \frac{\pm 1}{\sqrt{y_2}}$$

Fold relations $\mu_{\rm tot} = \sum_{i=\mathrm{A,B}} \mu_i = 0$

Cusp Images

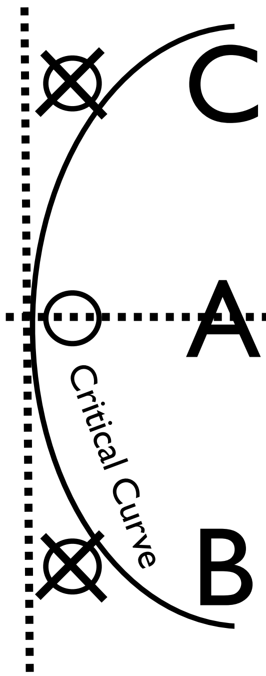

$y_1 < 0$ $y_1 > 0$

$$\boxed{\phi \approx y_1 x_1 + y_2 x_2 - \frac{1}{2}x_1^2 - \frac{1}{2}y_1 x_2^2 - \frac{1}{4}x_2^4}$$

$$\partial\phi/\partial x_1 = y_1 - x_1 = 0 \qquad x_1 = y_1$$

$$\partial\phi/\partial x_2 = y_2 - y_1 x_2 - x_2^3 = 0$$

Let's assume $y_2 = 0$ then $x_2^3 - y_1 x_2 = 0$

$$x_2 = 0$$

$$x_2 = \pm\sqrt{y_1}$$

Cusp Images

$$\partial^2\phi/\partial x_1^2 = -1 \quad \partial^2\phi/\partial x_2^2 = -y_1 - 3x_2^2 \qquad \partial^2\phi/\partial x_2\partial x_1 = 0$$

$$\mu = \frac{1}{y_1 - 3x_2^2}$$ with $x_1 = y_1$ and $\mu = 0$

Leads to a parabolic c.c. $x_2 = \pm\sqrt{x_1/3}$

$$\mu(x_2 = 0) = \frac{1}{y_1} \qquad \mu(x_2 = \pm\sqrt{y_1}) = \frac{-1}{2y_1}$$

Cusp relations $\mu_{\mathrm{tot}} = \sum_{i=A,B,C} \mu_i = 0$

Flux-ratio anomalies near folds/cusps

The sum of (parity-signed) magnifications is zero

Fold relation

$$\mu_{\rm tot} = \sum_{i=\rm A,B} \mu_i = 0$$

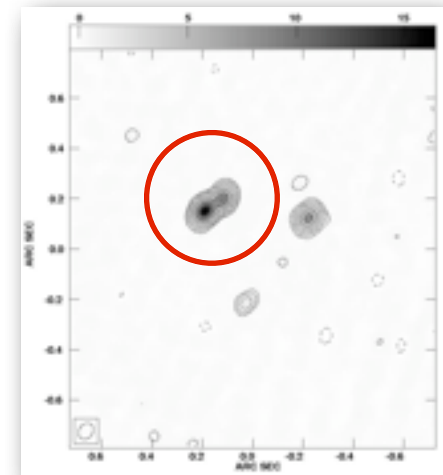

Cusp relation

$$\mu_{\rm tot} = \sum_{i=A,B,C} \mu_i = 0$$

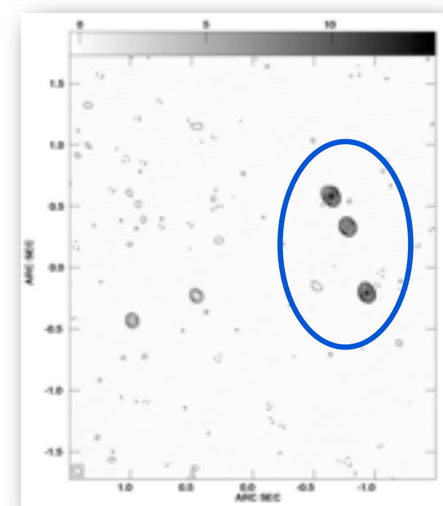

(e.g. Blandford 1989; Mao & Schneider 1998)

Perturbations to a SIE

Magnifications are very large near critical curves, and formally infinite on the critical curve. In fact one of the eigenvalues of matrix A goes to zero on the critical curve.

Let us take a simple example for the SIE. In that case, on the critical curve,

$$\kappa_{\rm SIE} = \gamma_{\rm SIE} = 1/2$$

The matrix A'' then becomes

$$A'' \approx \begin{pmatrix} -\,\delta\kappa - \delta\gamma_1 & 0 \\ 0 & 1\,-\delta\kappa + \delta\gamma_2 \end{pmatrix} \approx \begin{pmatrix} -\,\delta\kappa - \delta\gamma_1 & 0 \\ 0 & 1 \end{pmatrix}$$

Whereas w/o the perturbation the magnification was infinite (or very large), it can now become very different due to a shift in the critical curve. The images themselves will also shift, but by far less.

In short: a small perturbation can have a major impact on highly magnified images near critical curves. We will now examine this in greater detail.

Perturbations to the Lens Potential

Effects on the critical curve/caustic

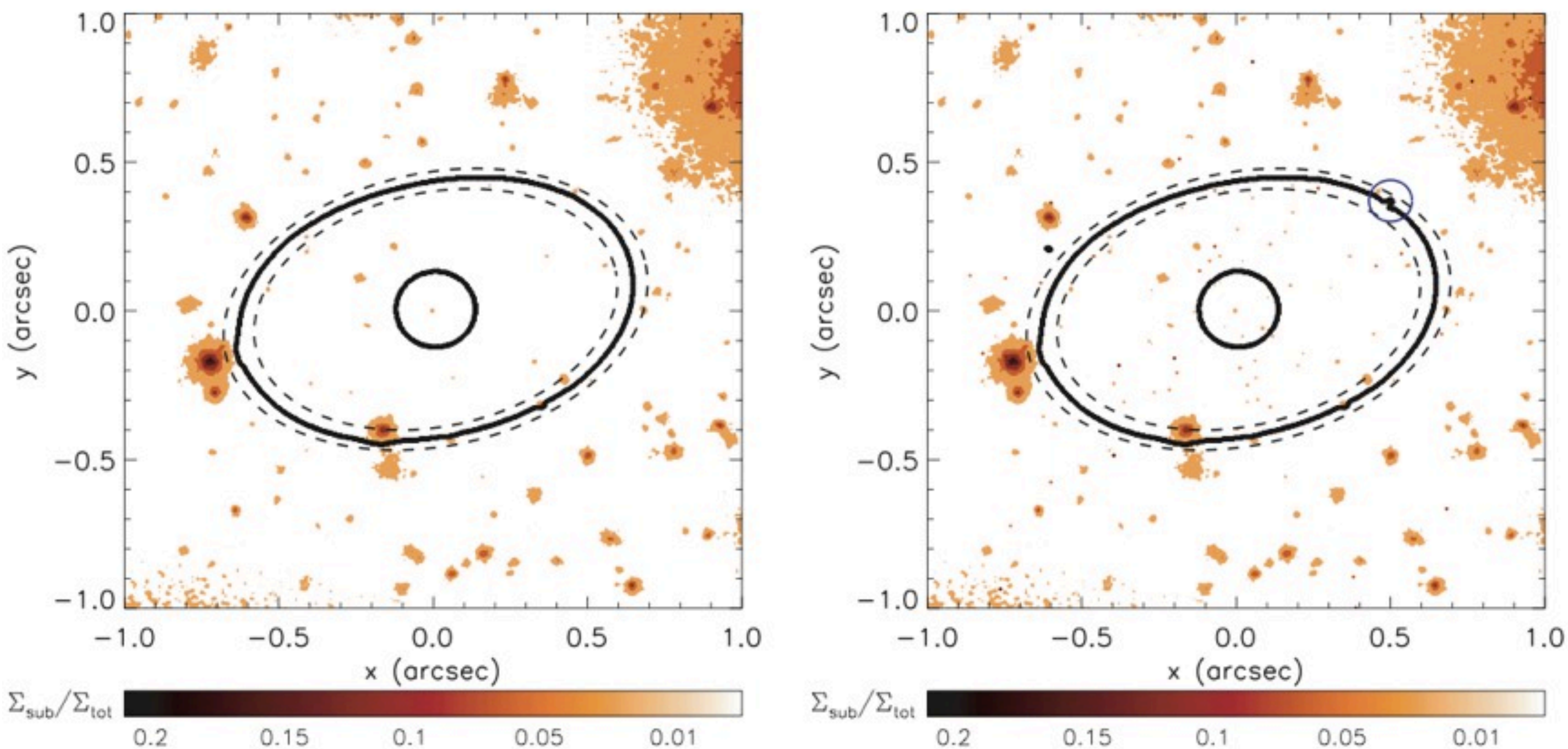

Xu et al. (2012)

Perturbations of Catastrophes

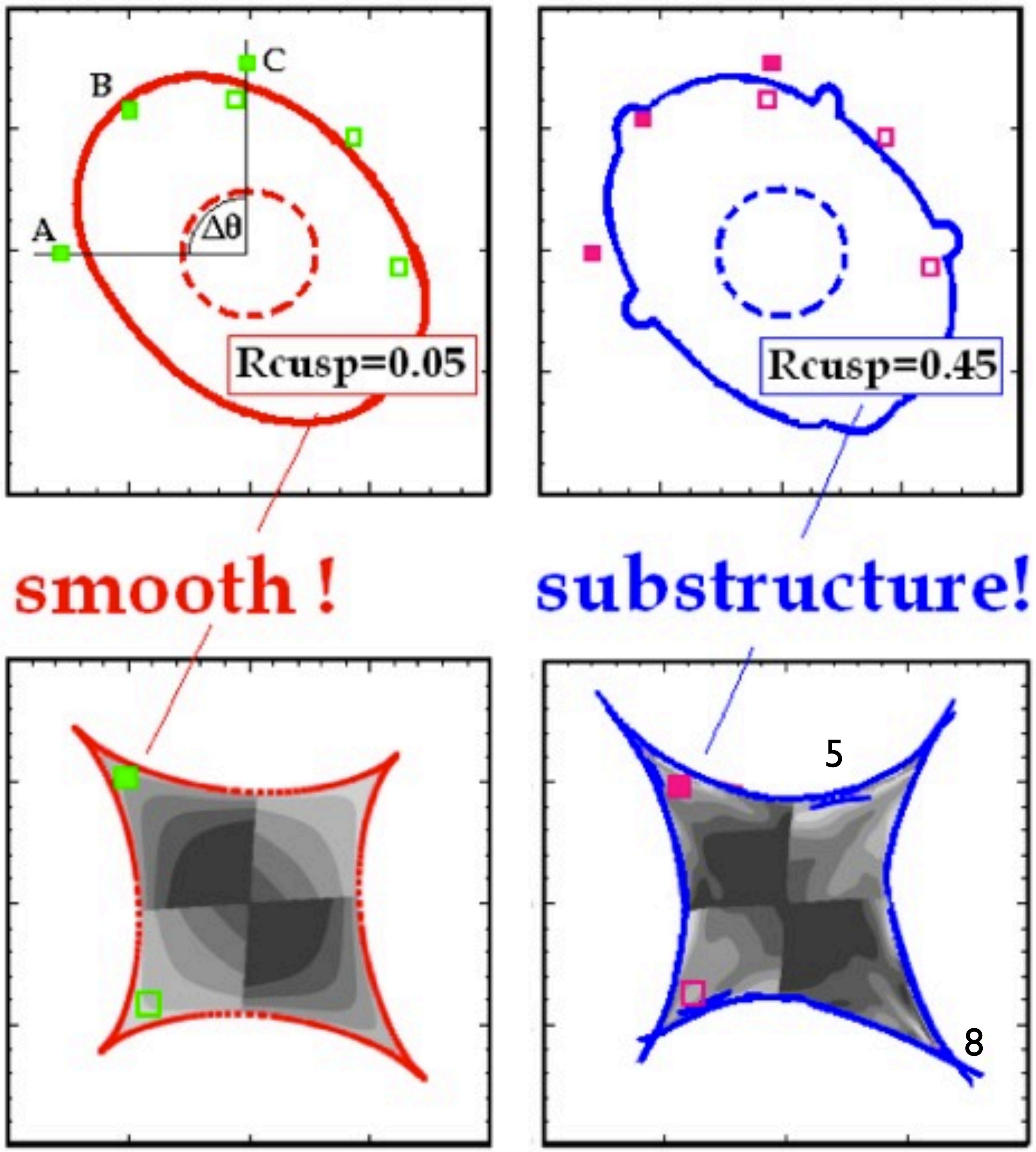

Xu et al. (2012)

Perturbations cause the critical curves to change and the caustics to transform as well, sometimes developing other types of catastrophes such as swallowtails and butterflies. This can cause a major change in the flux-ratio between cusp/fold images.

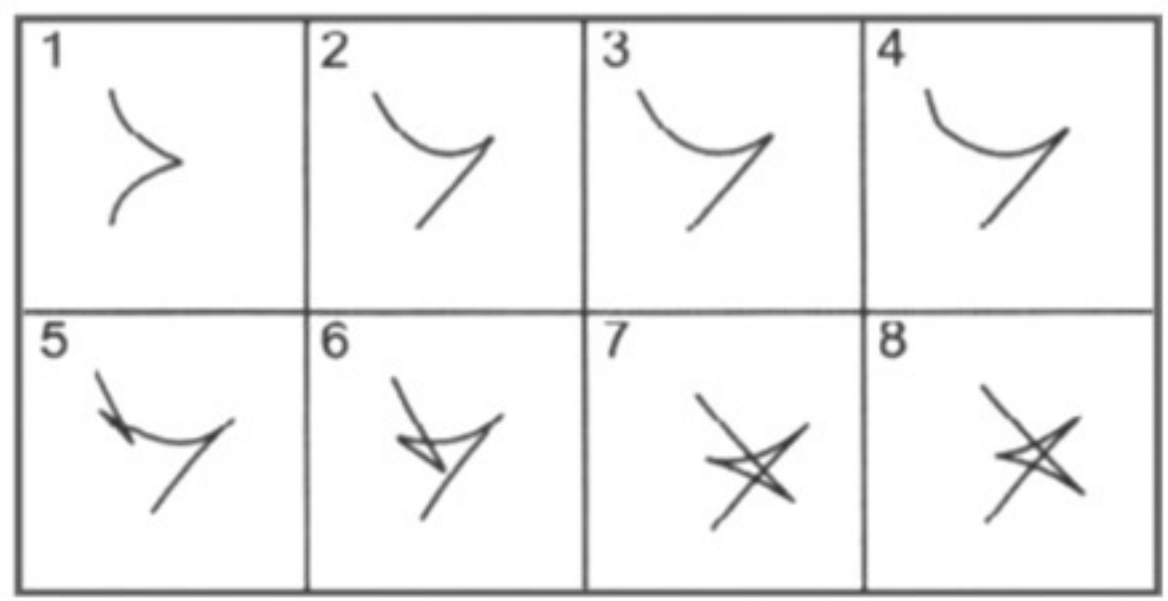

swallowtail butterfly

Petters et al. (2001)

Cusp Relation

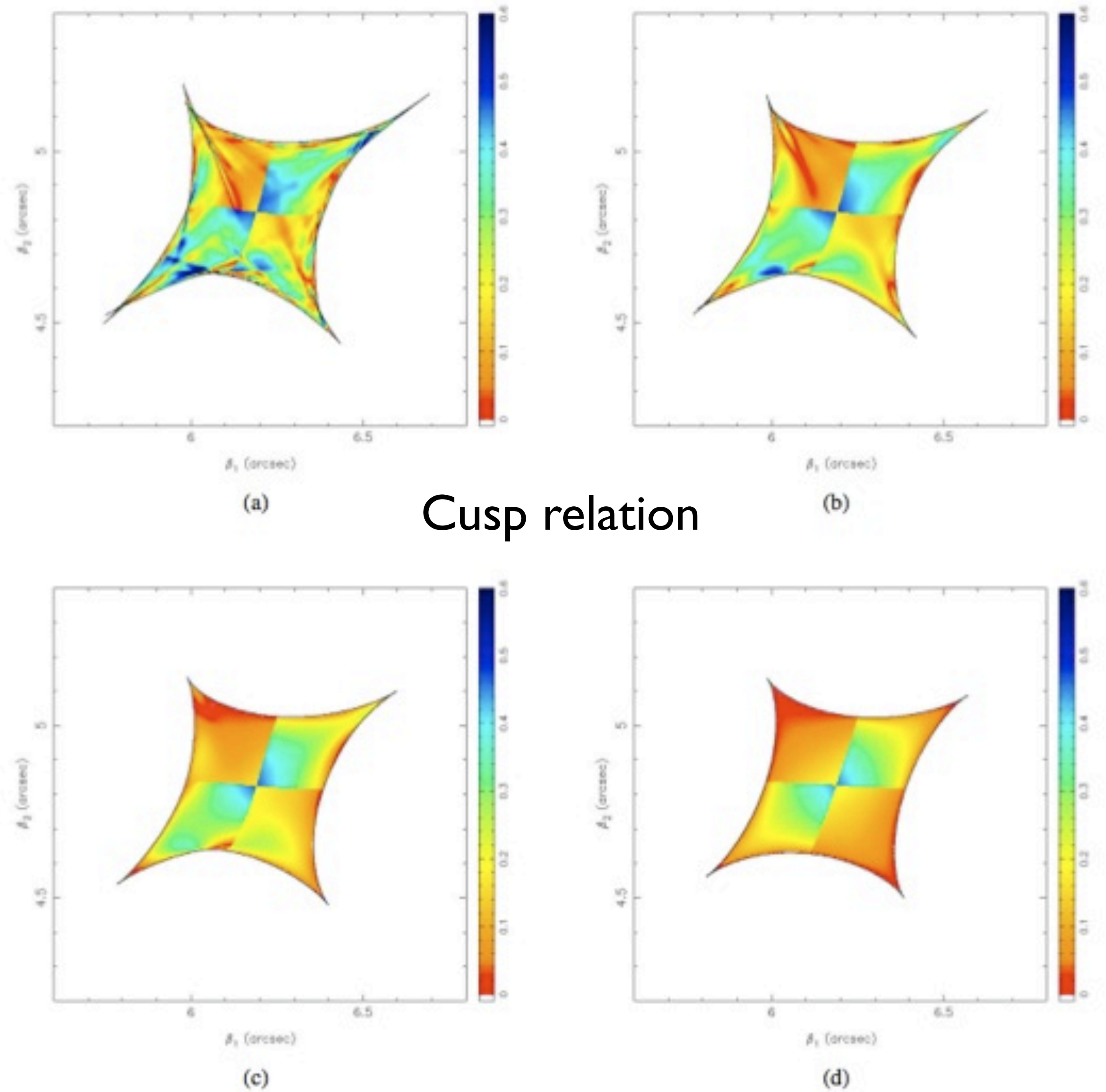

Cusp/fold magnification relation:
Measure of deviations from a perfectly smooth lens

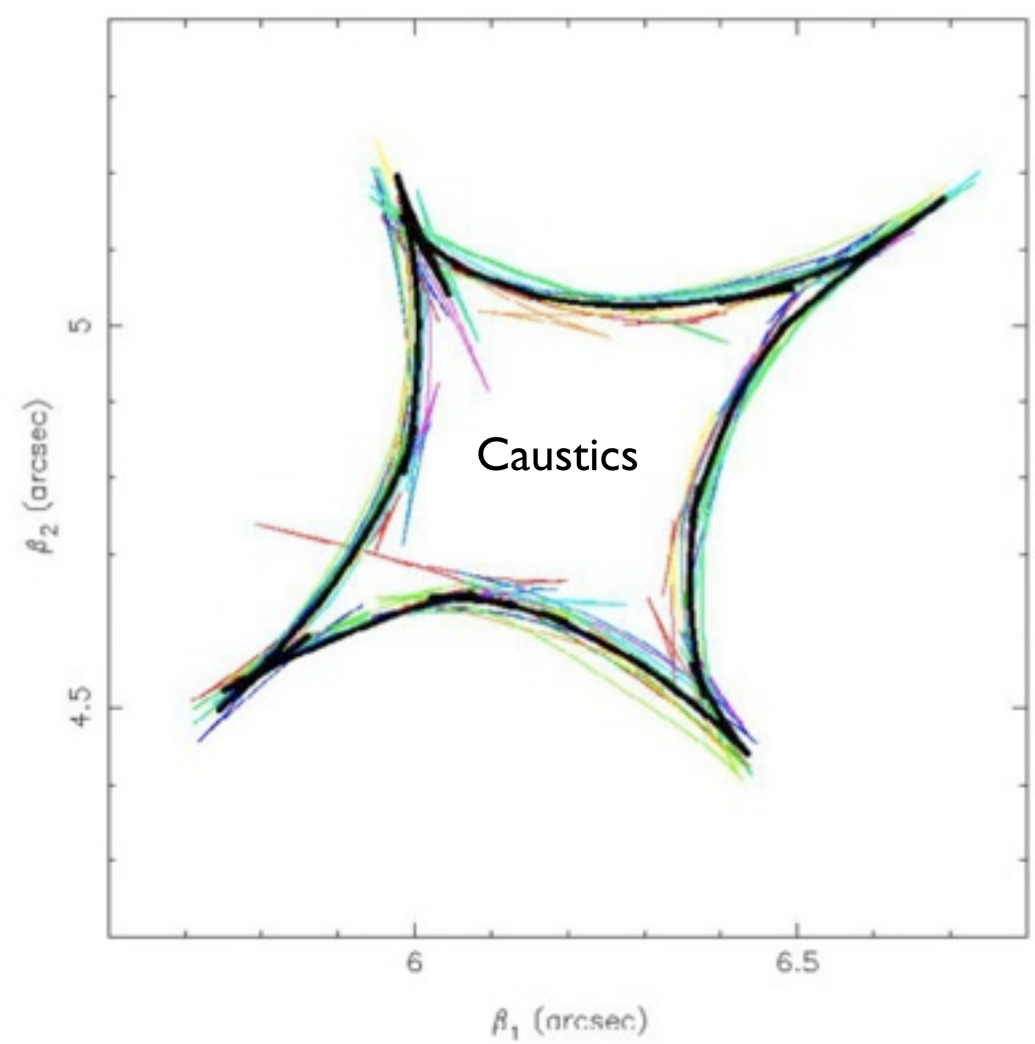

Bradac et al. 2004

Cusp Relation

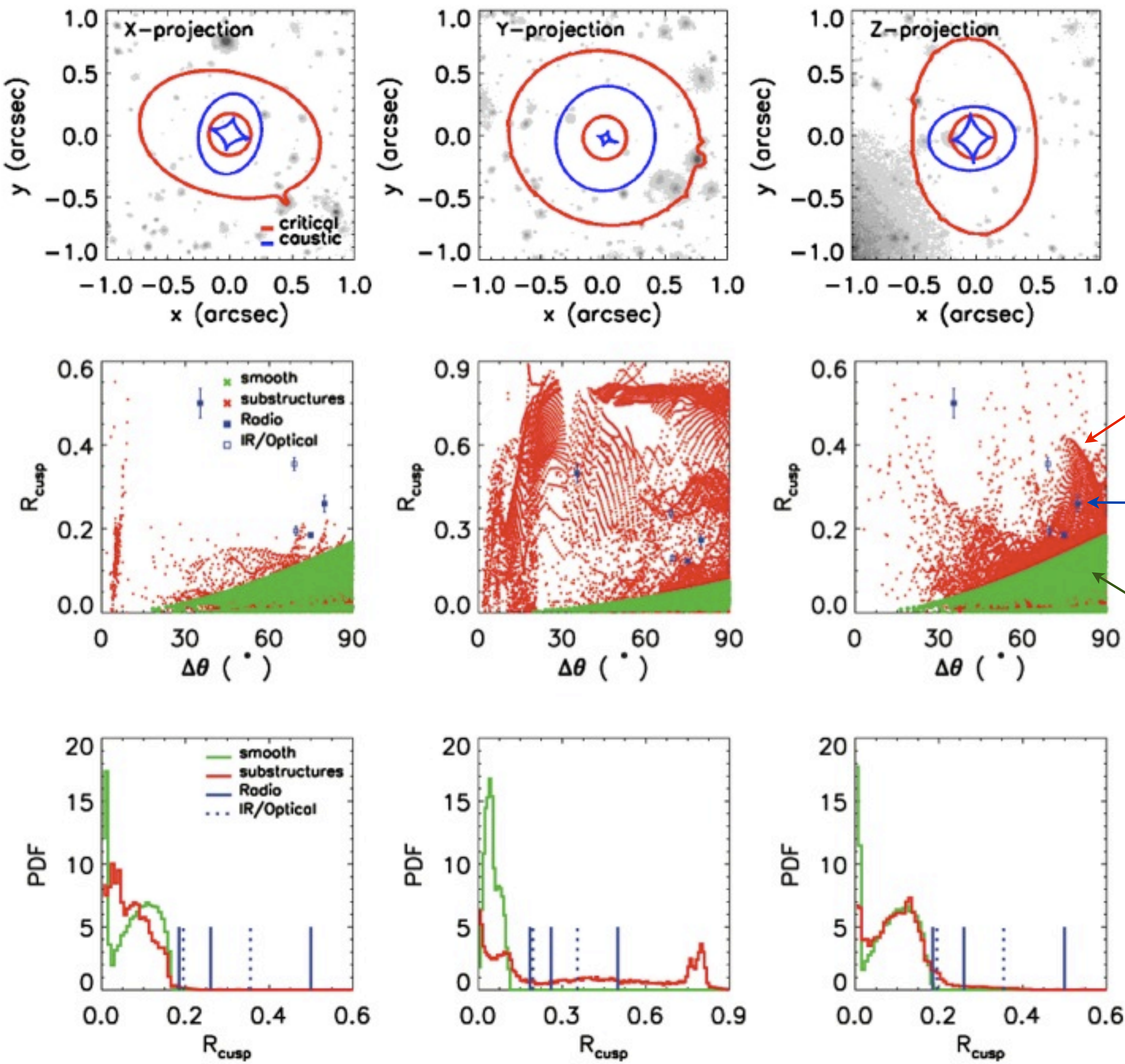

Cusp Relation

Expected for Perturbed Lens

Observed Lenses

Expected for Smooth Lens

Xu et al. 2009

Surface Brightness Anomalies

A difference in the surface brightness between extended images from that expected from a smooth lens model.

Surface Brightness Anomalies

To solve for (i) the source brightness distribution and (ii) the potential, using

$$S_x(\vec{x}) = S_y(\vec{y})$$

Conservation of source surface brightness

with

$$\vec{y} = \vec{x} - \vec{\alpha}(\vec{x})$$

The usual lens equation

Koopmans (2005)

Surface Brightness Anomalies

Conservation of surface brightness

$$S_x(\vec{x}) = S_y(\vec{y}) \longleftarrow \vec{y} = \vec{x} - \vec{\alpha}(\vec{x})$$

If

$$\psi \rightarrow \psi + \delta\psi$$

$$S_x \rightarrow S_x + \delta S_x$$

then

$$S_y + (\partial S_y / \partial \vec{y}) \cdot \delta \vec{y} \approx S_x + \delta S_x$$

$$(\partial S_y / \partial \vec{y}) \cdot \delta \vec{y} \approx \delta S_x$$

$$\boxed{\delta S_x \approx -\vec{\nabla}_y S_y \cdot \vec{\nabla}_x \delta\psi}$$

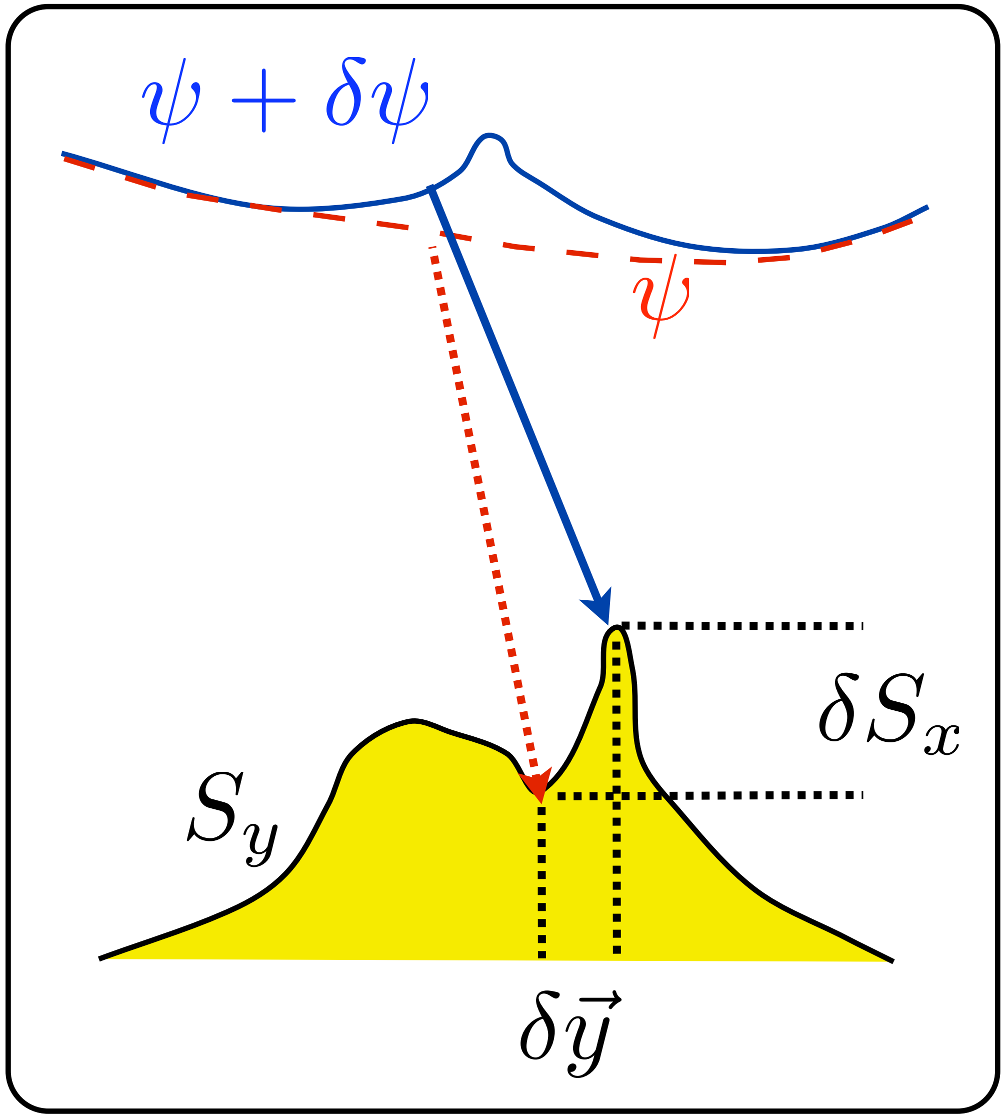

Surface Brightness Anomalies

Unperturbed smooth image

Perturbed smooth image

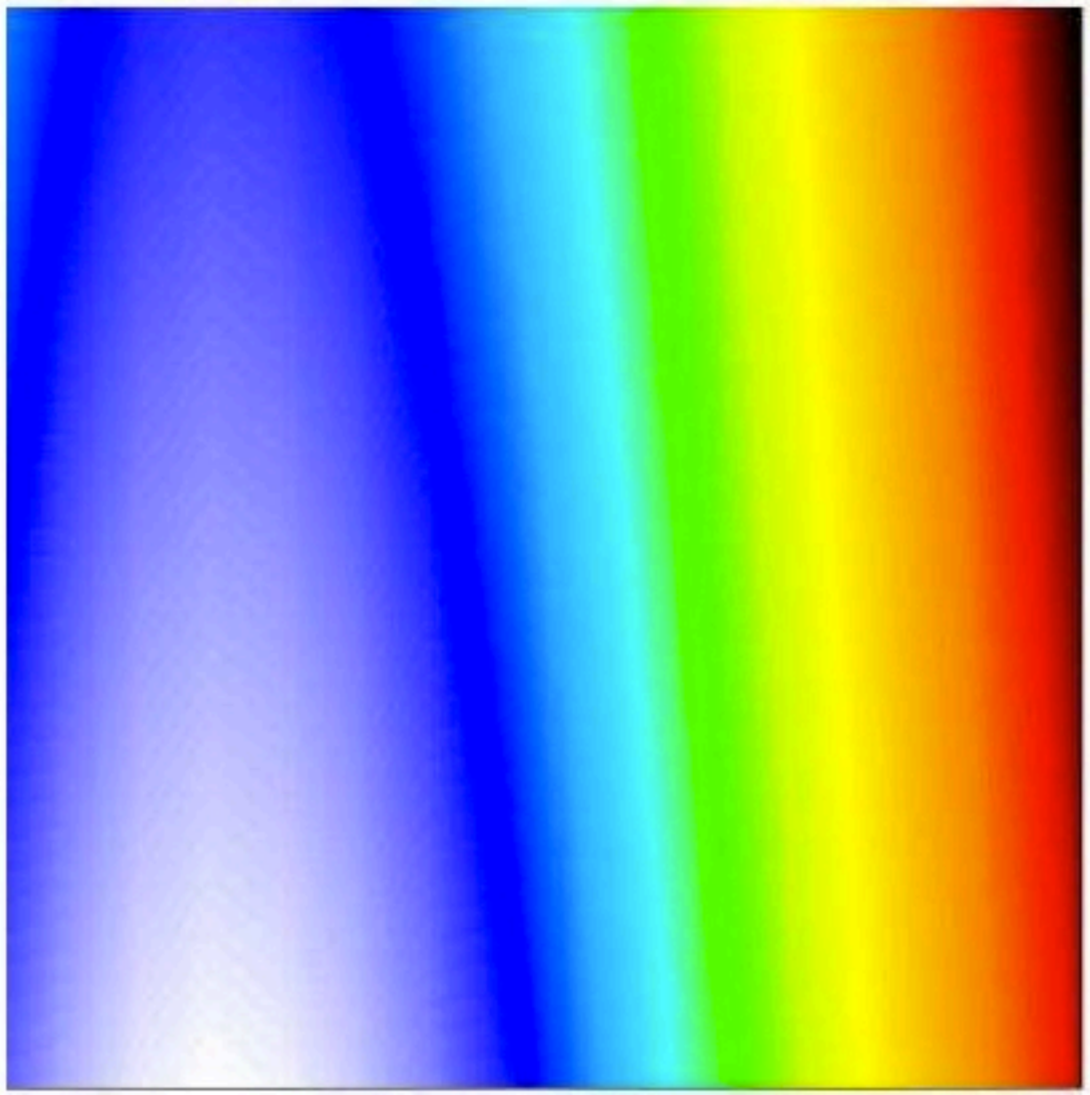

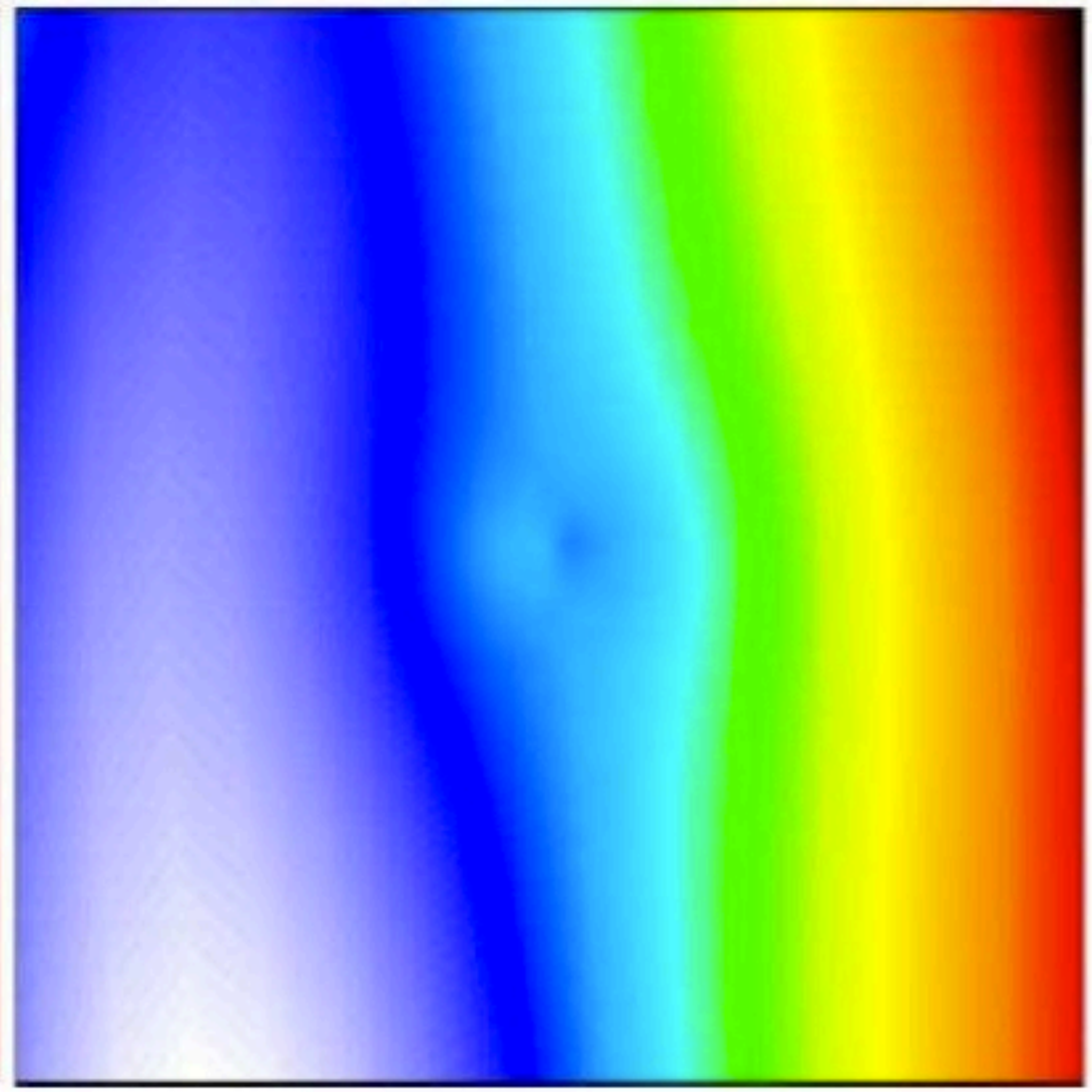

Can this small deviation from the smooth model be reconstructed from the image on the right? Yes under specific conditions!

Surface Brightness Anomalies

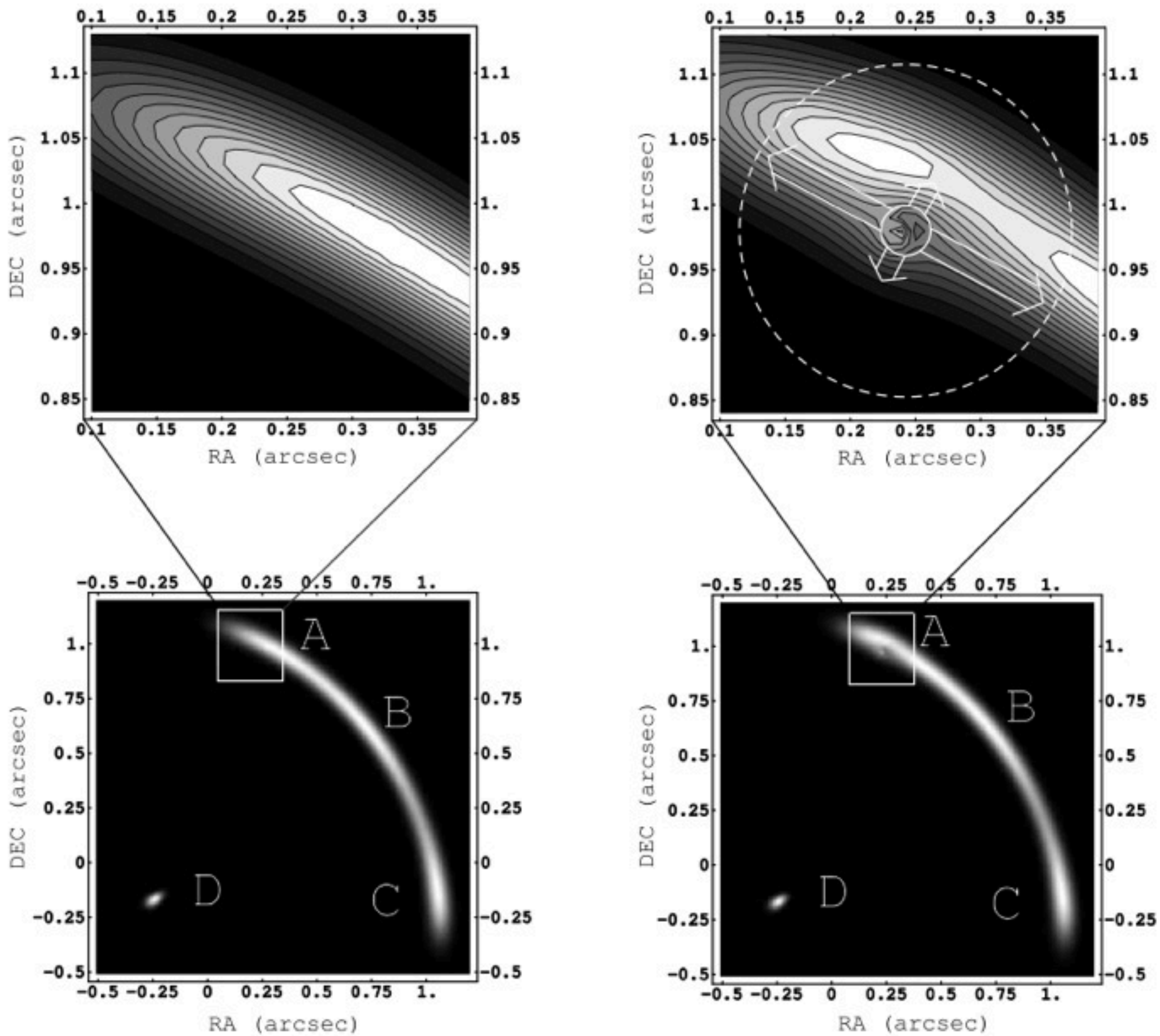

Inoue & Chiba 2005

Surface Brightness Anomalies

The first step is solving for S(x), given a smooth model. This is simple and leads to a linear equation (e.g. Warren & Dye 2003)

$$S_x(\vec{x}) = S_y(\vec{y}) = S_y(\vec{x}, \psi(\vec{x}))$$ Functional Form

or equivalently (see next lectures)

$$\mathbf{L}(\vec{\psi})\vec{s} = \vec{d}$$ Algebraic Form

(e.g. Warren &Dye 2003; Koopmans 2005; Suyu et al. 2006/8; Brewer & Lewis 2005; Vegetti & Koopmans 2009)

Surface Brightness Anomalies

In algebraic form this linearized equation reads (see next lectures):

$$\boldsymbol{B}[\boldsymbol{L}(\vec{\psi})\,|\overbrace{-\,\boldsymbol{D}_s(\vec{s}\,)\,\boldsymbol{D}_x}^{\equiv \boldsymbol{L}_{\delta\psi}}]\begin{pmatrix} \delta\vec{s} \\ \delta\vec{\psi} \end{pmatrix} = \vec{d} - \boldsymbol{B}\boldsymbol{L}(\vec{\psi})\vec{s} = \delta\vec{d}\,.$$

Gauss-Newton equation that can be solved iteratively

This linear algebraic equation can be solved using
a Bayesian penalty function for the residuals
and standard Cholesky/gradient methods

(Koopmans et al 2005;Vegetti & Koopmans 2008)

Simulations

Strong image distortion

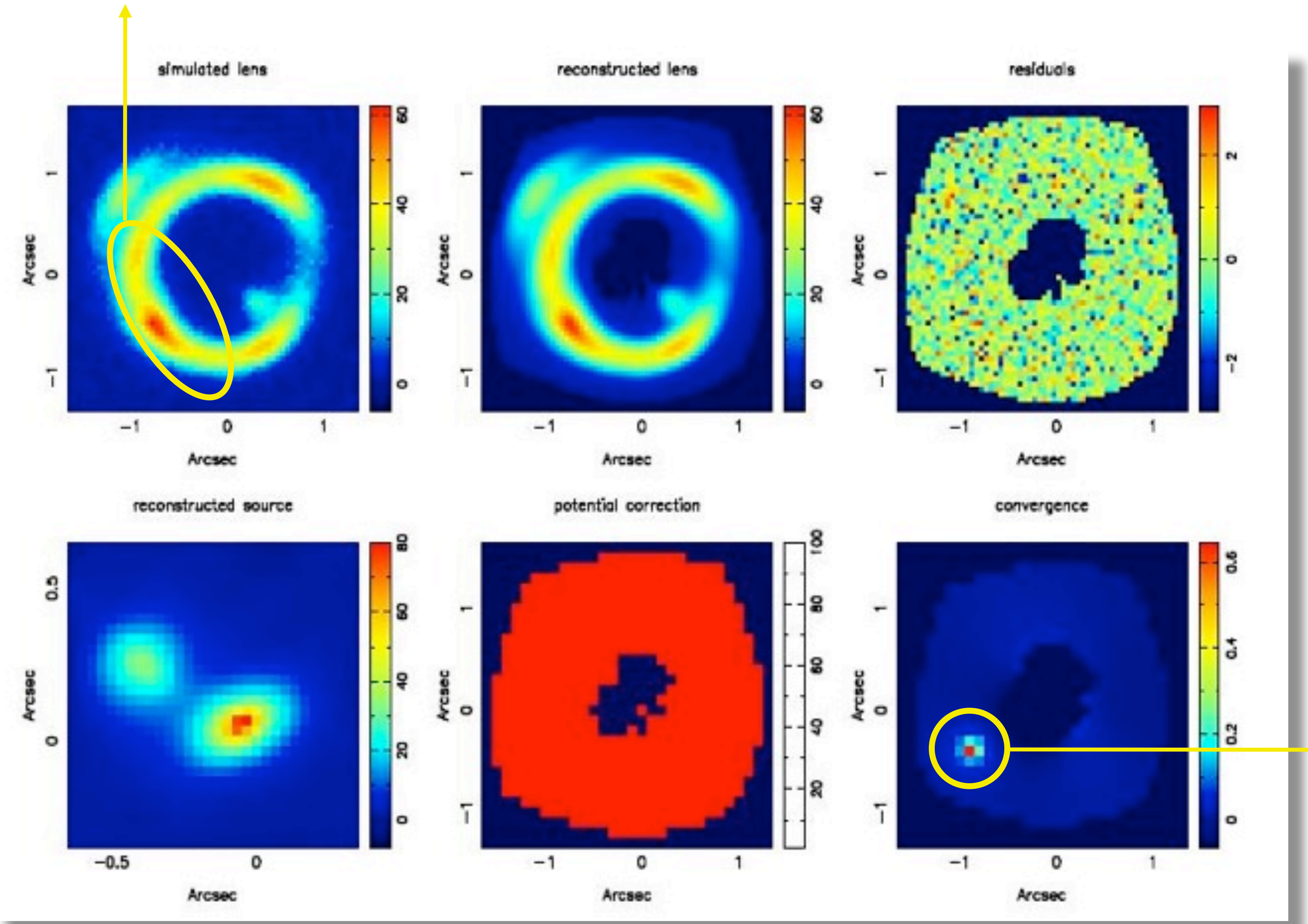

Simulation of lens system: SIE + SIS

SIE: 10^{11} solar mass

SIS substructure of 10^8 solar mass

Koopmans 2005

Simulations

Best Smooth Model Residuals

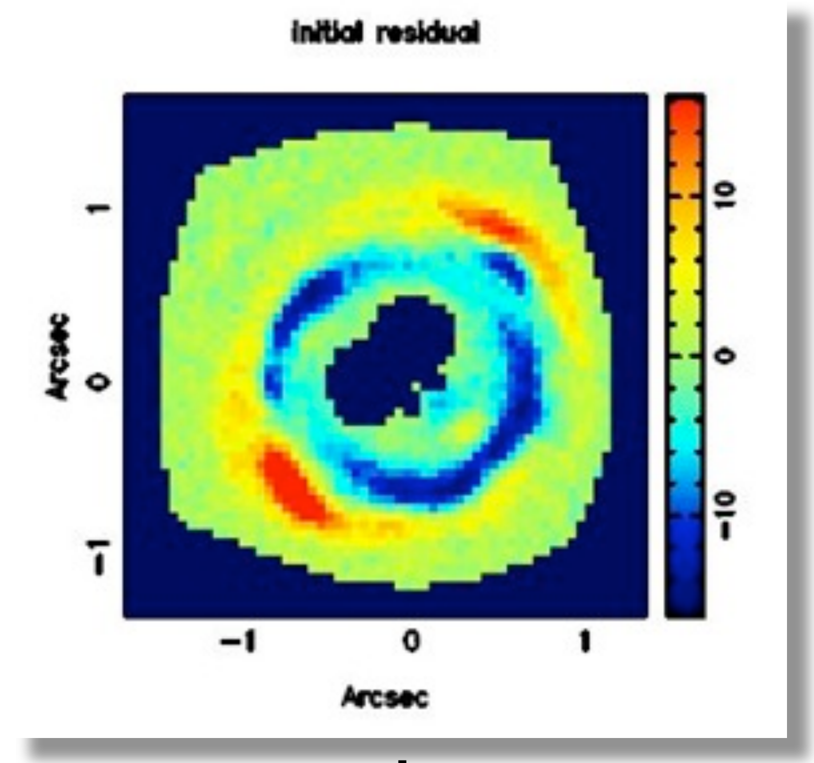

Potential Correction

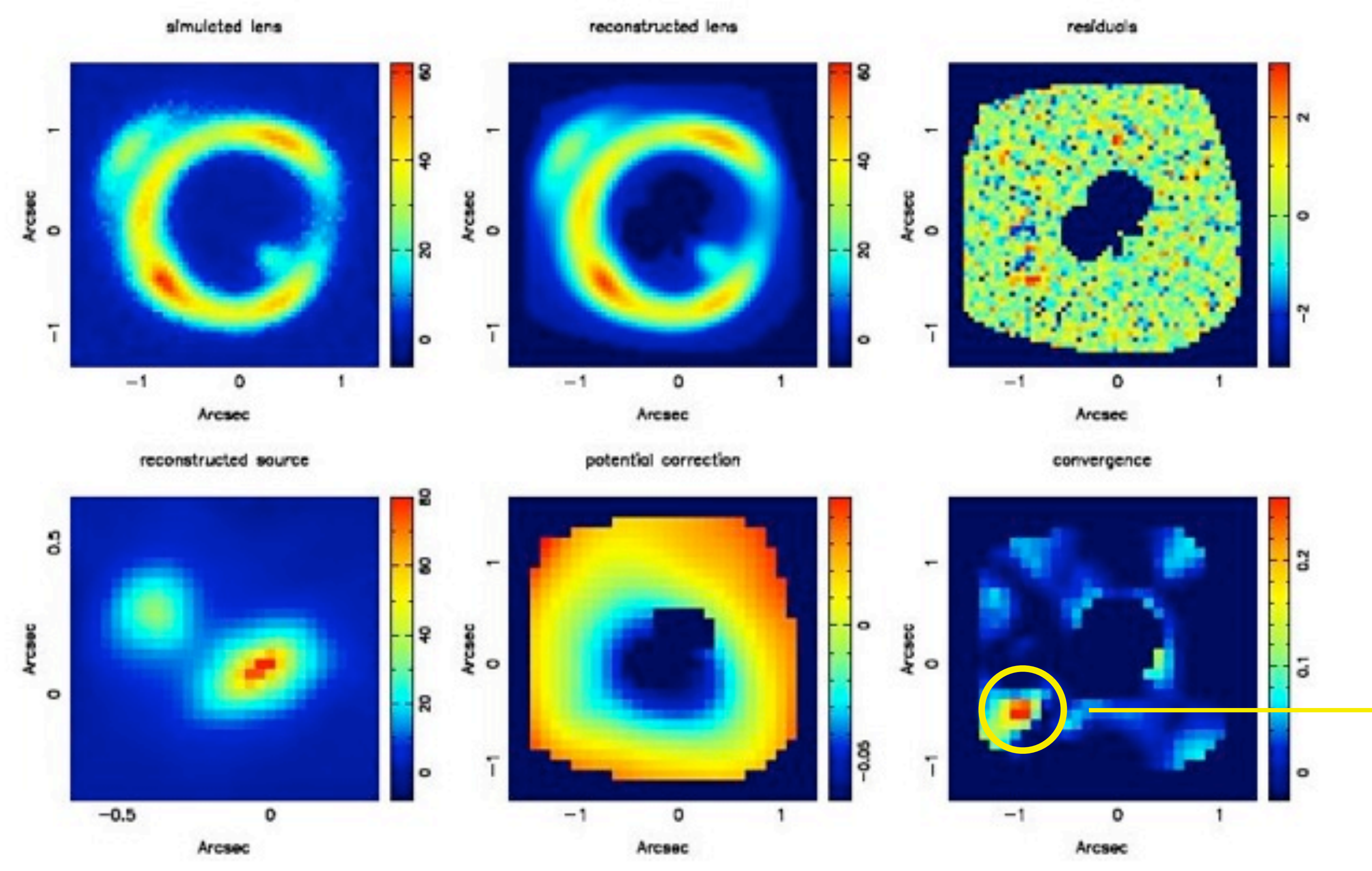

Koopmans 2005

Reconstruction:
SIS substructure
of ~10^8 solar mass

Summary

Flux-ratio anomalies:

- Caused by perturbations to the magnification of a point-like image where information on A is lost (only 1/det(A) is known).
- BUT, how do we know this is not caused by a difference in the smooth model?
- Near folds/cusps, catastrophe theory predicts that the sum of magnifications (including parity) adds to zero, INDEPENDENT of the global smooth model.
- The latter thus says that the potential must be locally perturbed.
- Since the sum of magnifications does not obey this relation in some observed lensed, we call them flux-ratio (better magnification-sum) anomalies.

Surface-brightness anomalies:

- Caused by perturbations to the surface brightness of an extended image, where information (apart from rotation) is retained. In principle $\delta\psi$ can be recovered.
- BUT, how do we know this is not caused by a difference in the smooth model?
- There are multiple extended images, i.e. maps of the source, hence a change in the source occurs in all lensed images. The local nature of a perturbation is not seen in the other images, hence we know it's due to the potential.

Observations/ Examples

Outline

Flux-ratio anomalies -

- Evidence for CDM substructure
- Be careful when assuming an anomaly is due to mass even in the radio/MIR
- Propagation effects?

Luminous Substructures

- Also substructure, but observable
- High-mass end of the mass-function

Dark Substructures

- Surface-brightness anomalies
- Two detections with mass estimates
- L.O.S. contamination

Flux-ratio Anomalies:

Evidence for CDM substructure
or are there also other effects
that can cause them?

“Aquarius” Simulation

Formation of a Galaxy (MW equivalent)

The "Missing Satellite Problem"

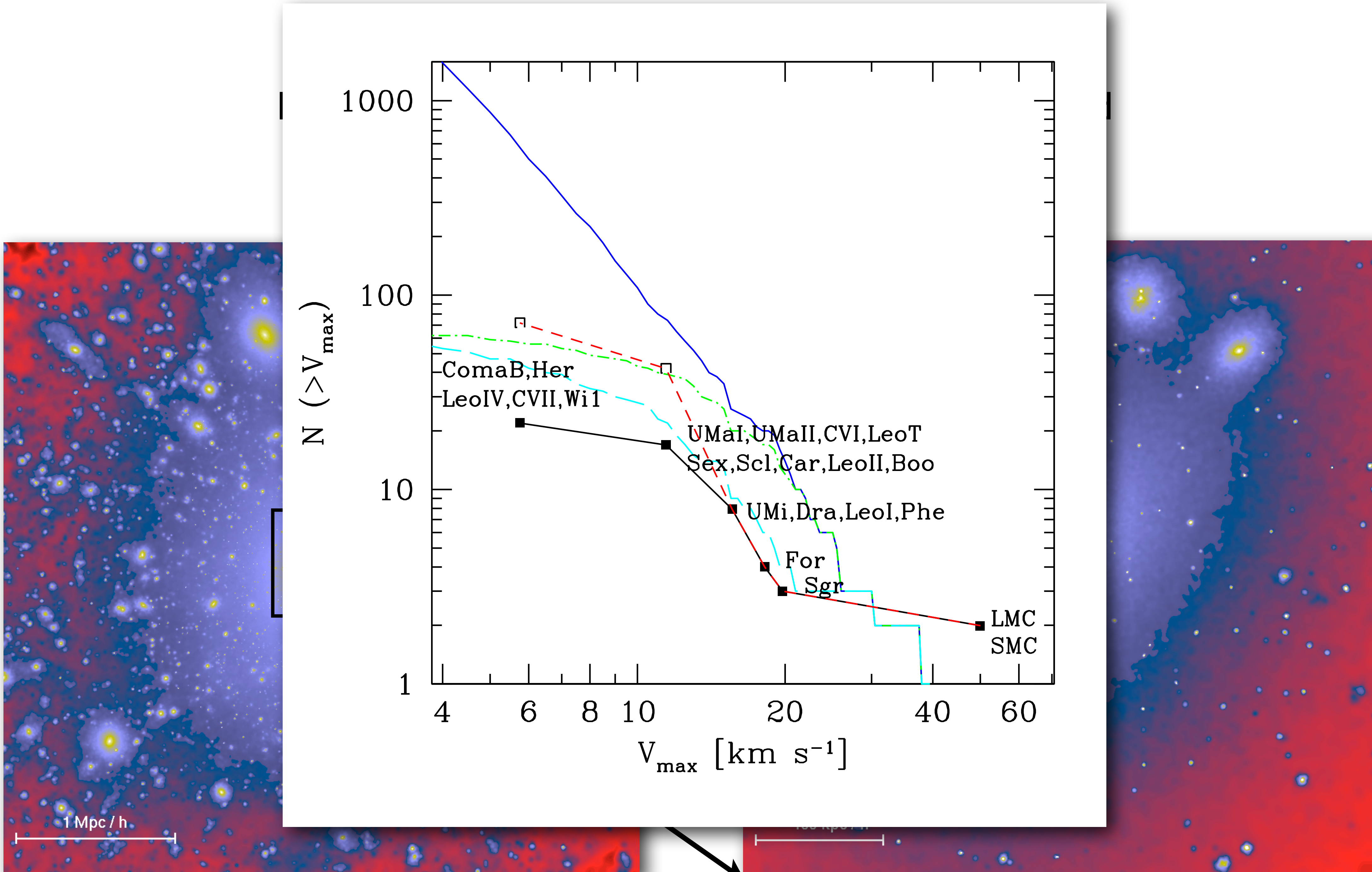

Springel et al. 1999

Substructure Mass Fraction

Substructure mass fraction is large outside, but decreases inward due to dynamical effects

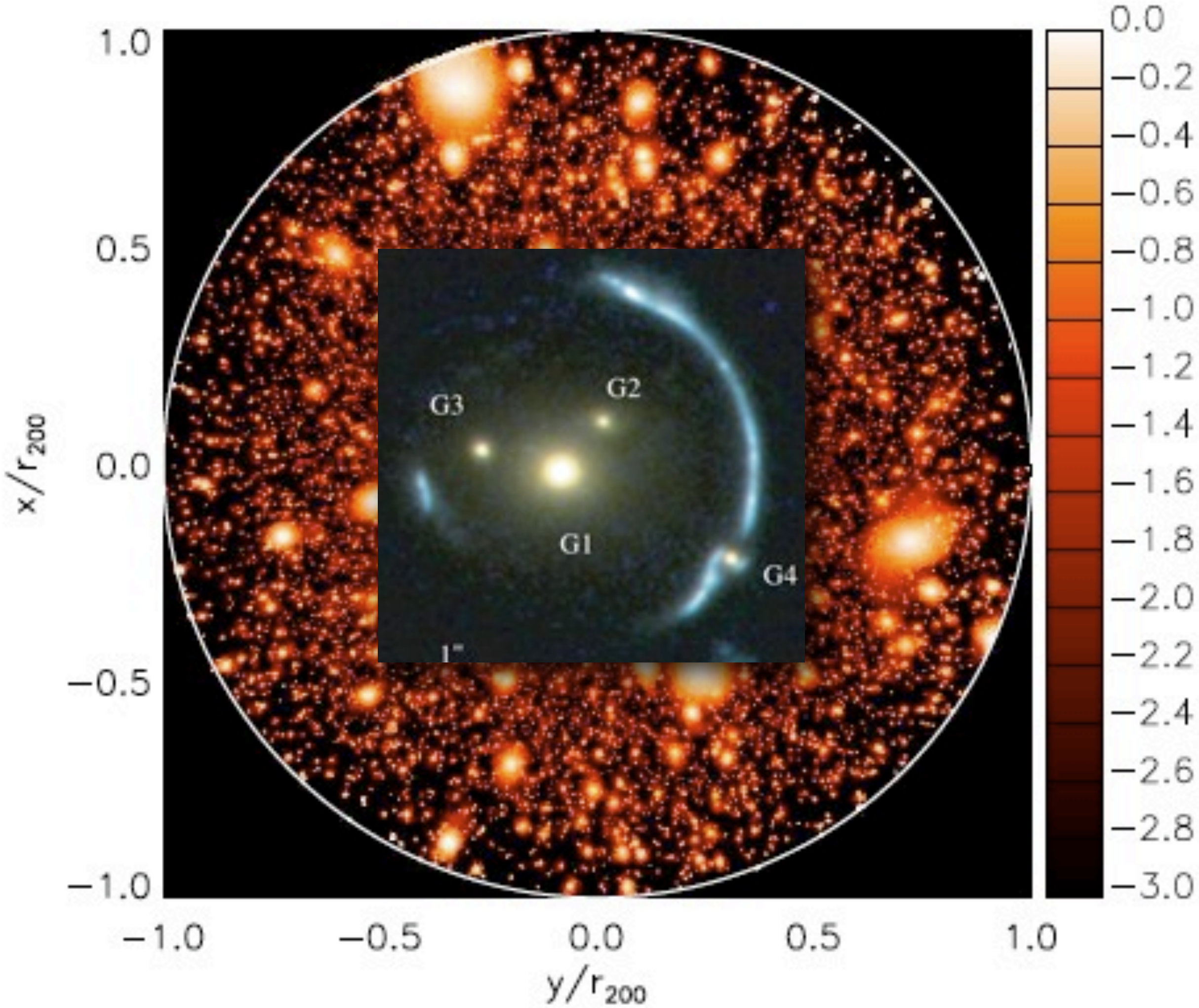

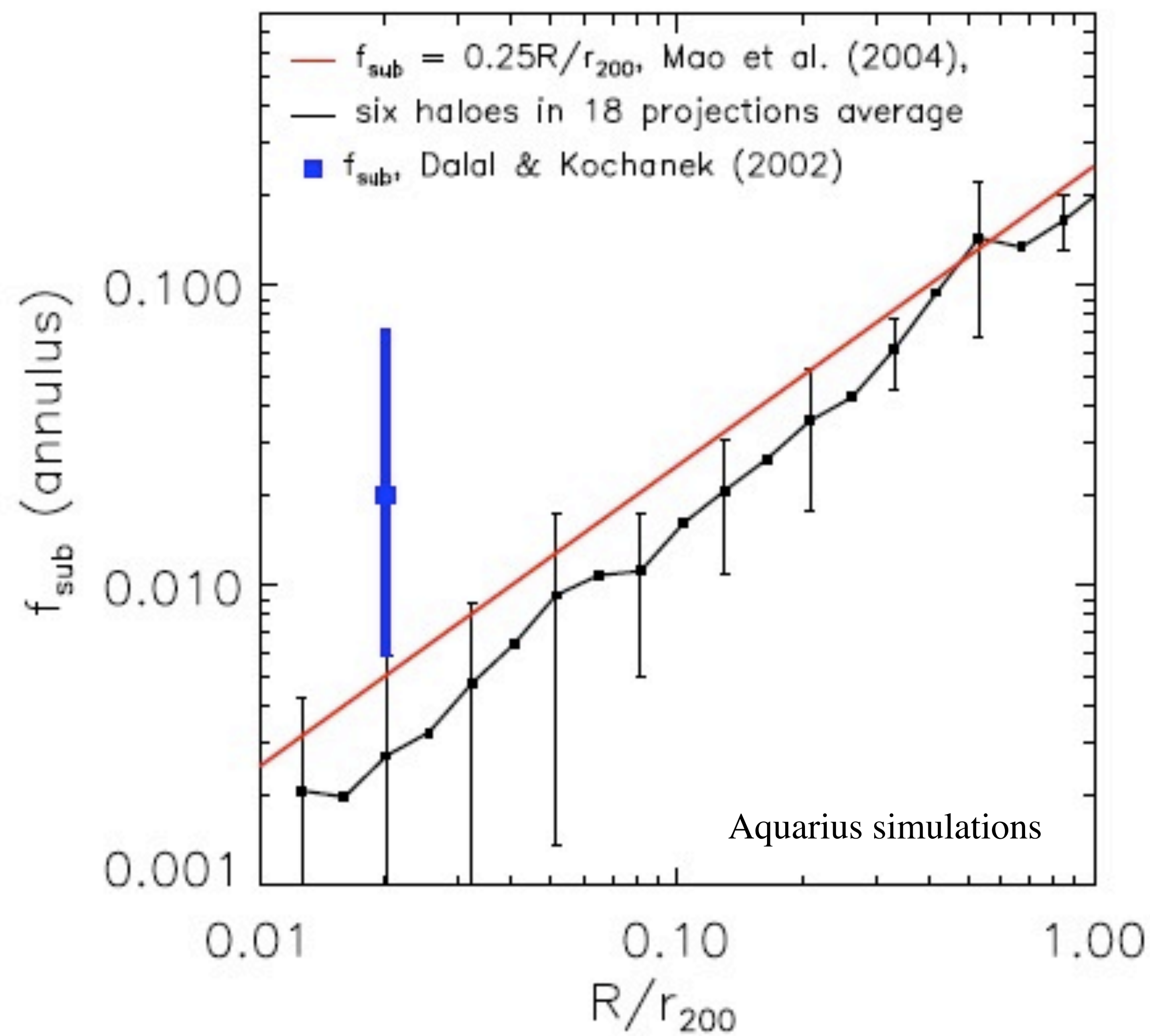

Aquarius Simulation

Xu et al. 2009

Anomalous Fold & Cusp Systems

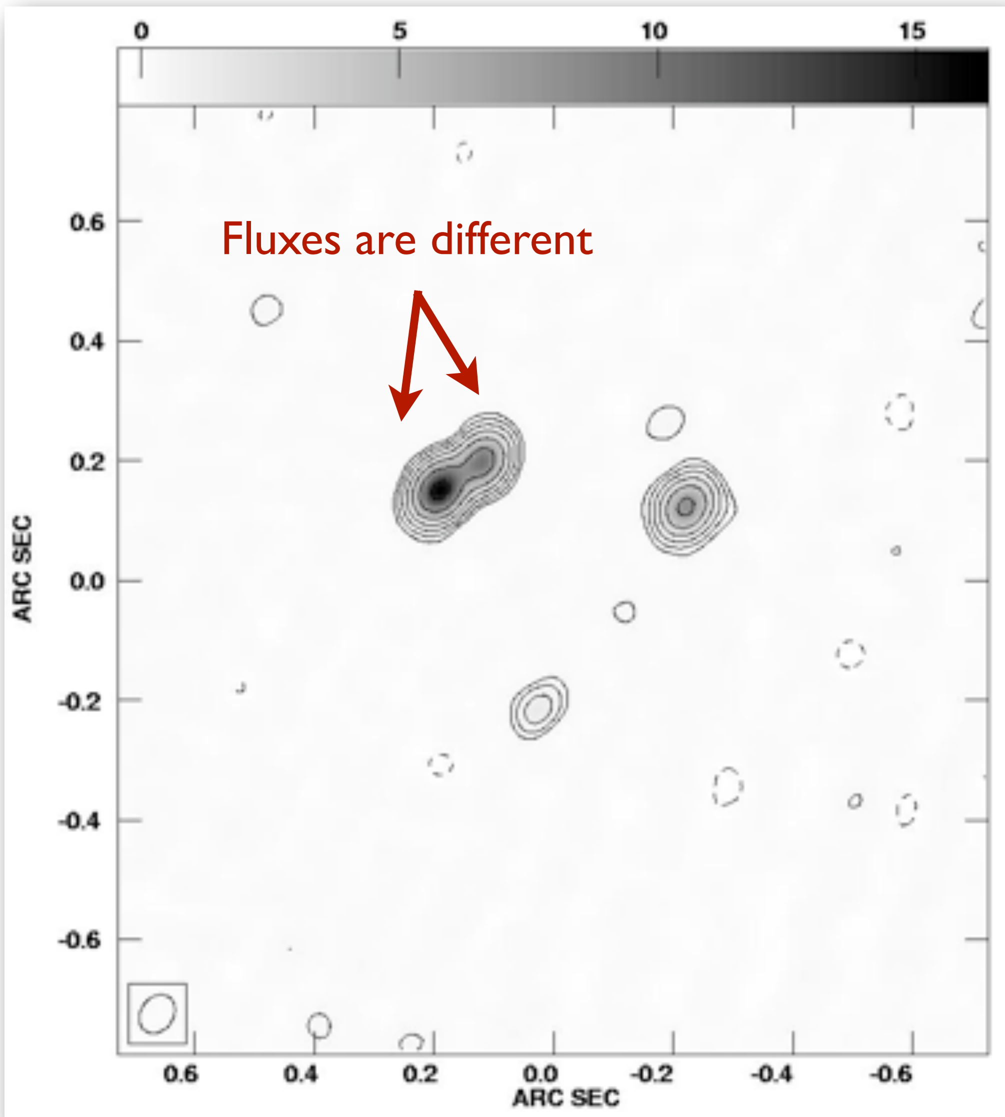

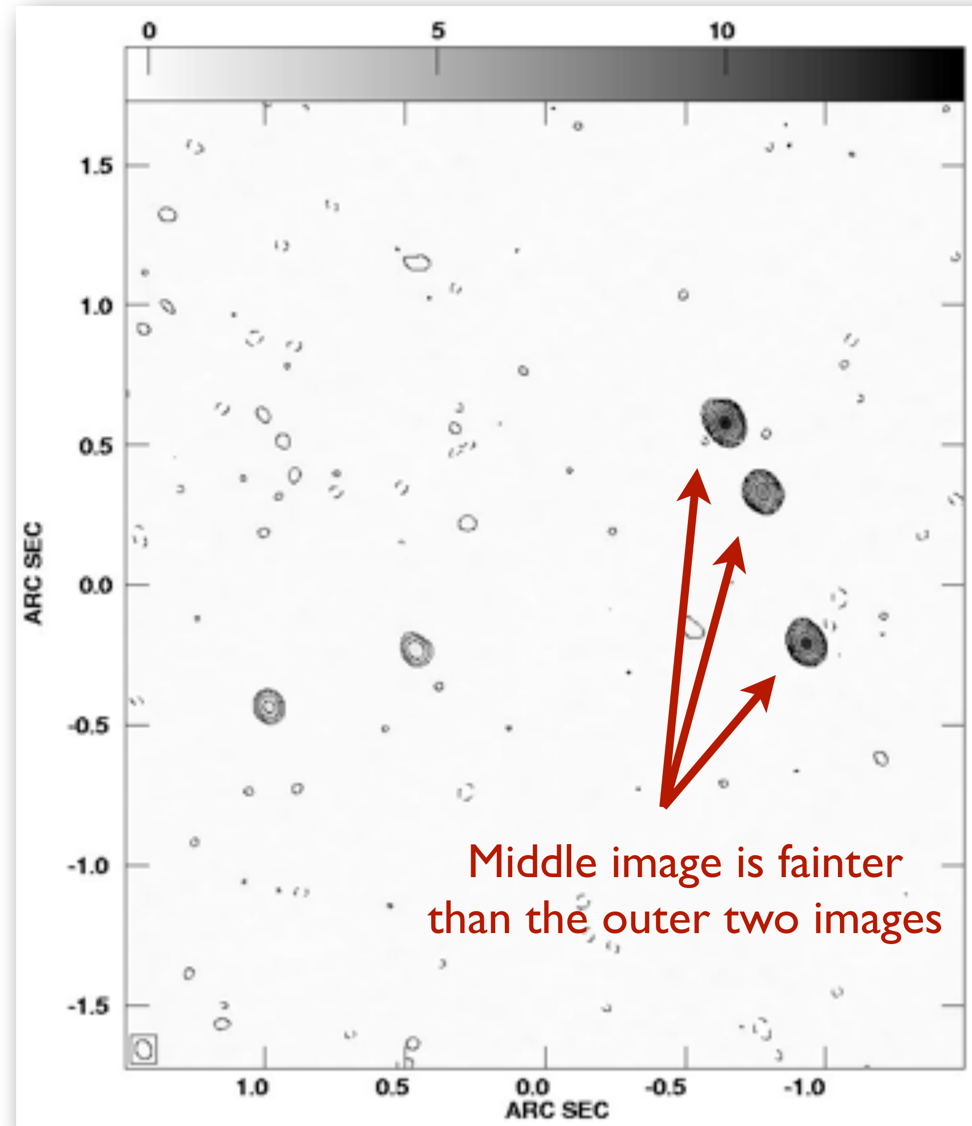

Do anomalous flux-ratios between merging fold/cusp images indicate the presence of mass substructure? (e.g. Mao & Schneider 1998; Dalal & Kochanek 2002).

Anomalous Fold & Cusp Systems

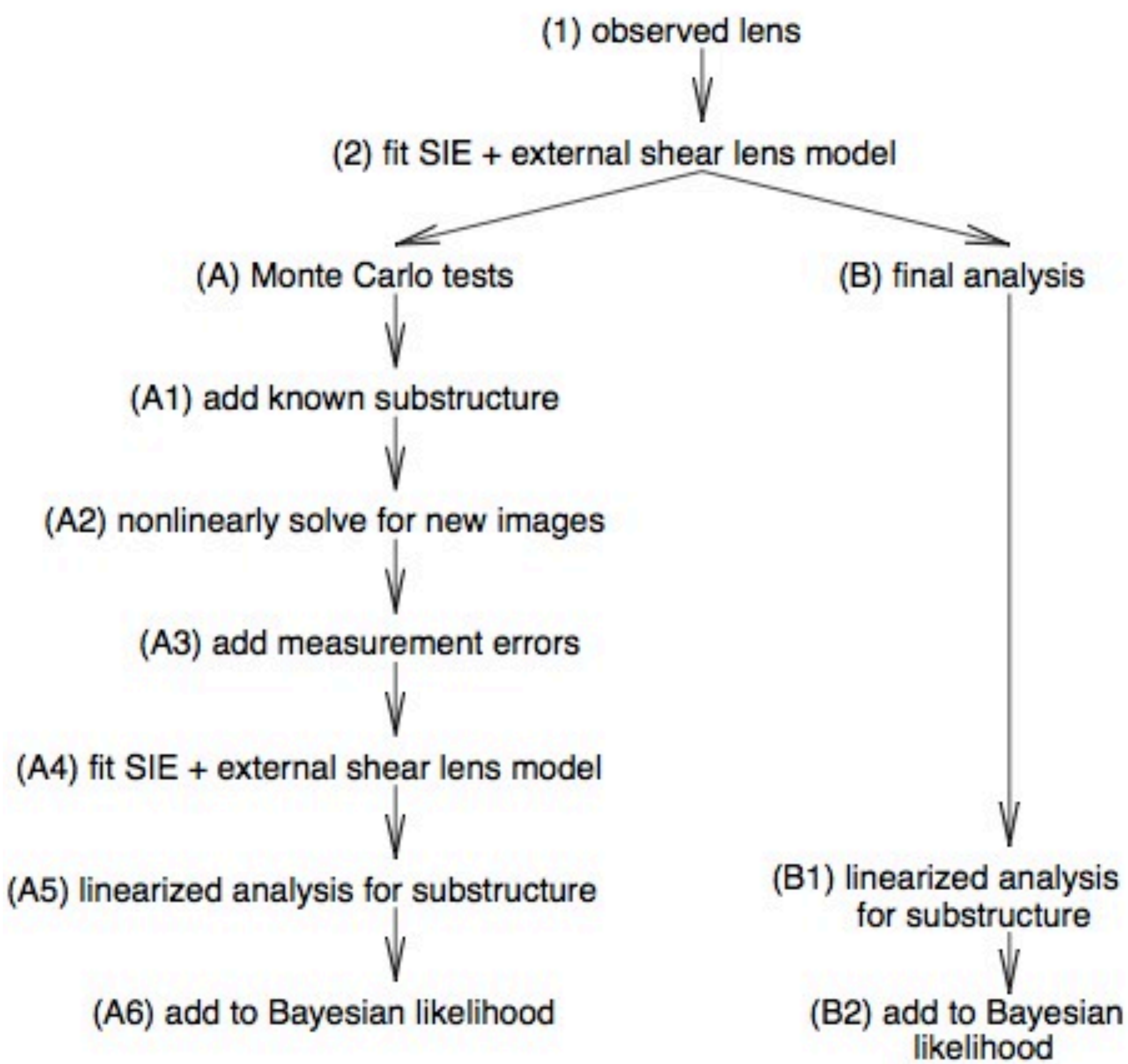

Dalal & Kochanek 2002

B1555+375

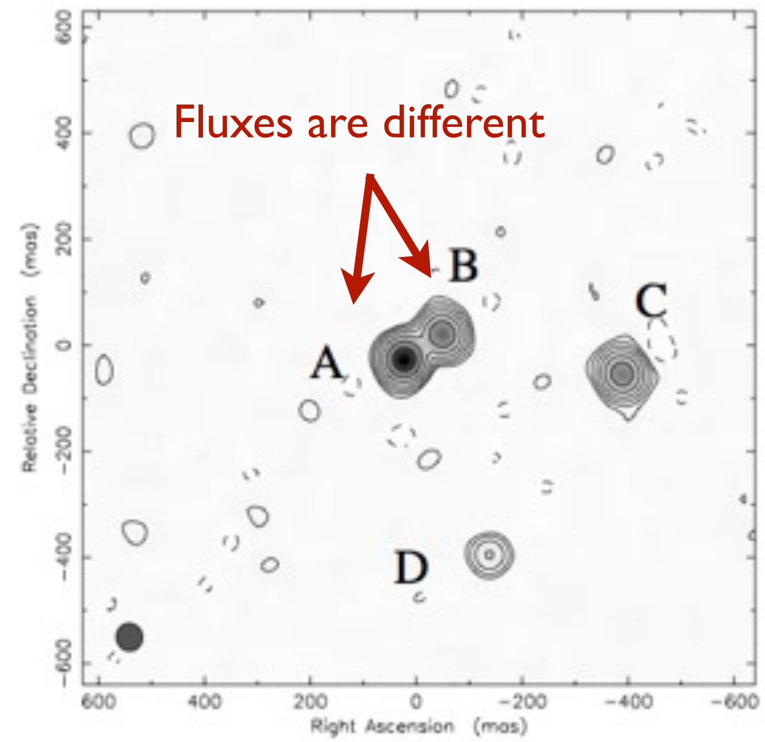

We analyzed the lenses MG 0414+0534 (Hewitt et al. 1992), B0712+472 (Jackson et al. 1998), PG 1115+080 (Weymann et al. 1980), B1422+231 (Patnaik et al. 1992), B1608+656 (Fassnacht et al. 1996), B1933+503 (Sykes et al. 1998), and B2045+265 (Fassnacht et al. 1999). Of these seven four-image lenses, six show anomalous flux ratios that might be due to the effects of substructure.

Anomalous Fold & Cusp Systems

Some issues

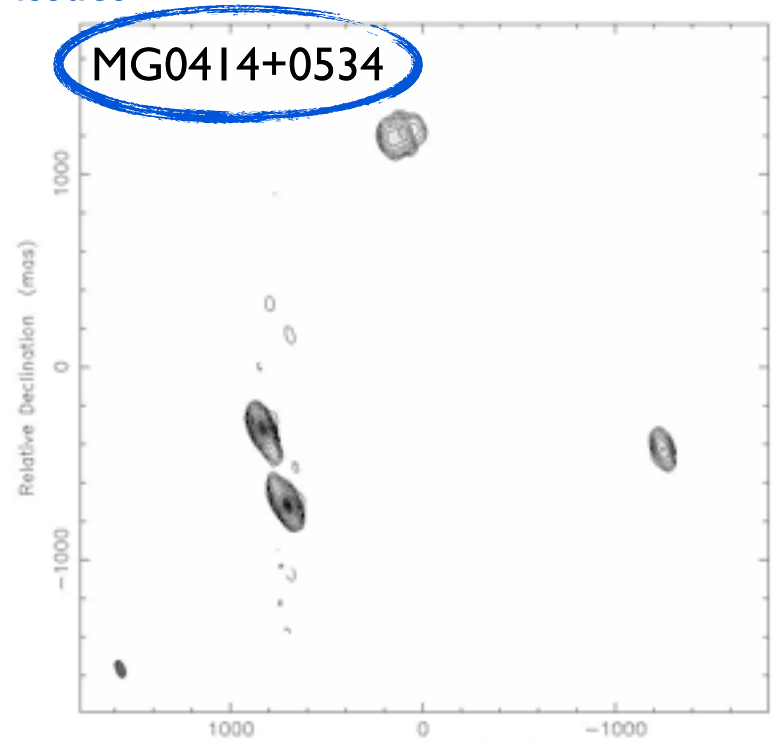

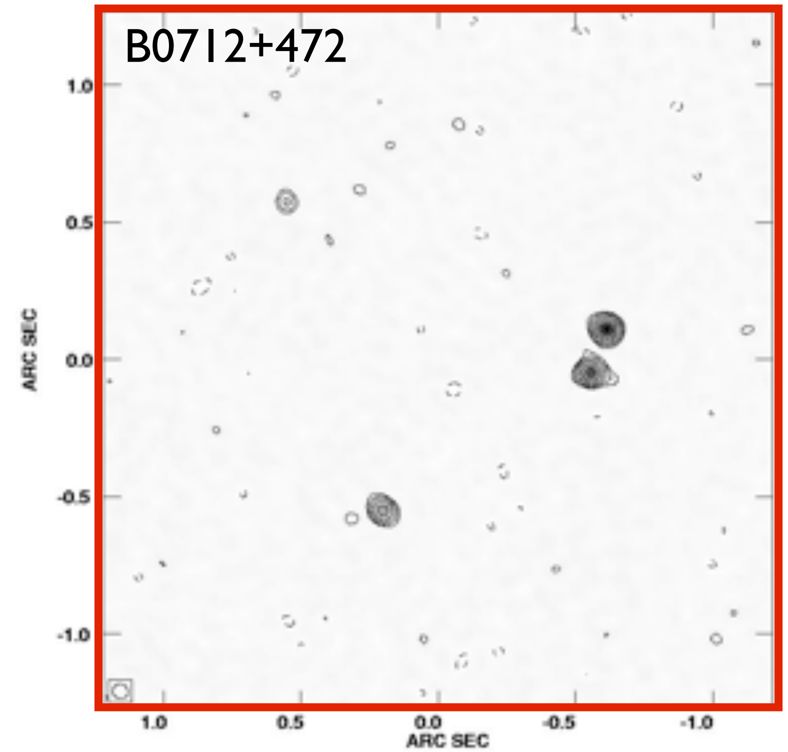

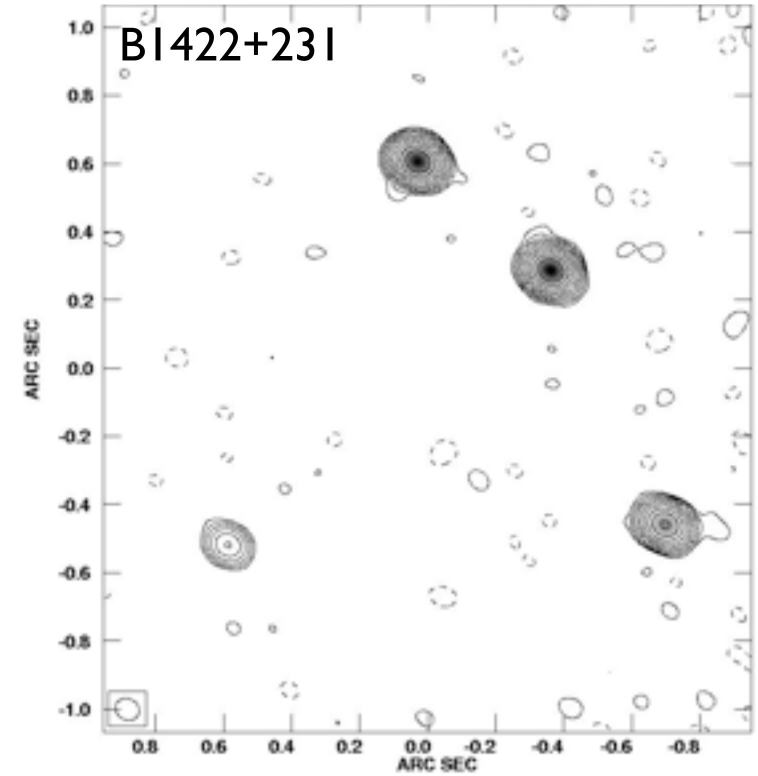

Some issues

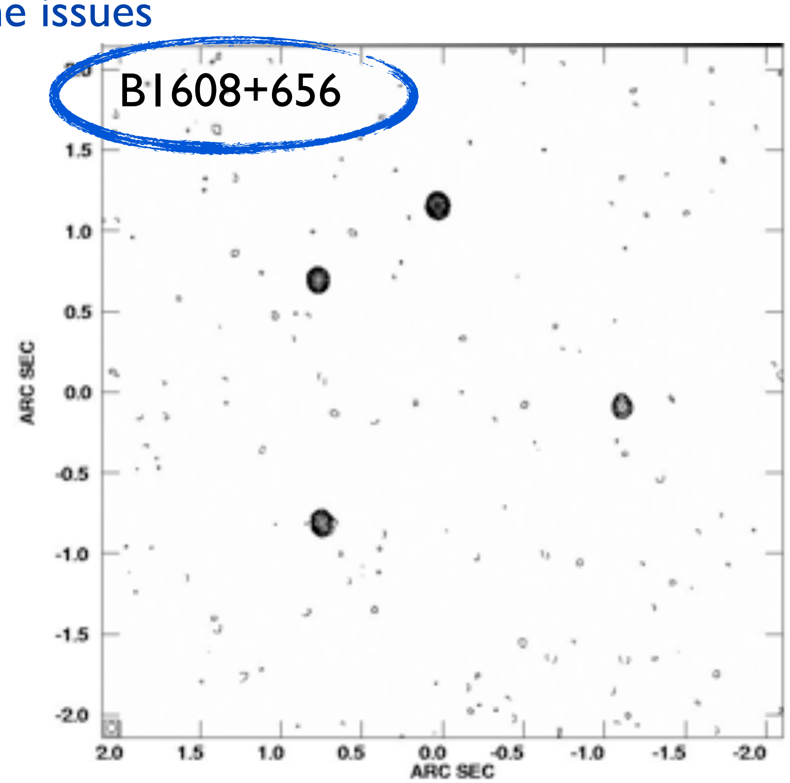

Some issues

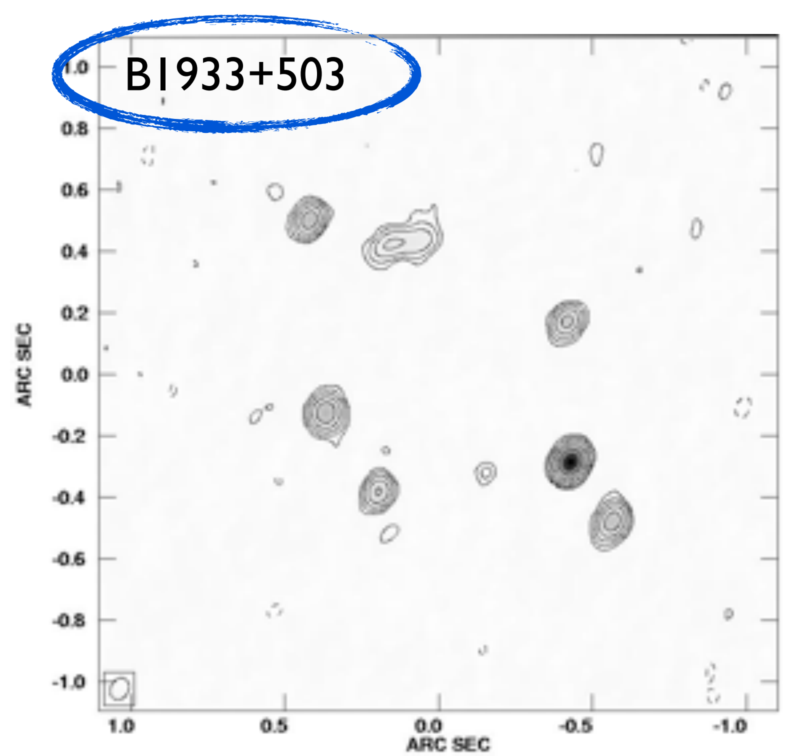

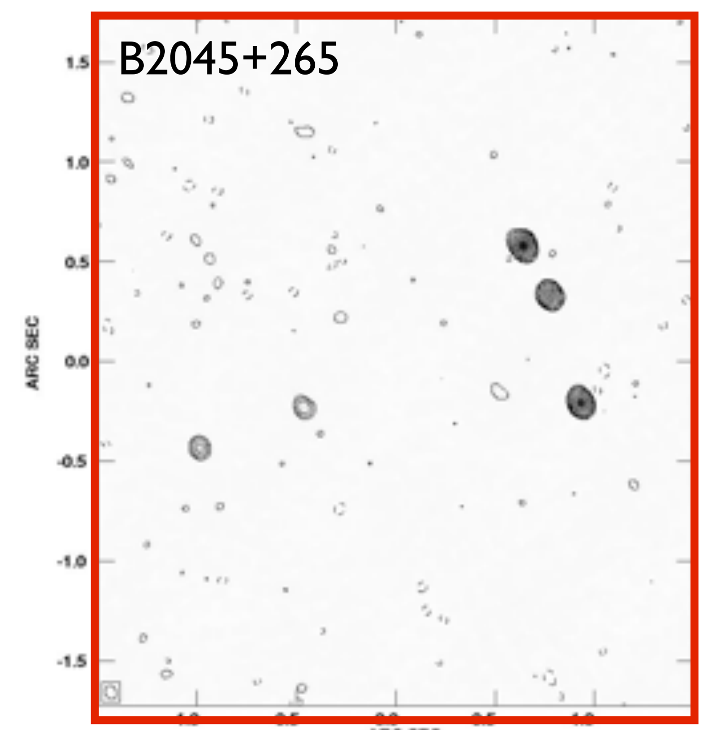

PG1115+080 not shown

Anomalous Fold & Cusp Systems

Anomalous in terms of the cusp-relation

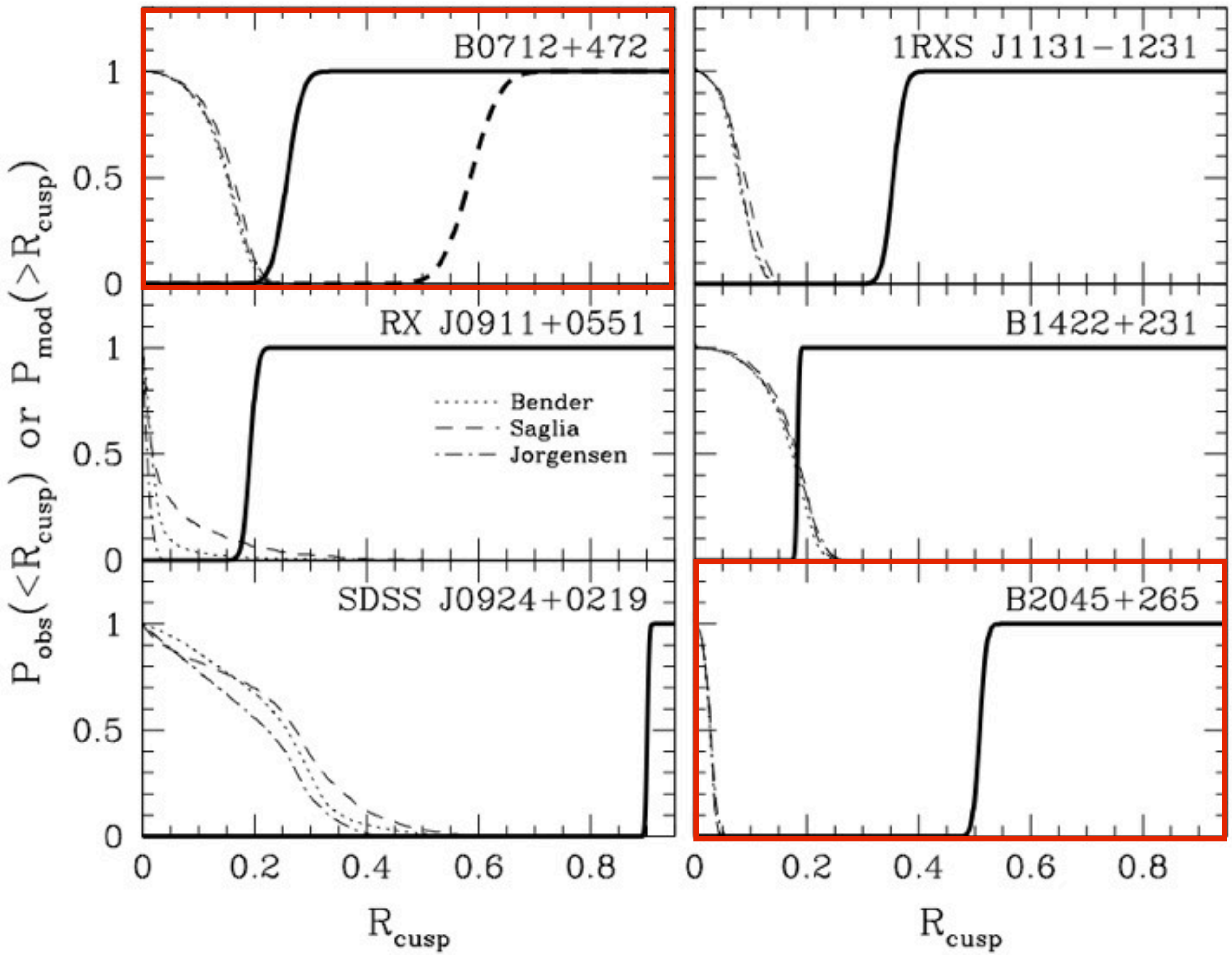

Keeton et al. 2003

Anomalous Fold & Cusp Systems

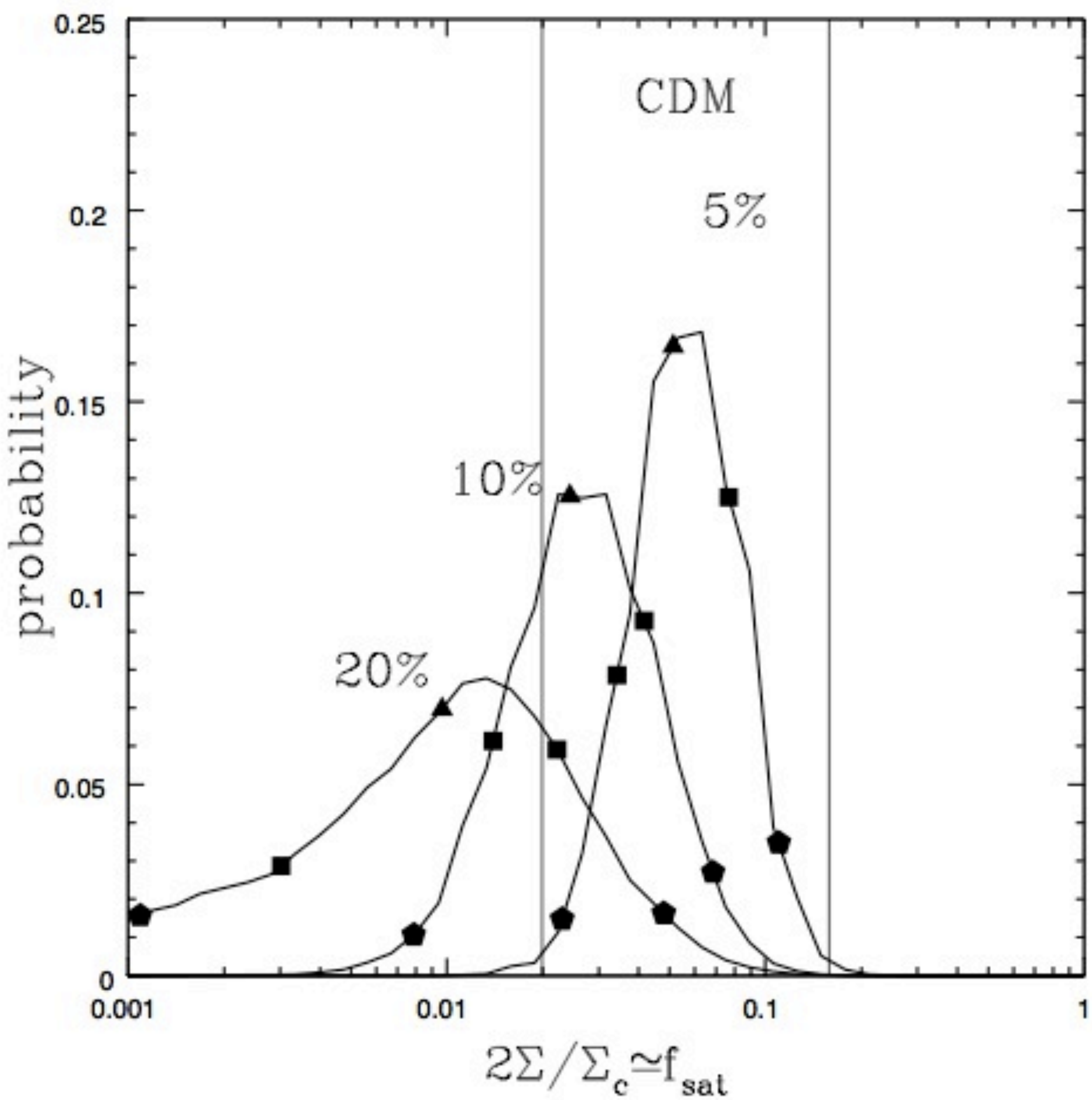

Based on 7 quad lenses from CLASS++ and PG1115+080.

f_{sat} = 0.6-7% (90%CL)

Dalal & Kochanek 2002
Kochanek & Dalal 2004

A gallery of issues with flux-ratio anomalies in the radio, optical, MIR

- Micro-lensing in the radio and MIR
- Extrinsic variability
- Scattering due to the ionized IGM
- Edge-one disks/disk-lenses
- Luminous satellites [also substructure!]

Flux-ratio anomalies in the mid-infrared

Chiba et al. 2008

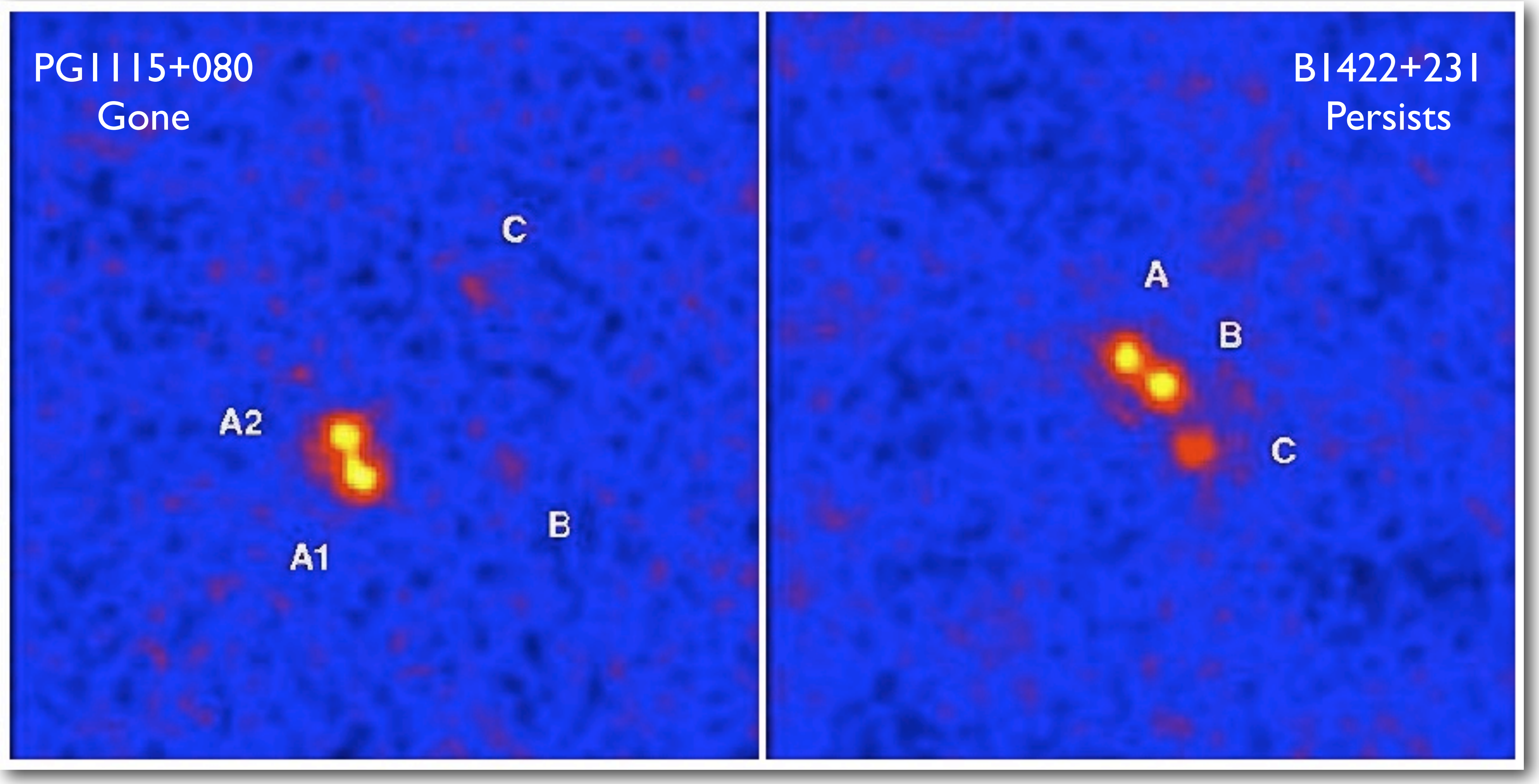

The MIR is dominated by the dust-torus and less affected by dust, scattering or microlensing, but still sensitive to substructure.

Flux-ratio anomalies in the mid-infrared

Microlensing magnification pattern

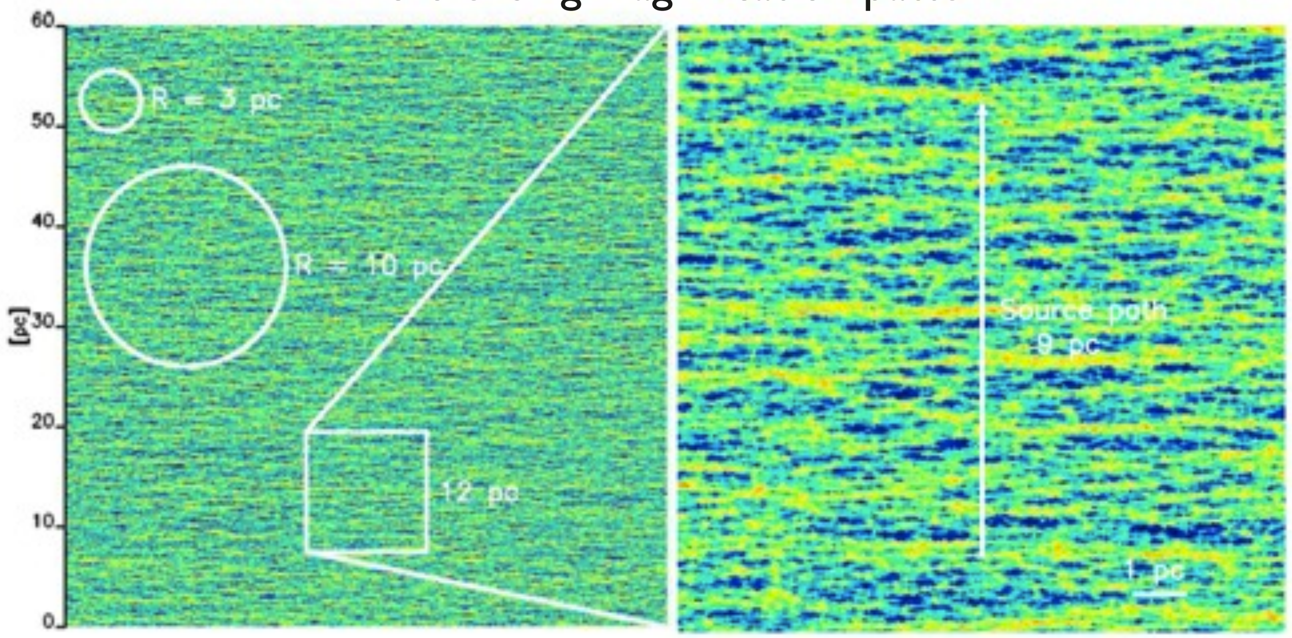

Microlensing can affect some compact quasars.
In the MIR most emission comes from
a few-pc dust-torus, smearing out this effect.

However, still anomalies of ~10% can be expected.

Dust torus

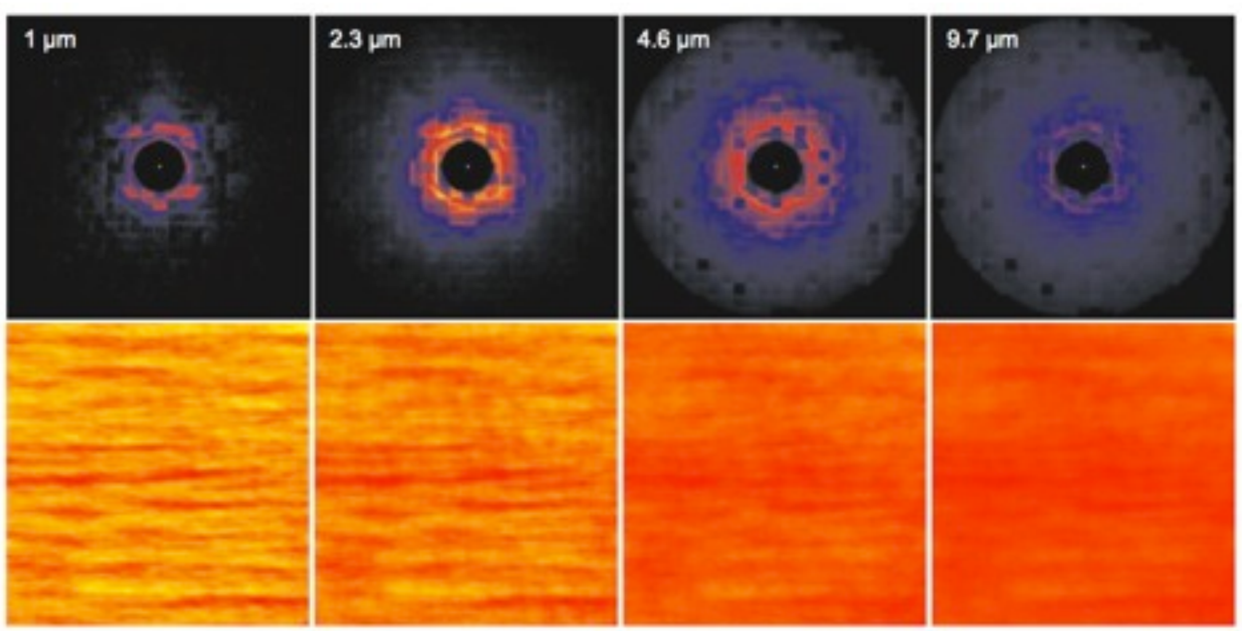

Magnification Pattern

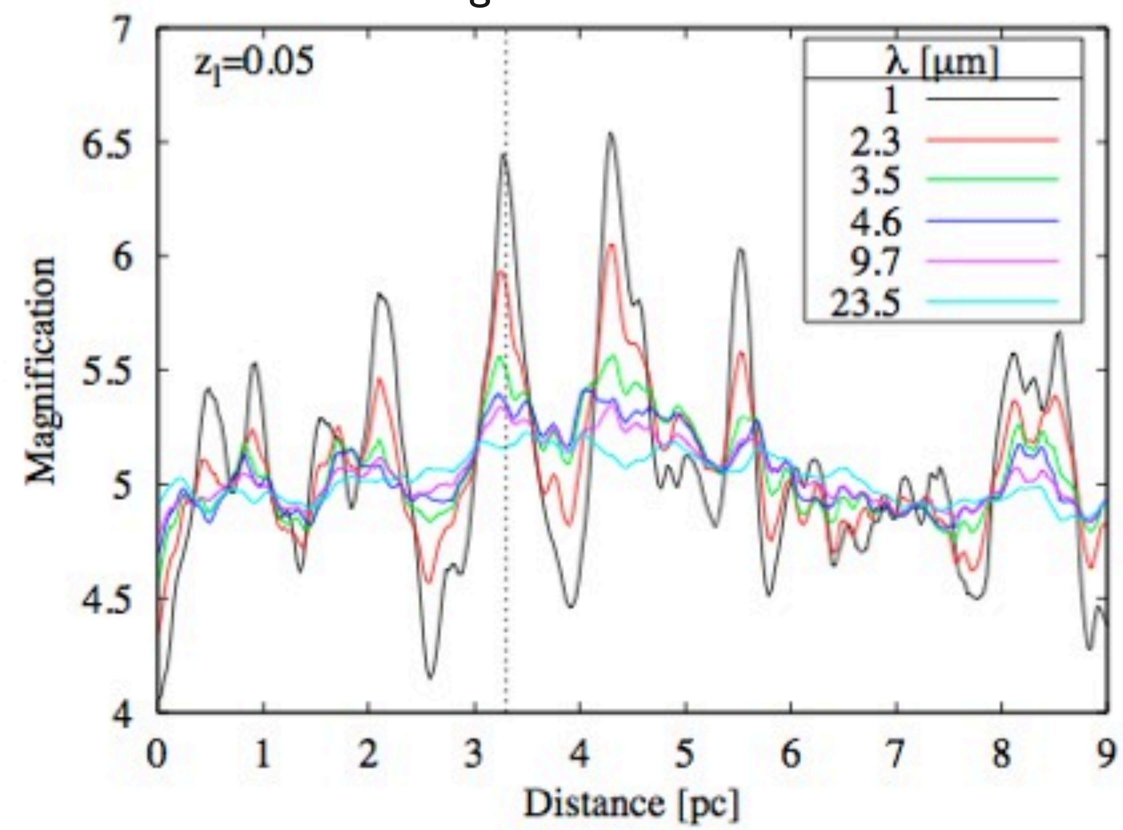

Stalevski et al. 2012

Flux-ratio anomalies and extrinsic variability

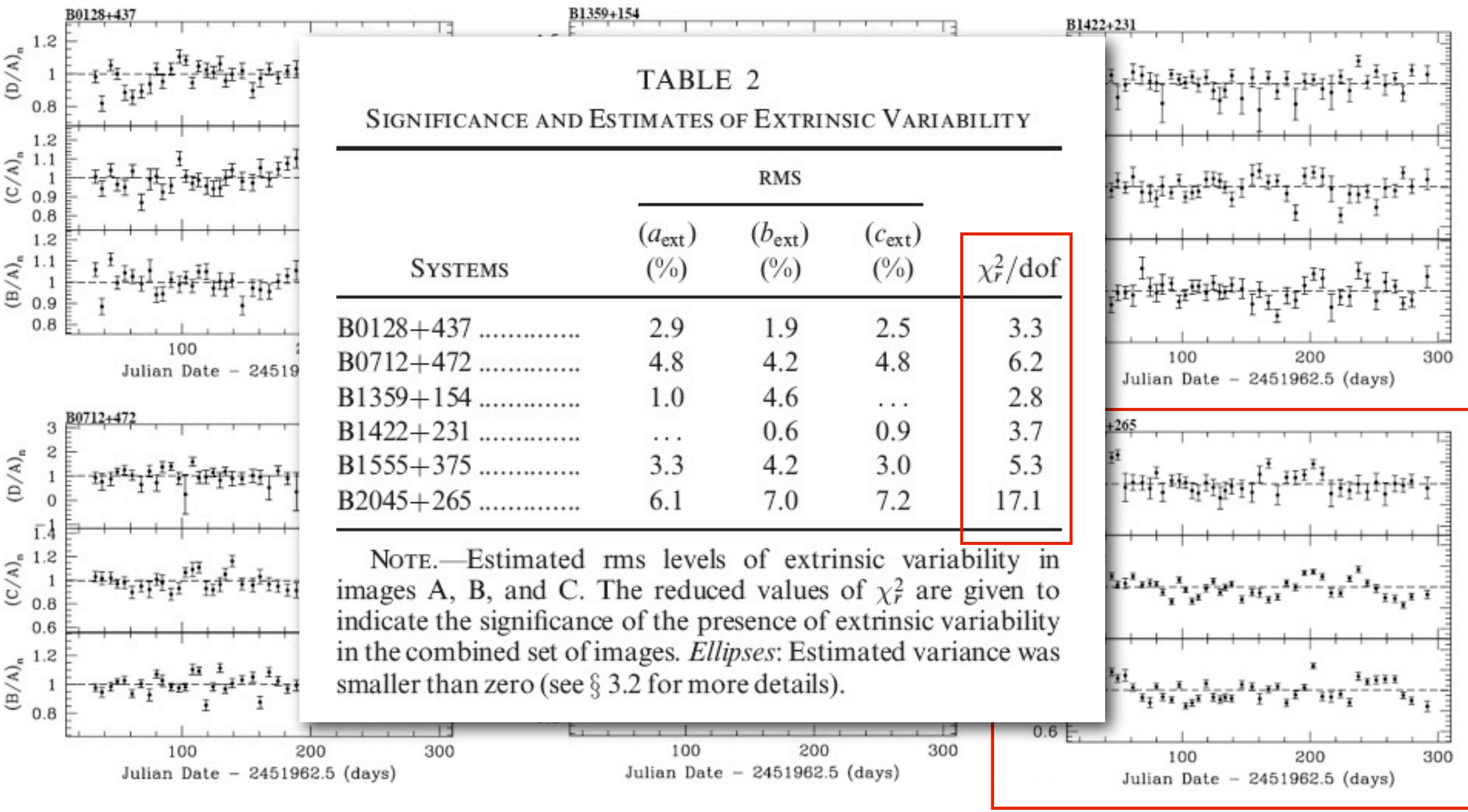

TABLE 2

SIGNIFICANCE AND ESTIMATES OF EXTRINSIC VARIABILITY

Systems	RMS (a_{ext}) (%)	RMS (b_{ext}) (%)	RMS (c_{ext}) (%)	χ_r^2/dof
B0128+437	2.9	1.9	2.5	3.3
B0712+472	4.8	4.2	4.8	6.2
B1359+154	1.0	4.6	. . .	2.8
B1422+231	. . .	0.6	0.9	3.7
B1555+375	3.3	4.2	3.0	5.3
B2045+265	6.1	7.0	7.2	17.1

NOTE.—Estimated rms levels of extrinsic variability in images A, B, and C. The reduced values of χ_r^2 are given to indicate the significance of the presence of extrinsic variability in the combined set of images. *Ellipses*: Estimated variance was smaller than zero (see § 3.2 for more details).

Koopmans et al. 2003

Radio Microlensing in B1600+434?

B1600+434

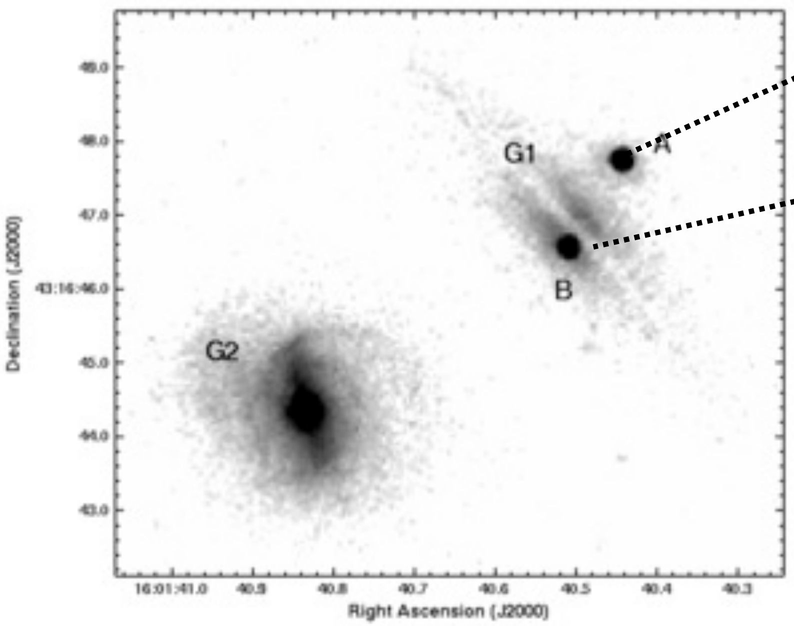

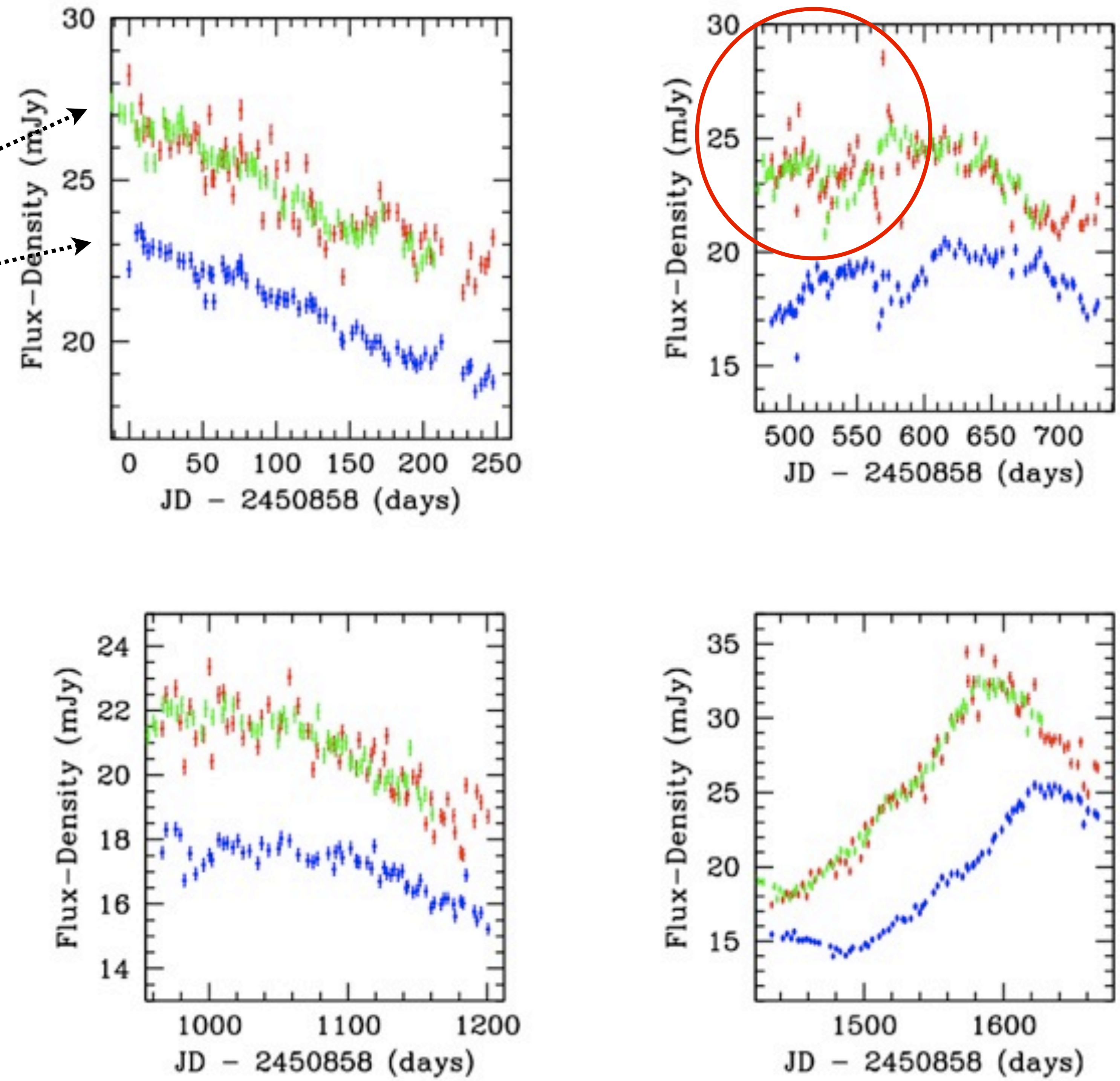

Do we really understand radio source to the level we should? i.e. what about scintillation and microlensing

Berciano-Alba, LVEK, et al. 2011, submitted

Radio Microlensing in B1600+434?

Caustic Pattern (code: Wambsganss)

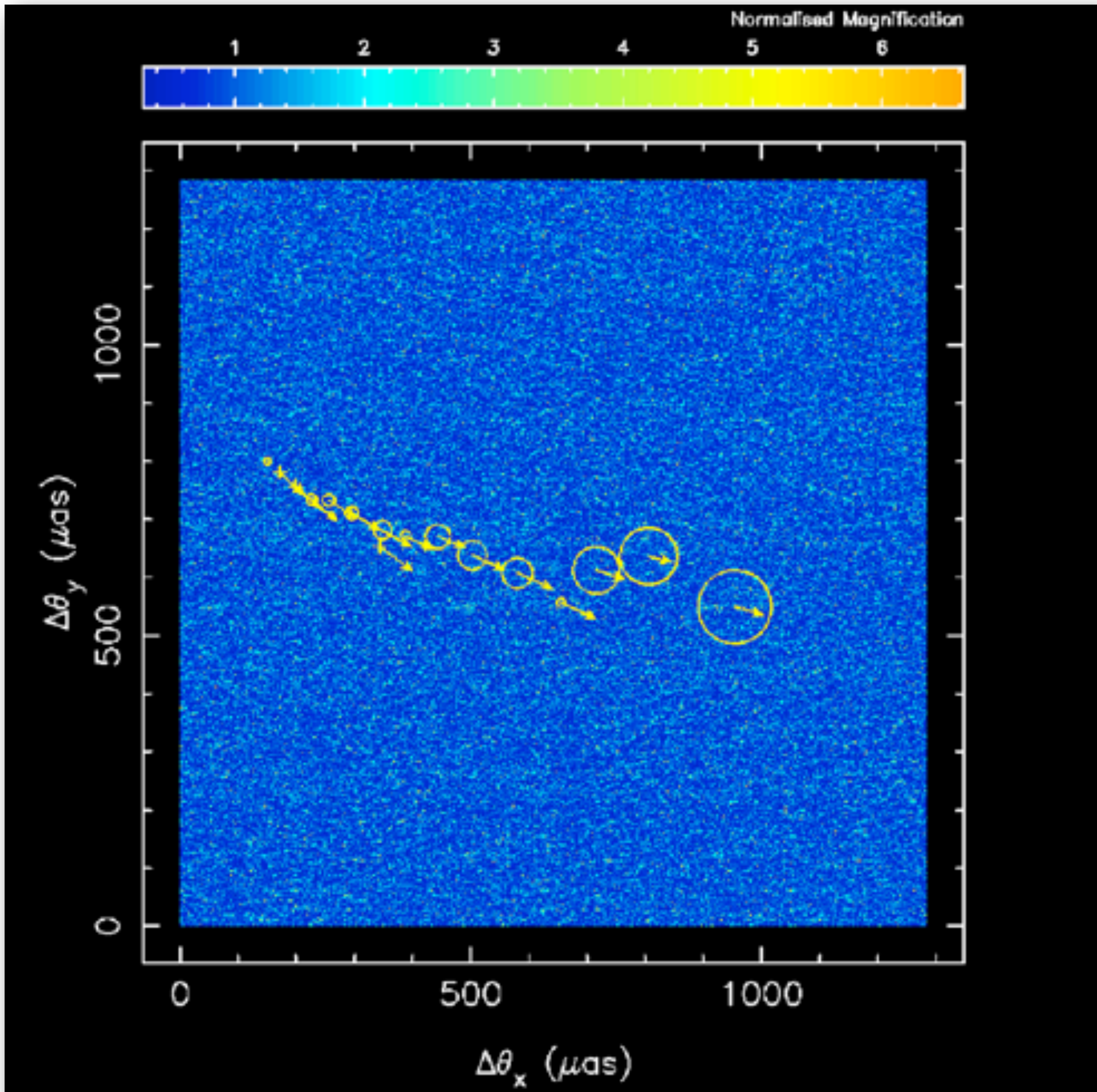

A test carried out in K&dB 2000 was to place one of the best studied nearby relativistic jets on to a caustic network, 3C120, scaled to z=1.59 and see what happens

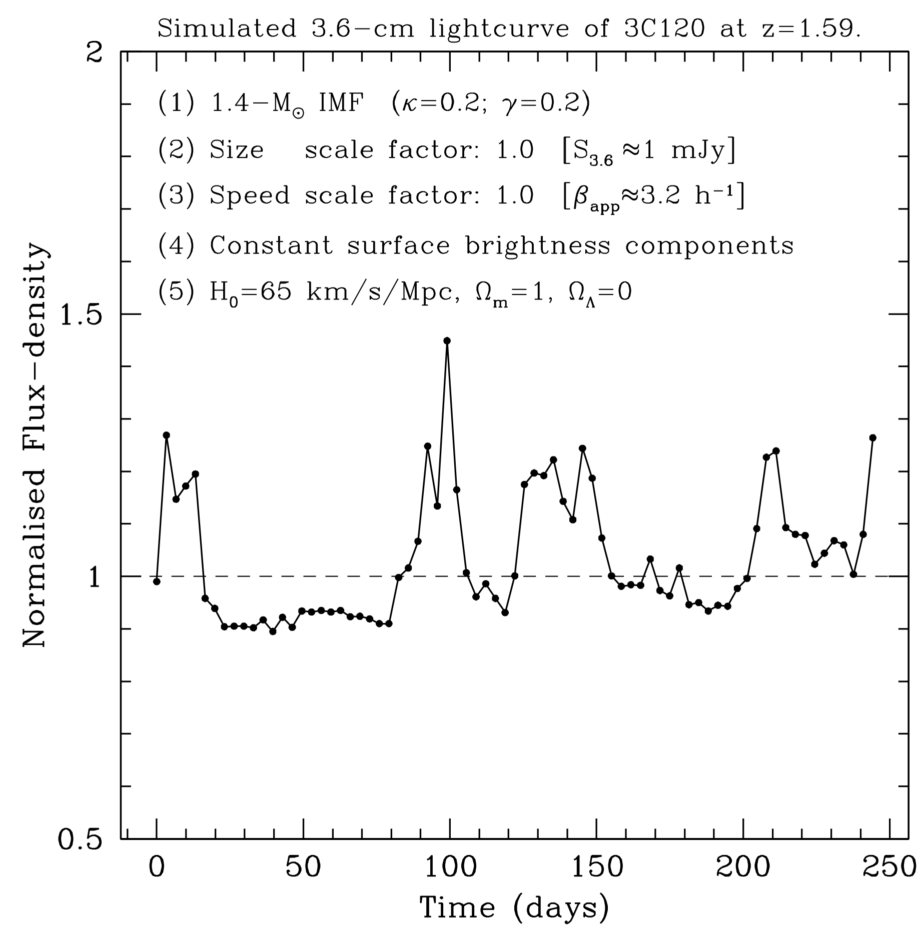

Radio Microlensing in B1600+434?

Simulated Light curves

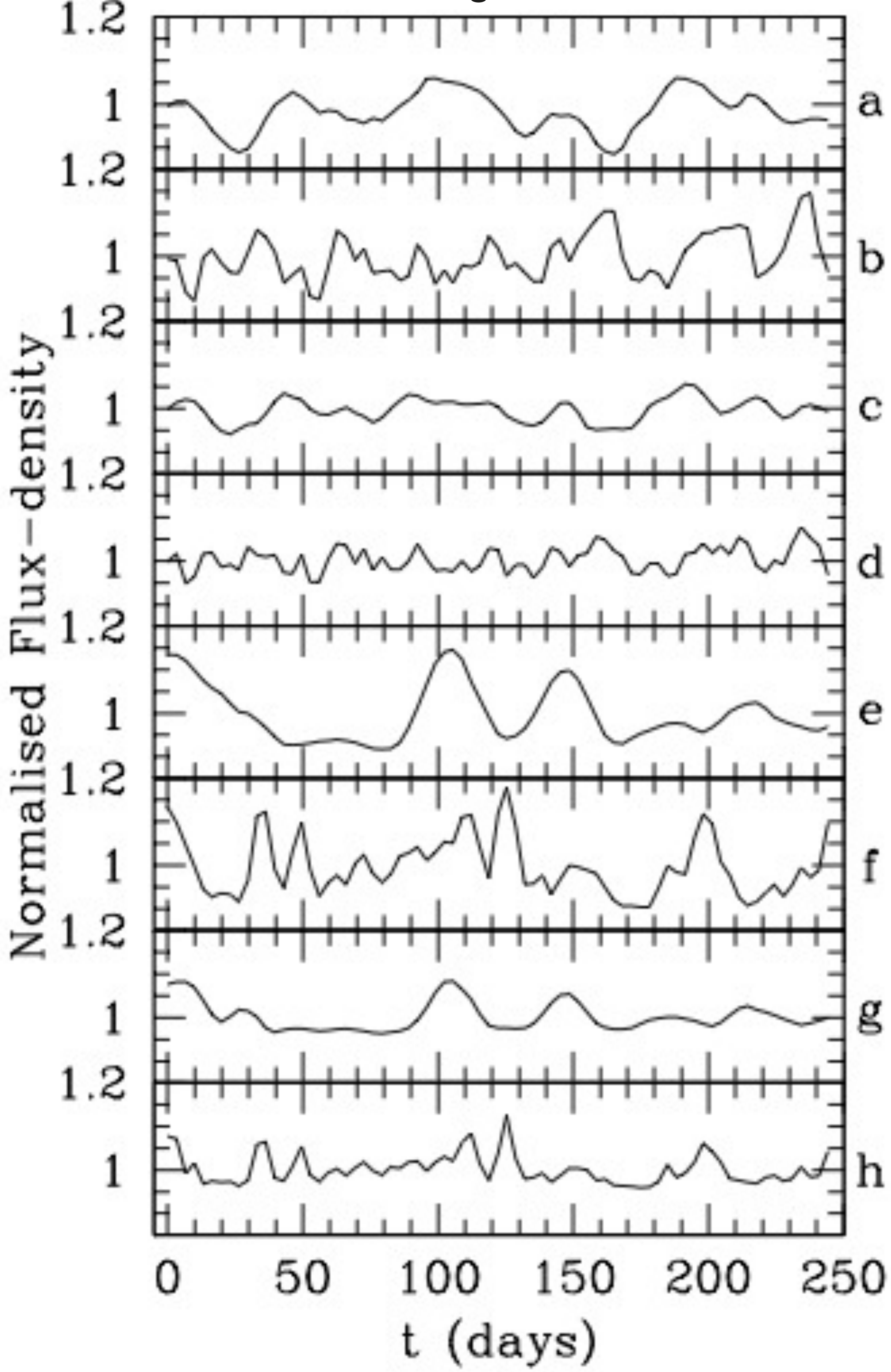

Observed Light curves

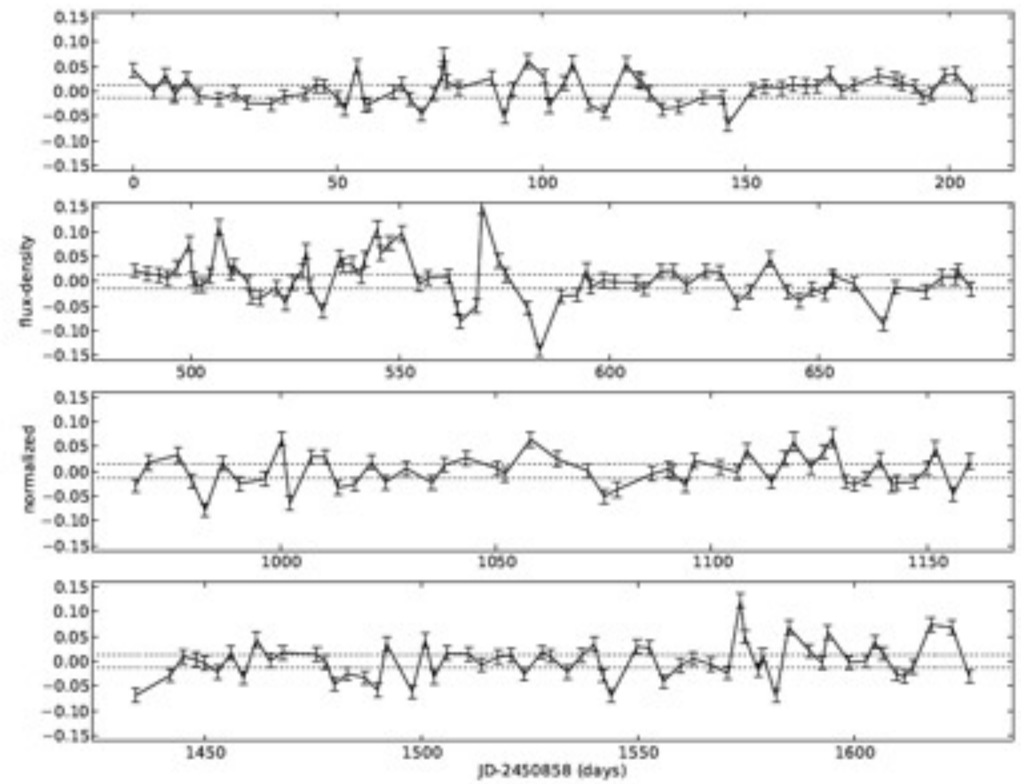

season 1

season 2

season 3

season 4

Level and duration of fluctuations

LC	α_r	α_v	rms (%)	t_{typ} (d)
a	5.7	1	4.5	~50
b	5.7	3	5.4	~15
c	3.7	1	2.6	~35
d	3.7	3	2.9	~10
e	5.7	1	6.4	~50
f	5.7	3	6.7	~20
g	3.7	1	3.3	~40
h	3.7	3	3.4	~15

Flux-ration anomalies and differential scattering

CLASS 0128+437

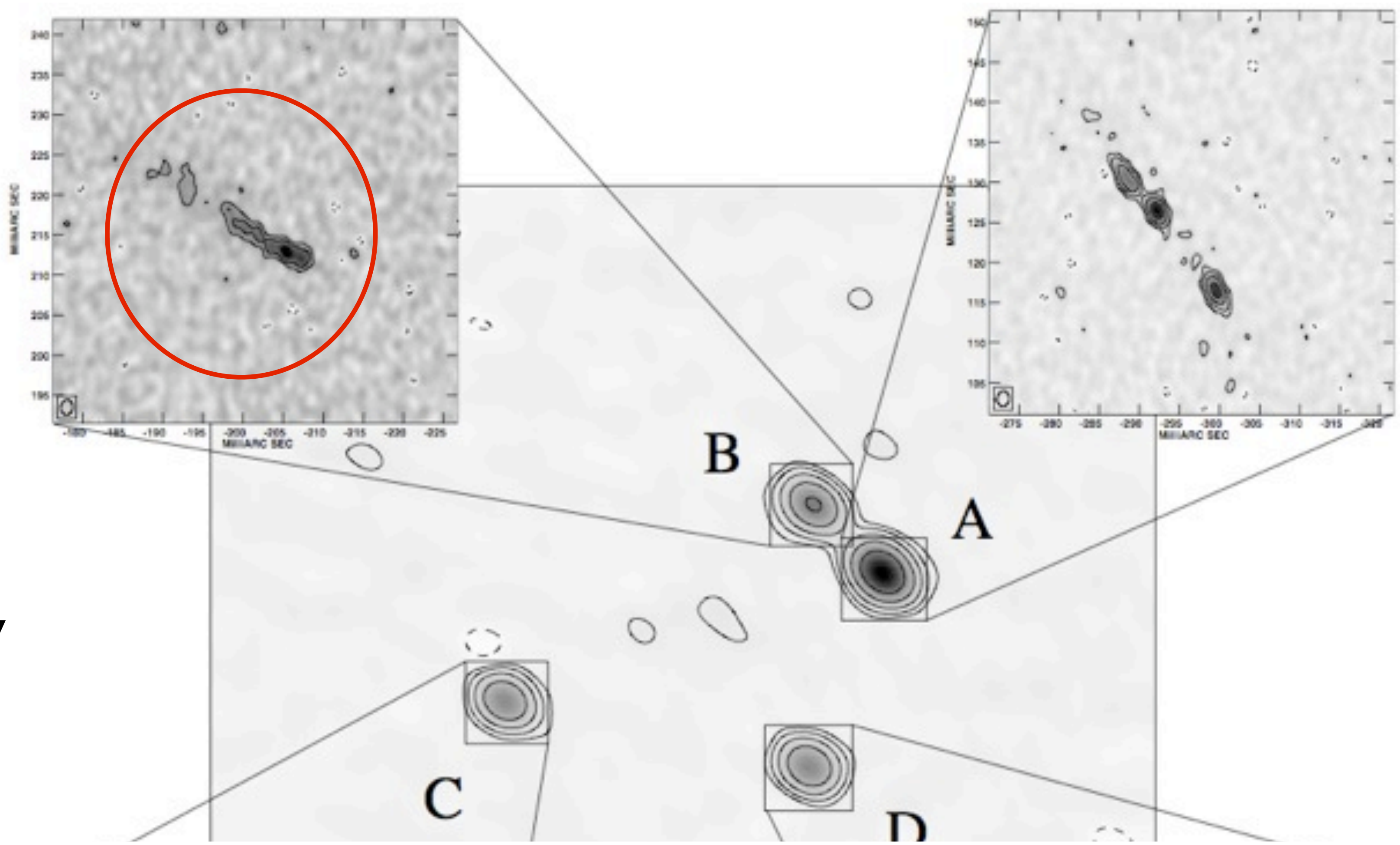

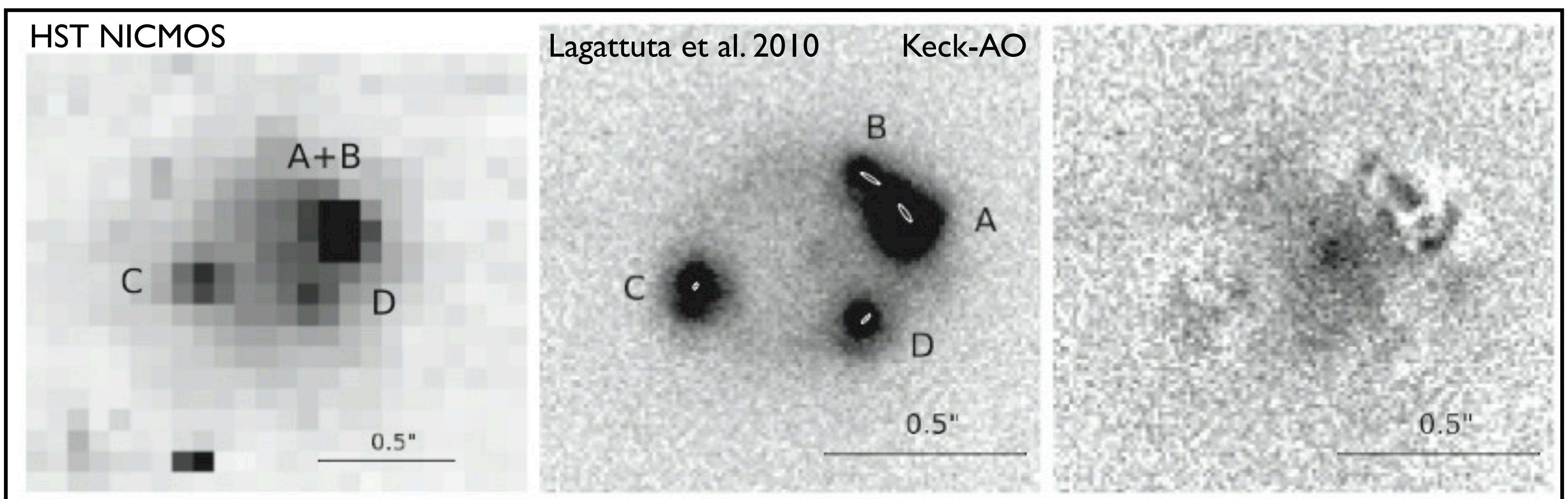

Anomalous Fold & Cusp Systems

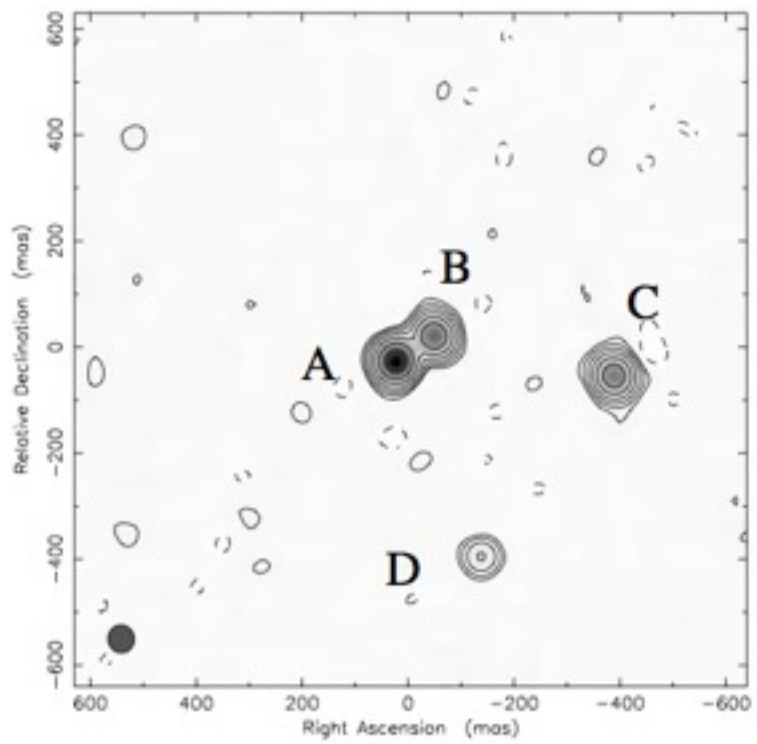

Mass model: 2006

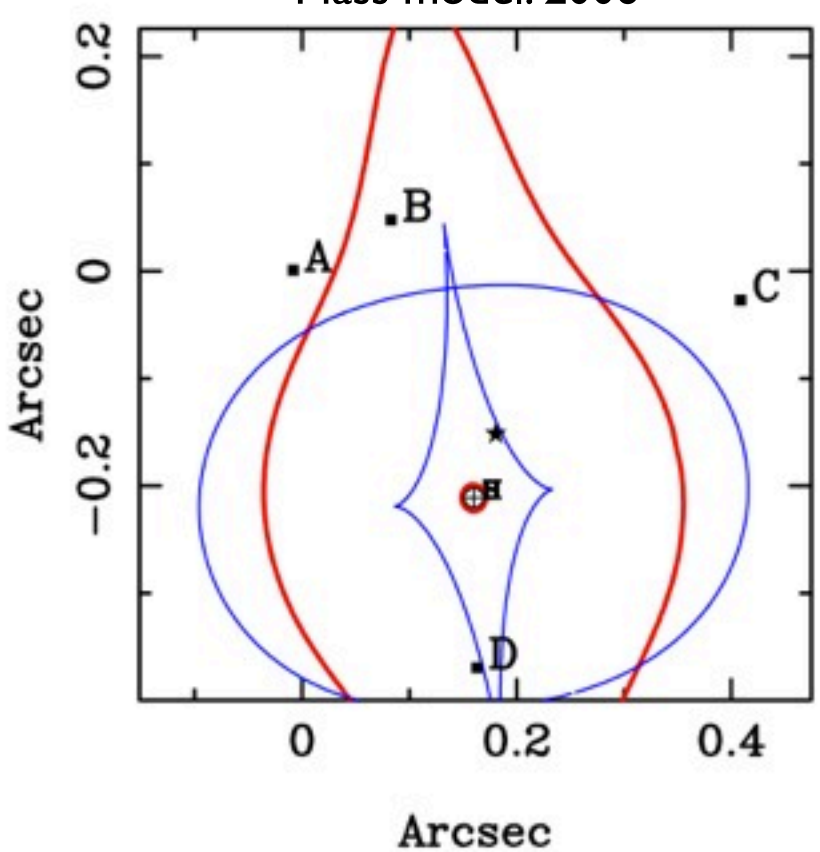

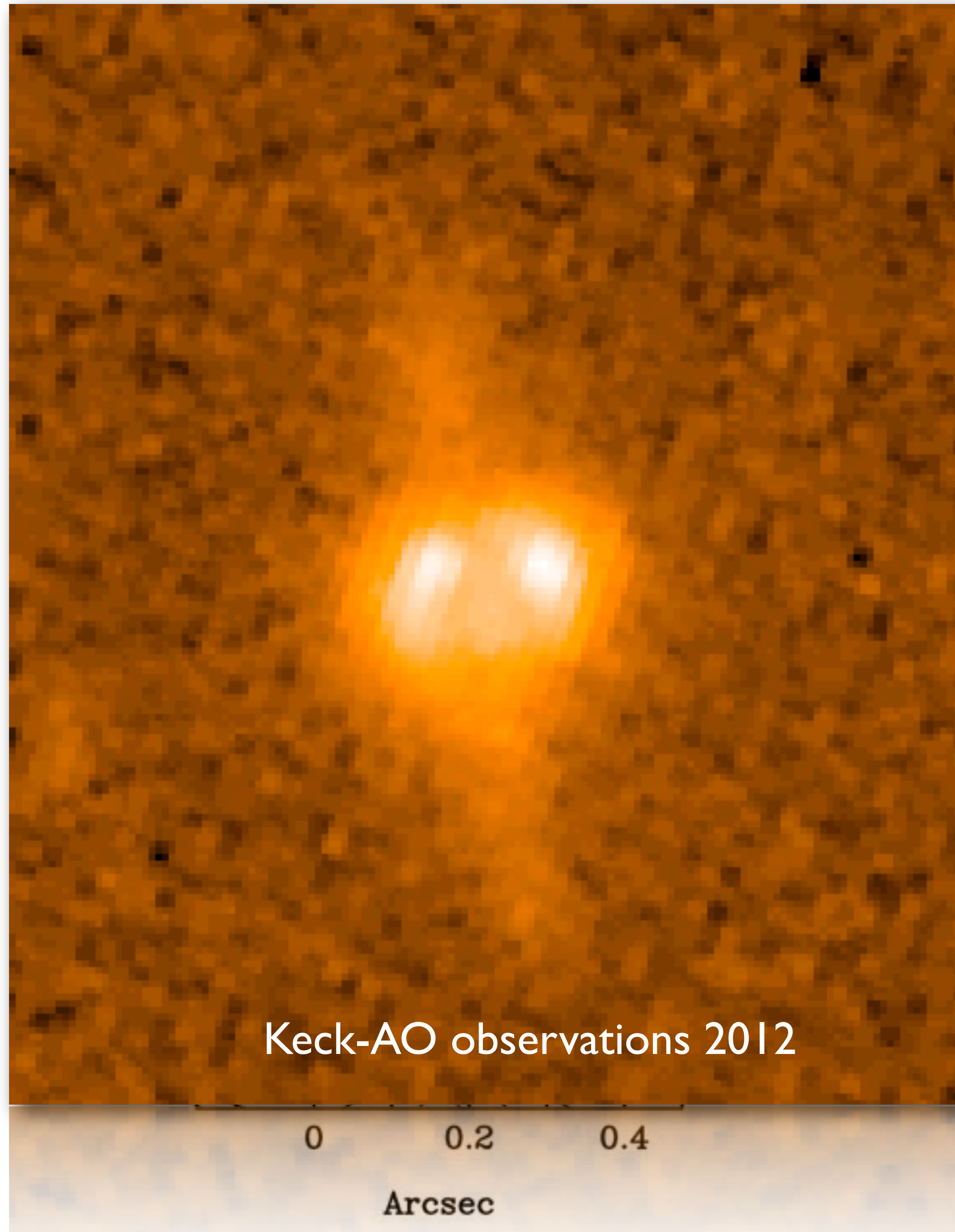

Luminous Satellites

Astrometric Anomalies Due to Luminous Substructure

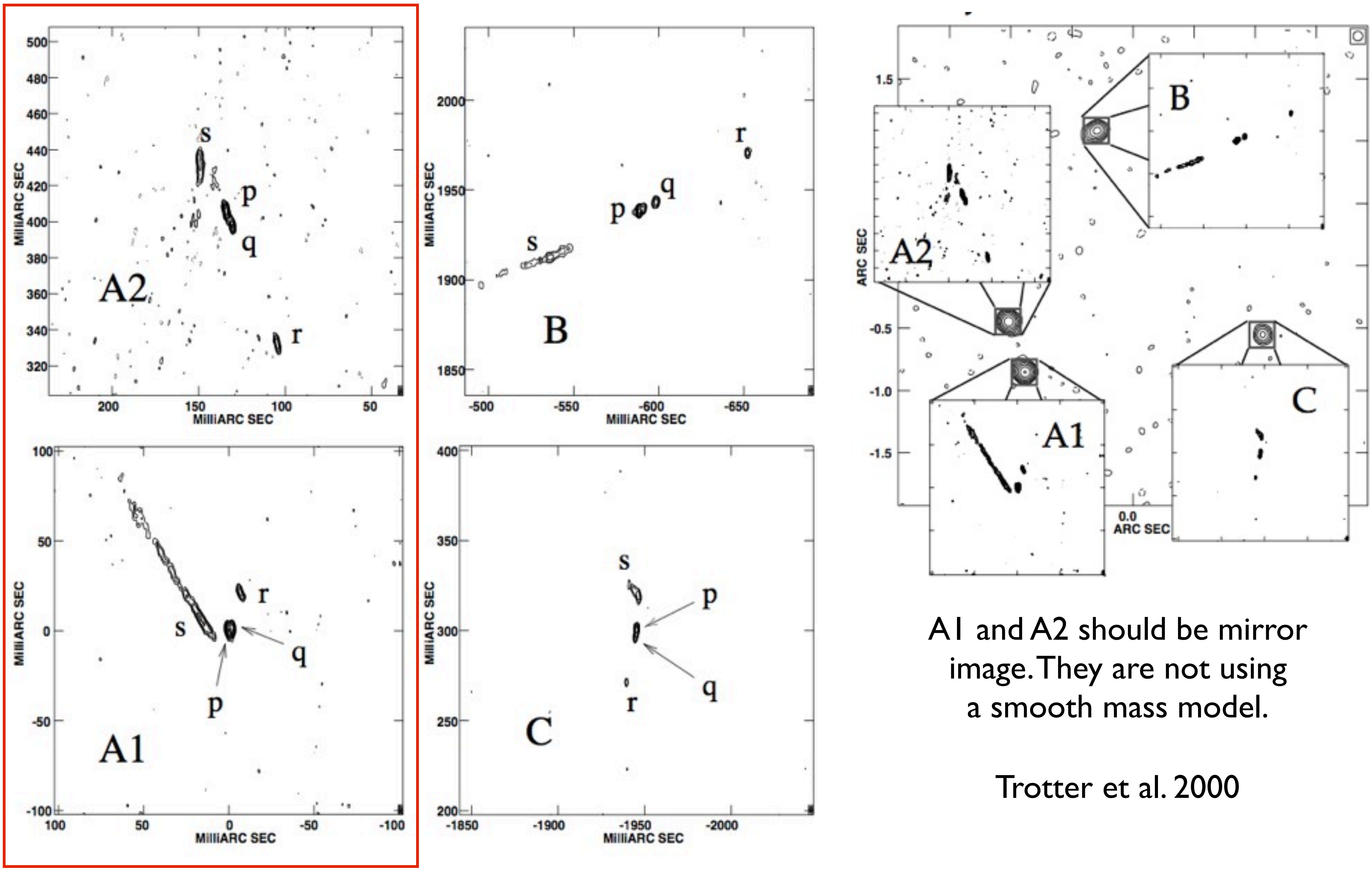

A1 and A2 should be mirror image. They are not using a smooth mass model.

Trotter et al. 2000

Astrometric Anomalies Due to Luminous Substructure

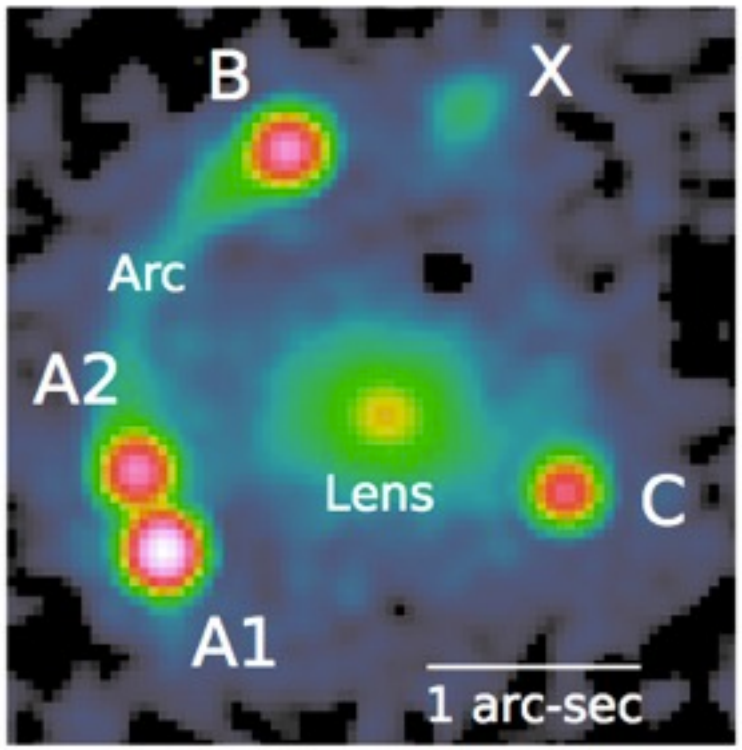

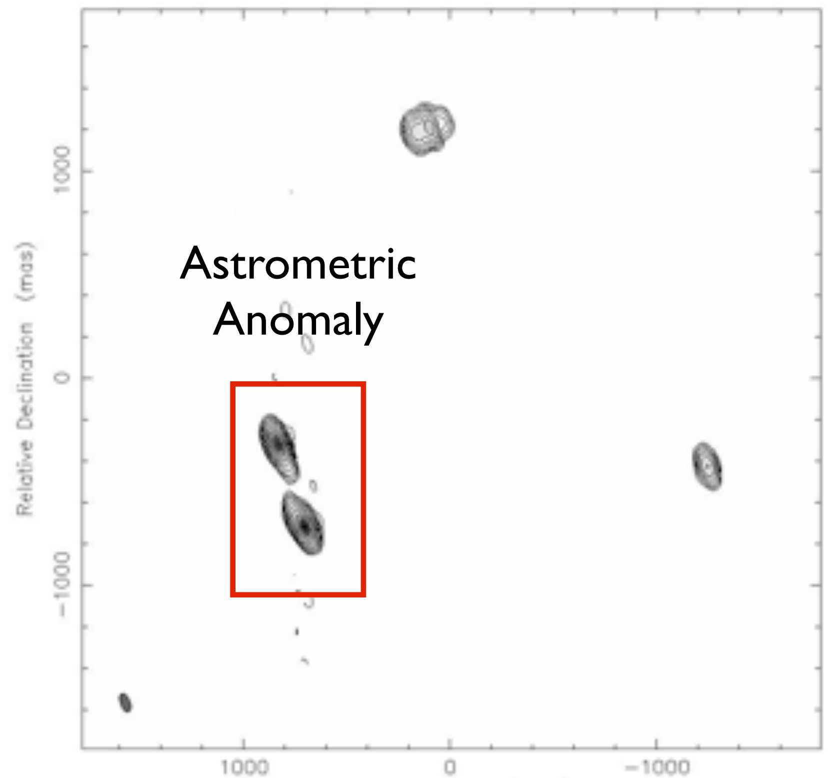

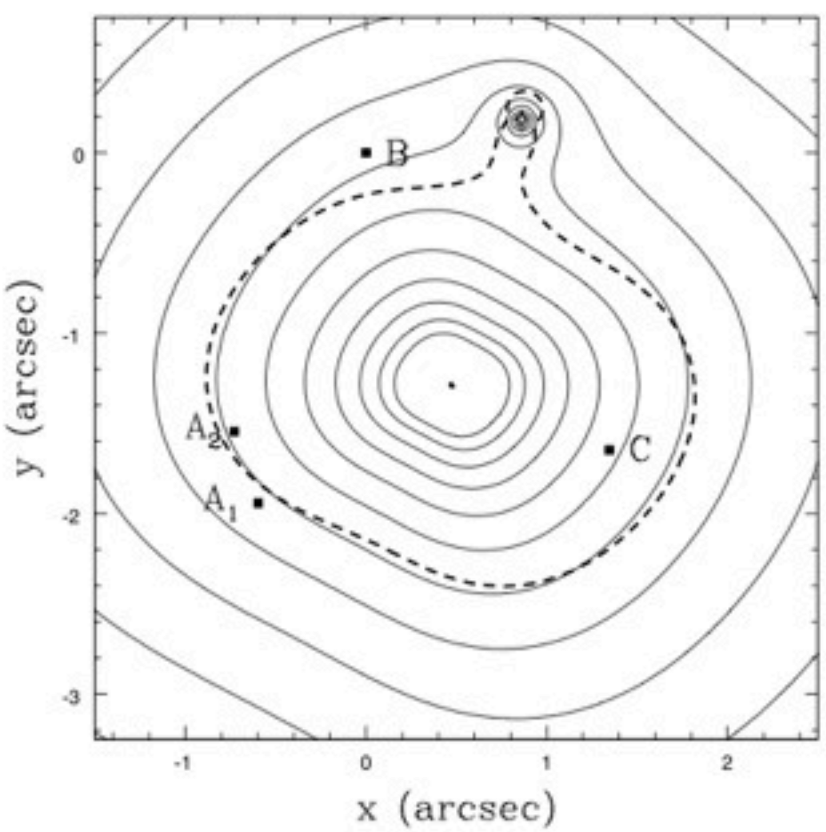

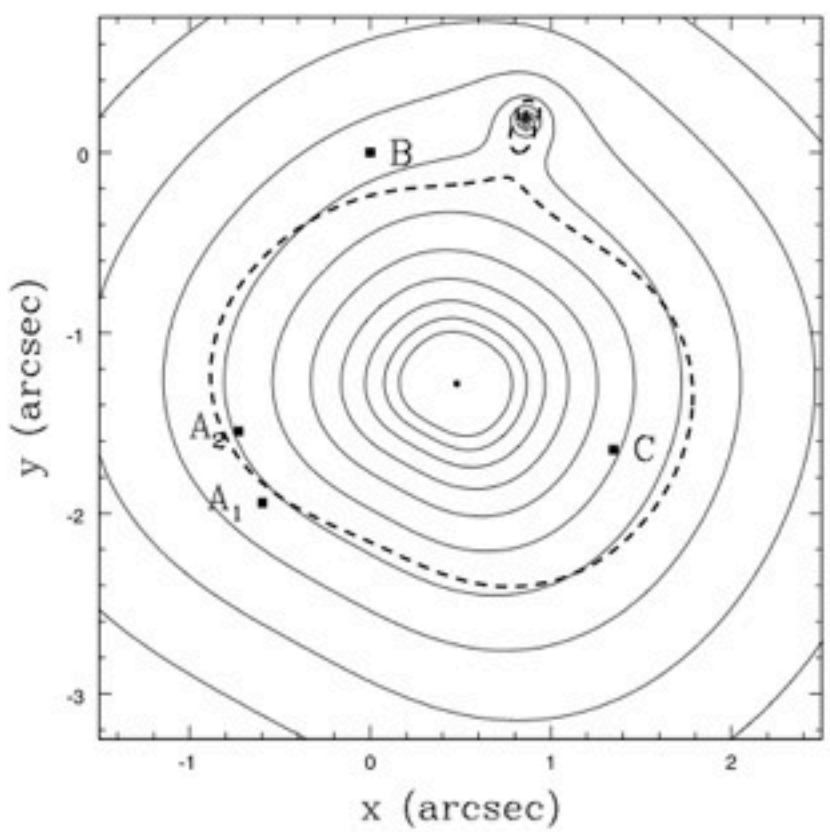

MG0414+0534

A visible luminous satellite largely causes this anomaly. They can be accounted for in the macro-model.

Model-fit improves by $\Delta\chi^2$=100 when object X is included in the mass model.

Kochanek & Dalal 2004

Astrometric Anomalies Due to Luminous Substructure

MG2016+112

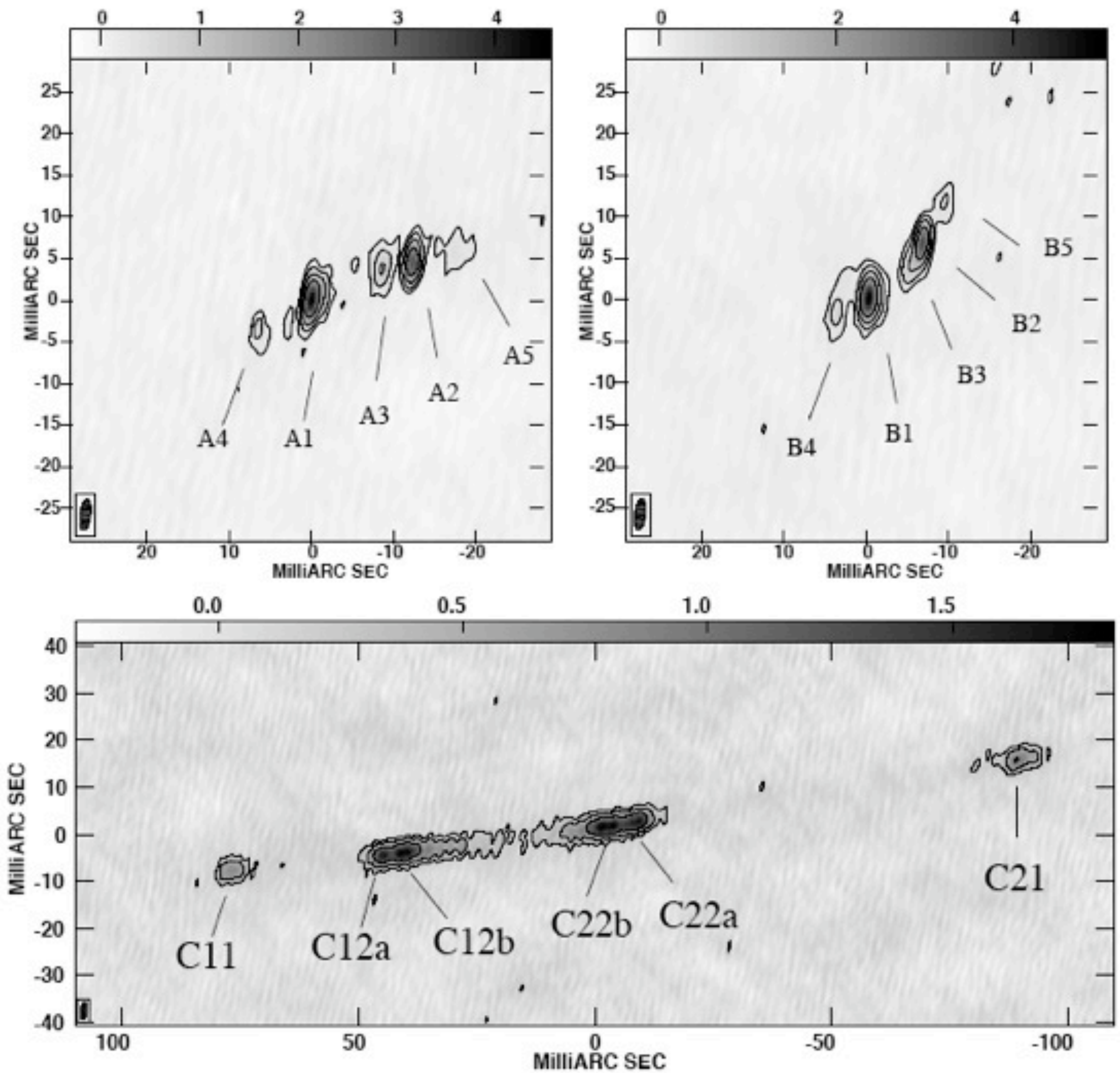

More et al. 2009

Koopmans & Treu 2002

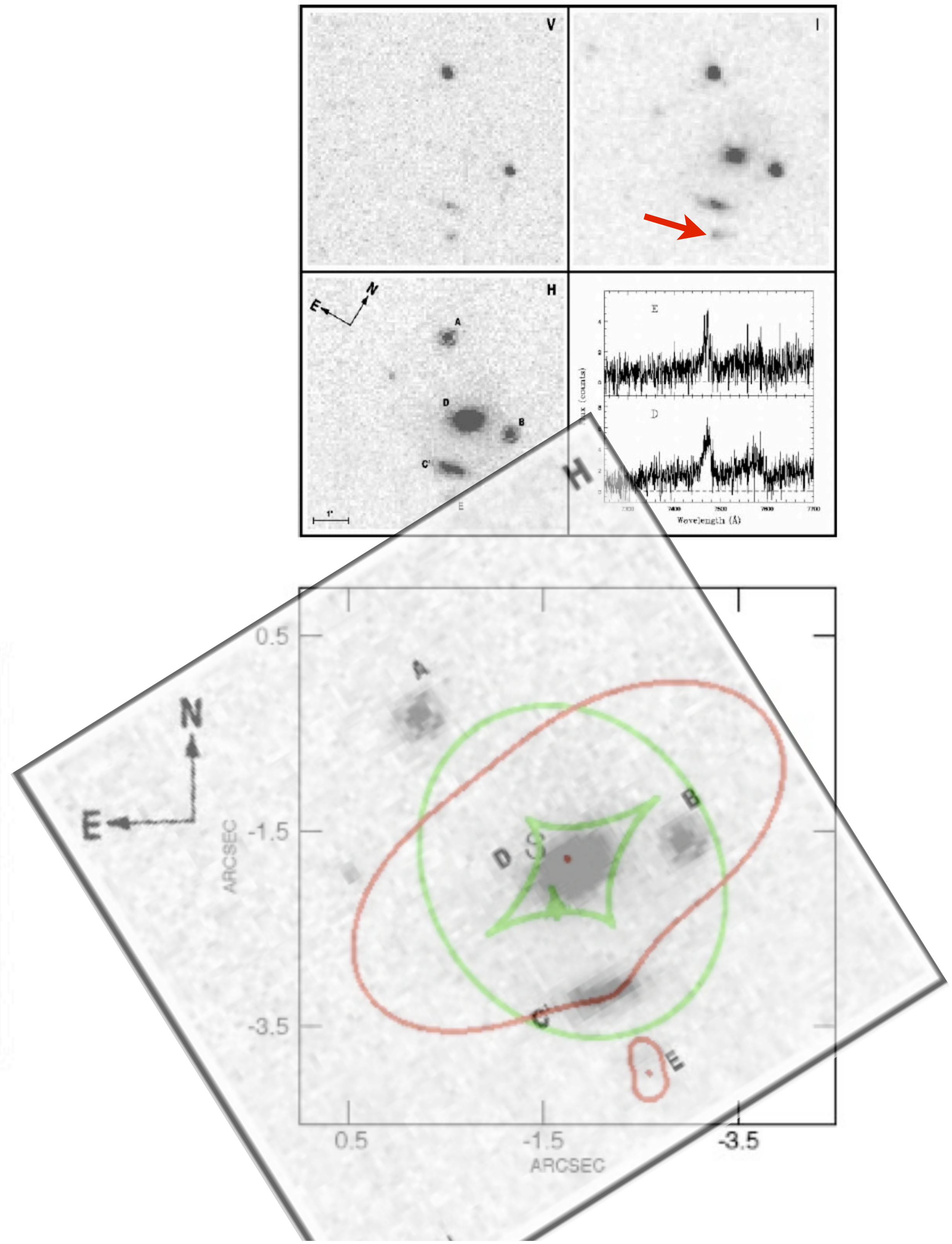

Luminous Substructure as Proxy for Dark Substructure

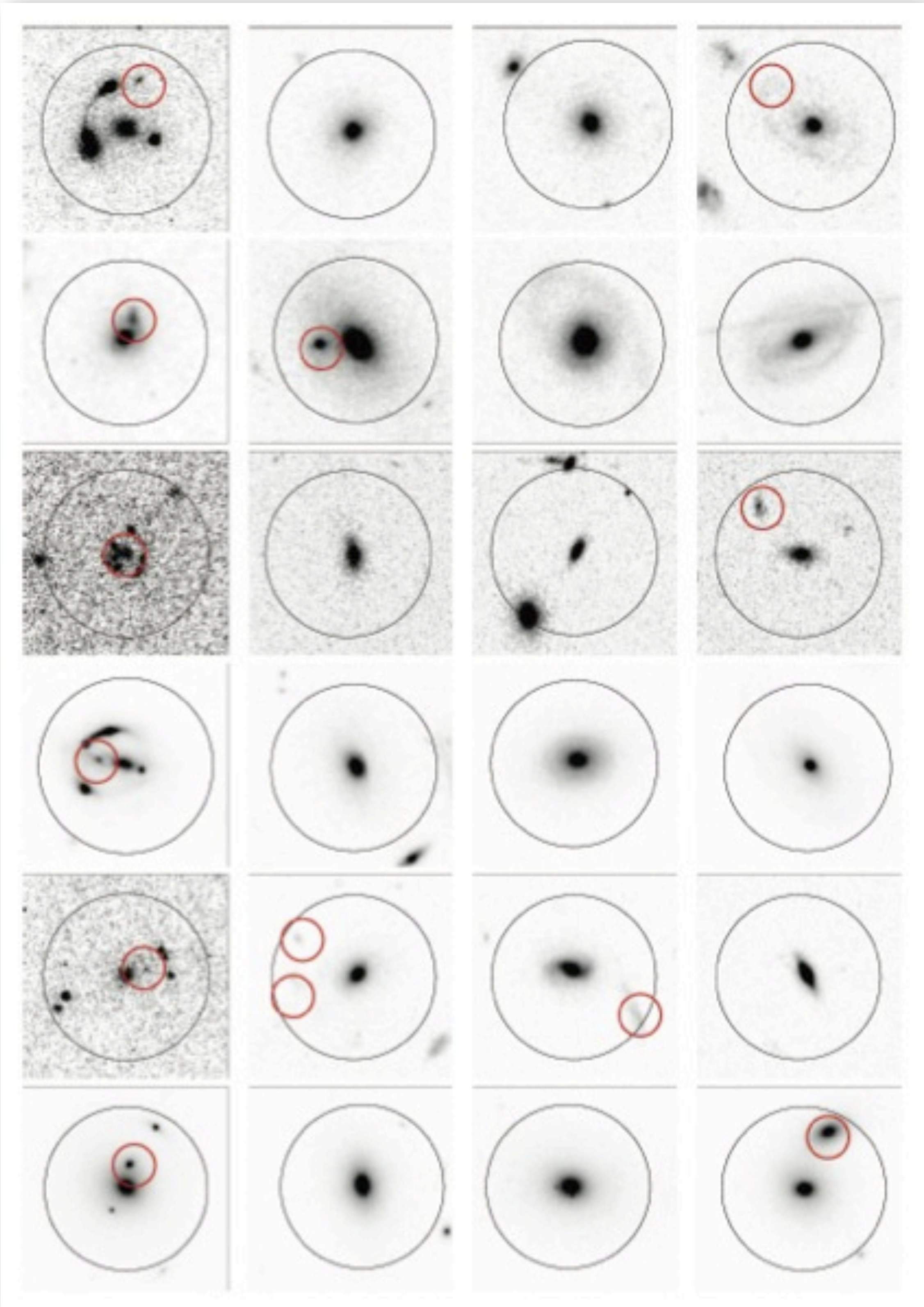

CLASS (radio) lenses seem to have too many nearby bright secondaries compared to e.g. COSMOS [or GOODS].

(see also Nierenberg et al. 2011)

This is not yet explained, but could explain some of the anomalies observed in this sample.

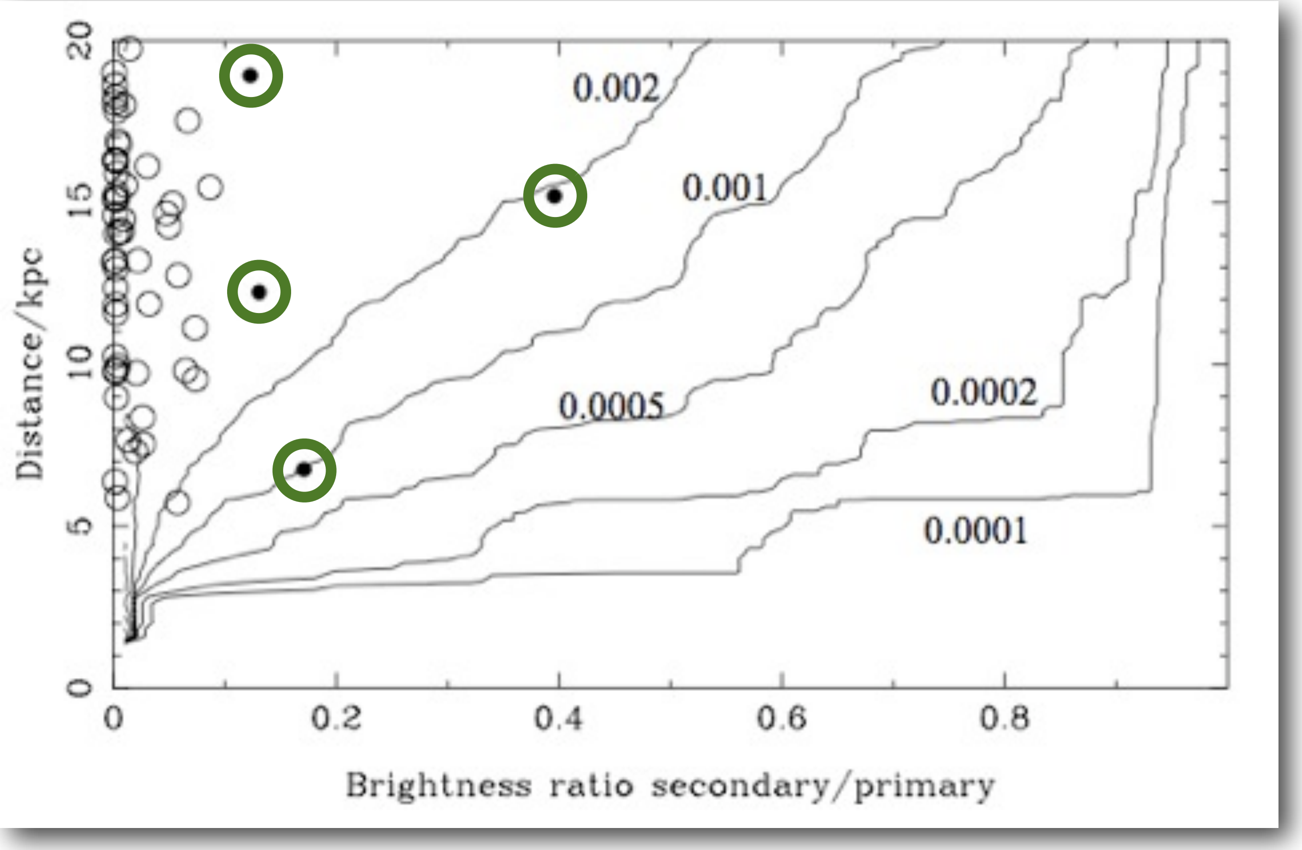

Jackson et al. 2010

Luminous Substructure on an arc

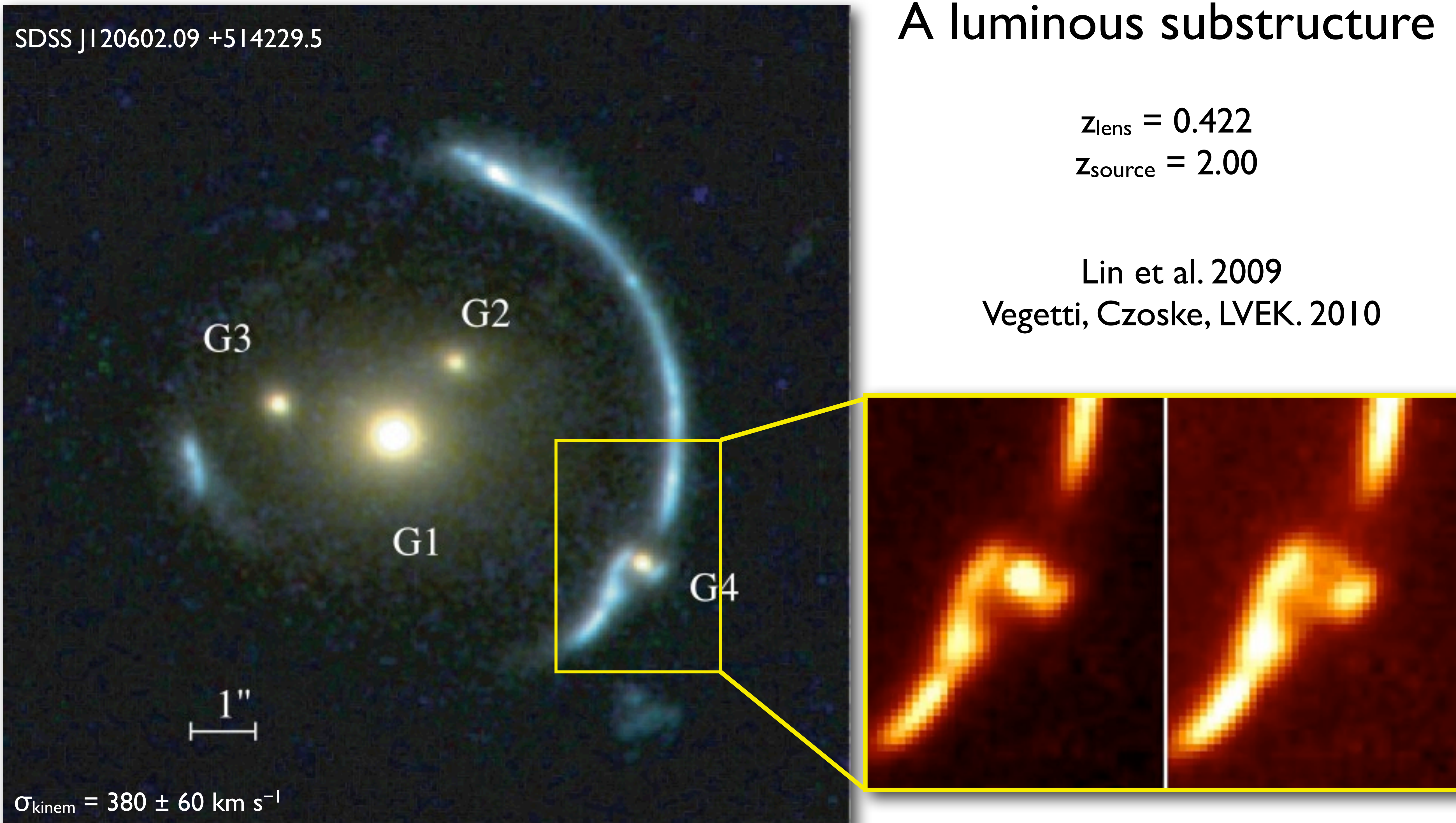

A luminous substructure

z_{lens} = 0.422
z_{source} = 2.00

Lin et al. 2009
Vegetti, Czoske, LVEK. 2010

Luminous Substructure on an arc

Vegetti et al. 2010

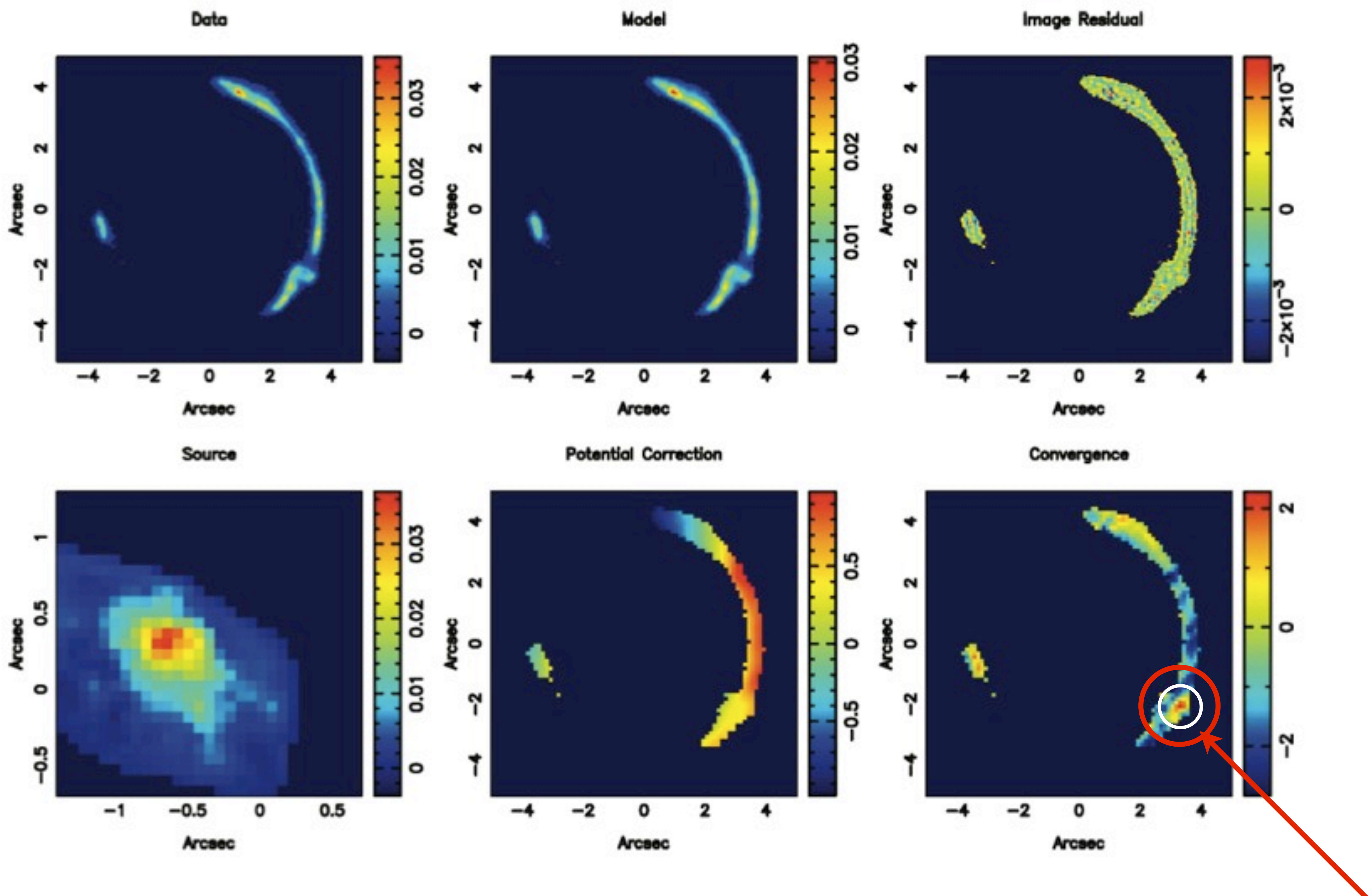

$M_{sub} = (2.75 \pm 0.04) \times 10^{10}\ M_\odot$ ($\sigma \sim 100$ km/s)
inside its tidal radius of $r_t = 0.68$ arcsec
$(M/L)_B = (17.2 \pm 8.5)\ M/L_\odot$

The potential reconstruction recovers the substructure in mass

Dark Structures?

The Double Einstein Ring

Data minus Galaxy

Best Lens Image Model

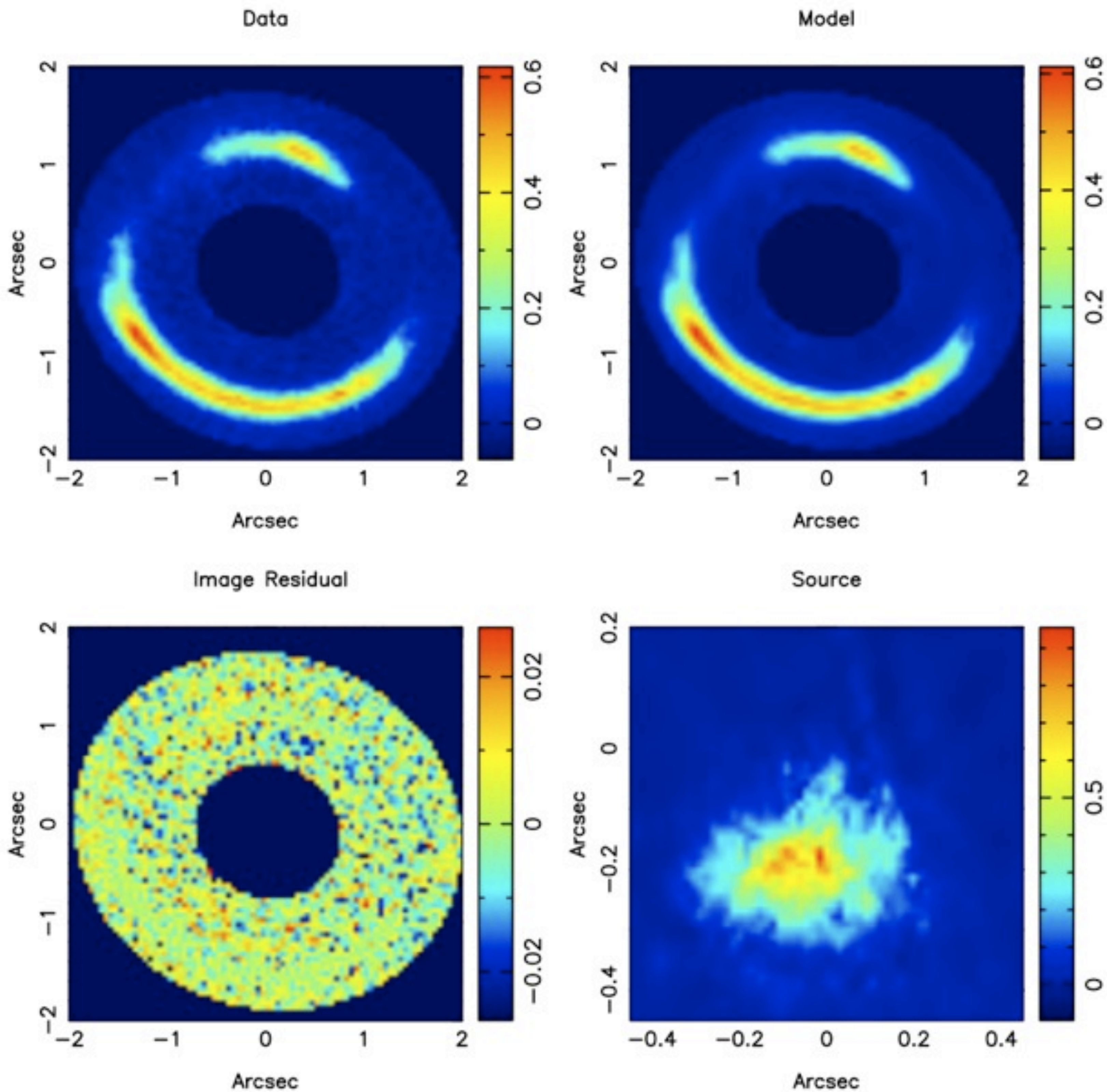

Residuals (data-model)

Best Source Model

Vegetti, LVEK, et al. 2010

The Double Einstein Ring

Vegetti, LVEK, et al. 2010

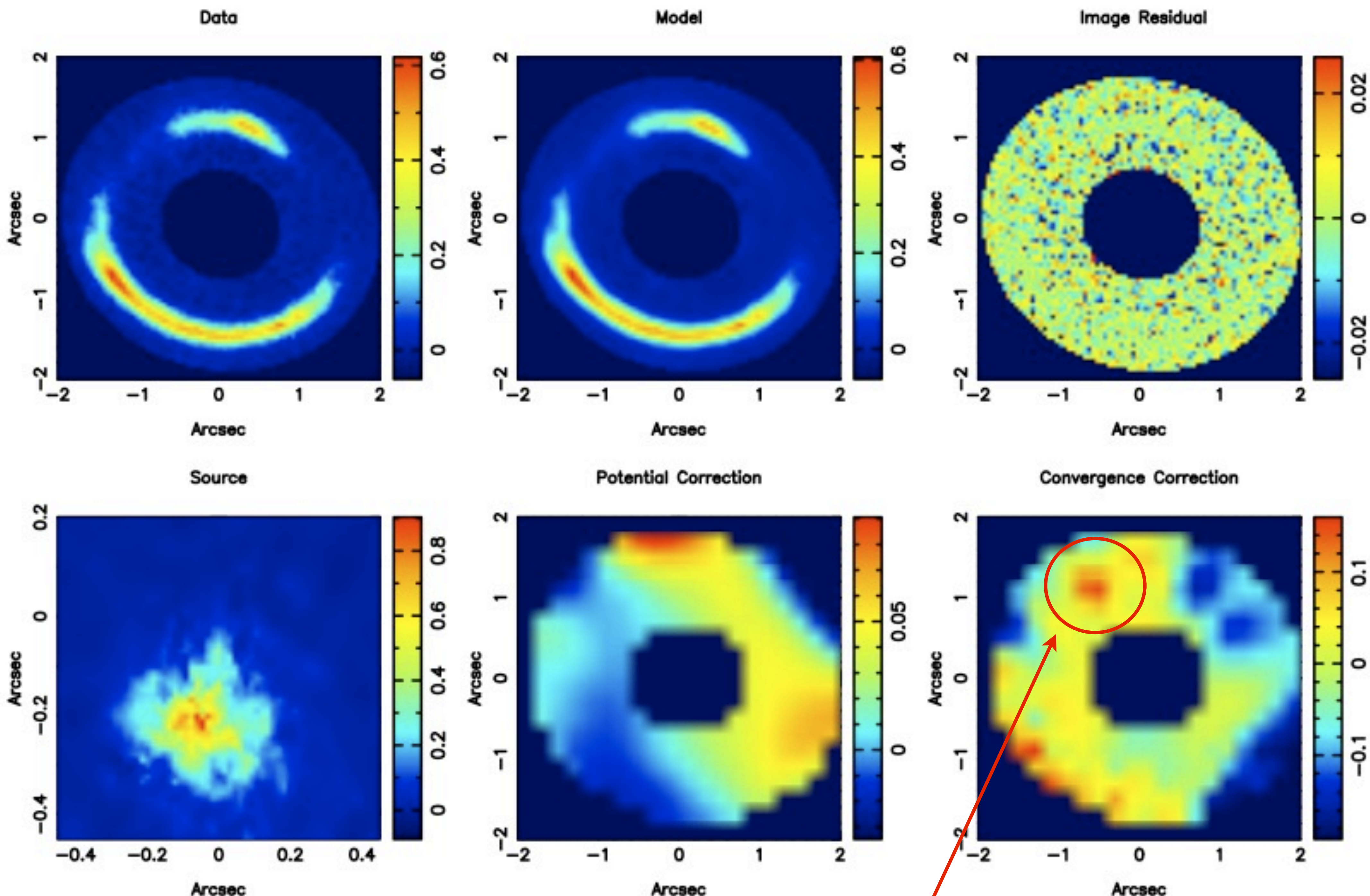

This overdensity seems robust

Double Einstein Ring: Parameters & Bayesian Evidence

Table 1. Parameters of the mass model distribution for the lens SDSSJ0946+1006. For each parameter we report the best recovered value and the relative Likelihood for a smooth model (PL) in column (2), for a smooth over-regularized smooth model in column (3), for a perturbed model (PL+PJ) in column (4), for a smooth and perturbed model (PL+PJ) with rotated PSF respectively in columns (5) and (6) and a smooth and perturbed model (PL+PJ) for different galaxy subtraction respectively in columns (7) and (8). We note that the models in the final two columns use a different (also rotated) data set and the evidence values, position angles and positions can therefore not be directly compared.

	$(PL)_0$	$PL_{0,over}$	$(PL+PJ)_0$	PL_{psf90}	$(PL+PJ)_{psf90}$	PL_{subt}	$(PL+PJ)_{subt}$
α (arcsec)	1.329	1.329	1.328	1.329	1.328	1.280	1.272
θ (deg)	65.95	65.80	69.26	64.97	71.04	-60.99	-60.96
f	0.961	0.961	0.962	0.962	0.963	0.982	0.982
q	0.598	0.597	0.599	0.597	0.600	0.641	0.646
Γ_{sh} (arcsec)	0.081	0.081	0.086	0.080	0.087	-0.092	-0.097
θ_{sh} (deg)	-20.83	-20.65	-22.32	-20.63	-22.12	-39.83	-40.58
$\log(\lambda_s)$	1.152	2.028	2.028	1.059	1.988	0.036	0.052
m_{sub} ($10^{10} M_\odot$)			0.323		0.333		0.342
x_{sub} (arcsec)			-0.686		-0.682		-1.286
y_{sub} (arcsec)			0.989		0.9956		-0.391
$\log \mathcal{L}$	20350.97	20328.11	20511.14	20358.49	20525.32	61520.63	61674.63

Vegetti et al. 2010

Adding a tidally truncated SIS (Pseudo-Jaffe) model to the model finds a substructure at the convergence over density with a mass of 3×10^9 solar mass (16-σ CL)

Double Einstein Ring: Substructure Mass Fraction?

The detection of such a high mass substructure implies a high substructure mass fraction of 2.2% [+2.1% / -1.3%; 68% CL])

Some lenses (e.g. 0414, 2016, 2045) have nearby luminous companions.
Do lenses or galaxies have too many of these in their vicinity?

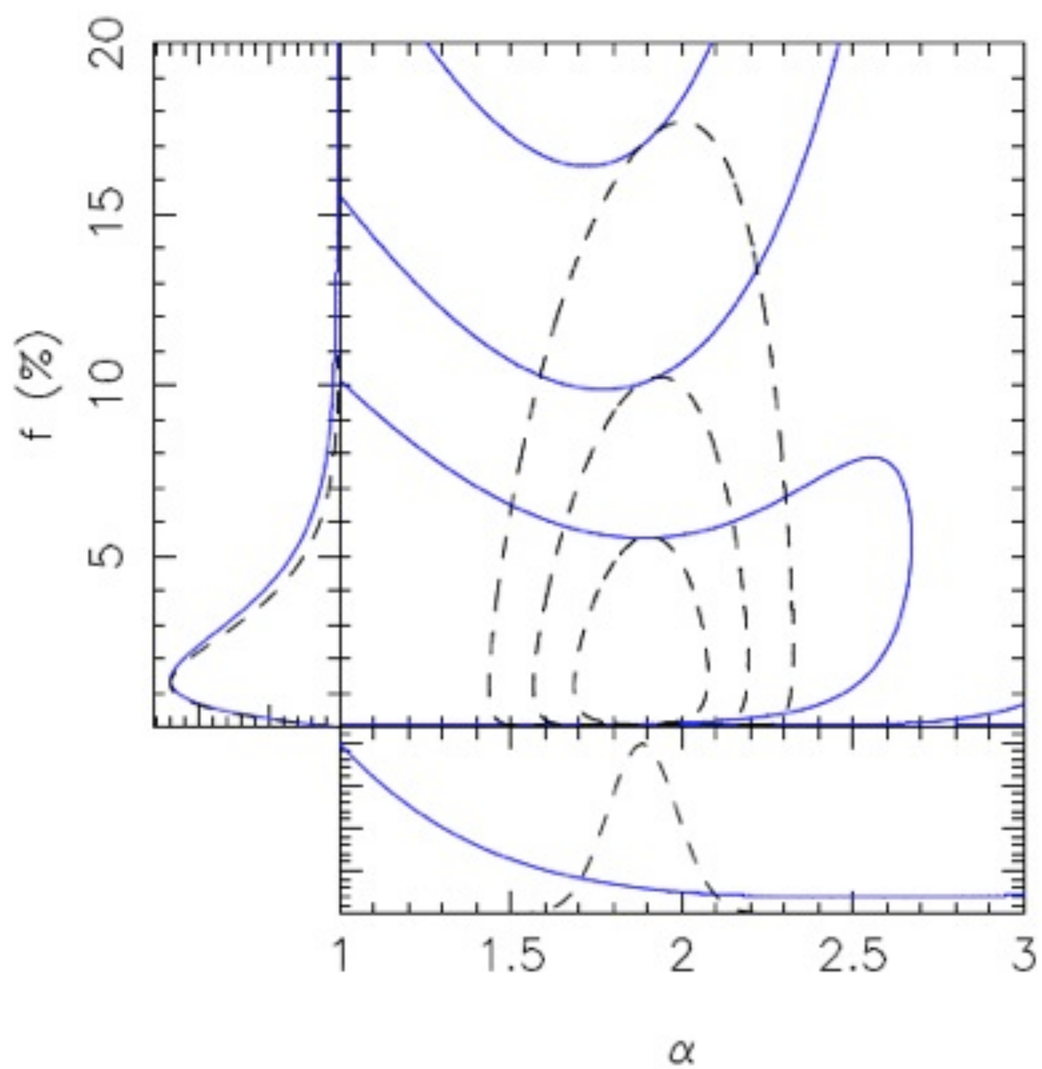

Vegetti & LVEK 2009; Vegetti et al. 2010

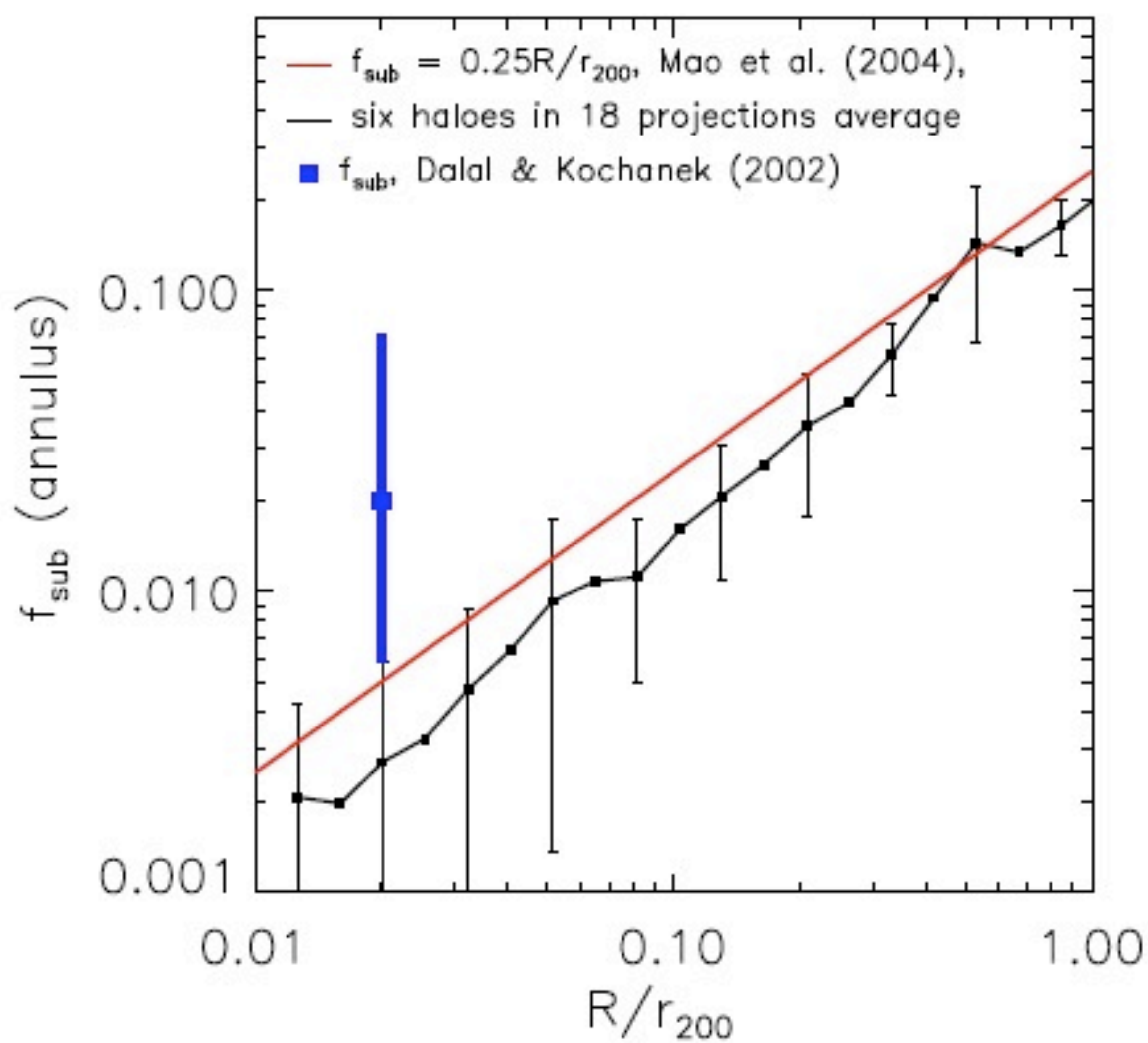

Dalal & Kochanek 2002; Xu et al. 2009

Double Einstein Ring: Substructure M/L?

M/L ratio of the substructure is large compared to MW satellites, but this might not be unexpected near a massive elliptical (e.g. stronger feedback)

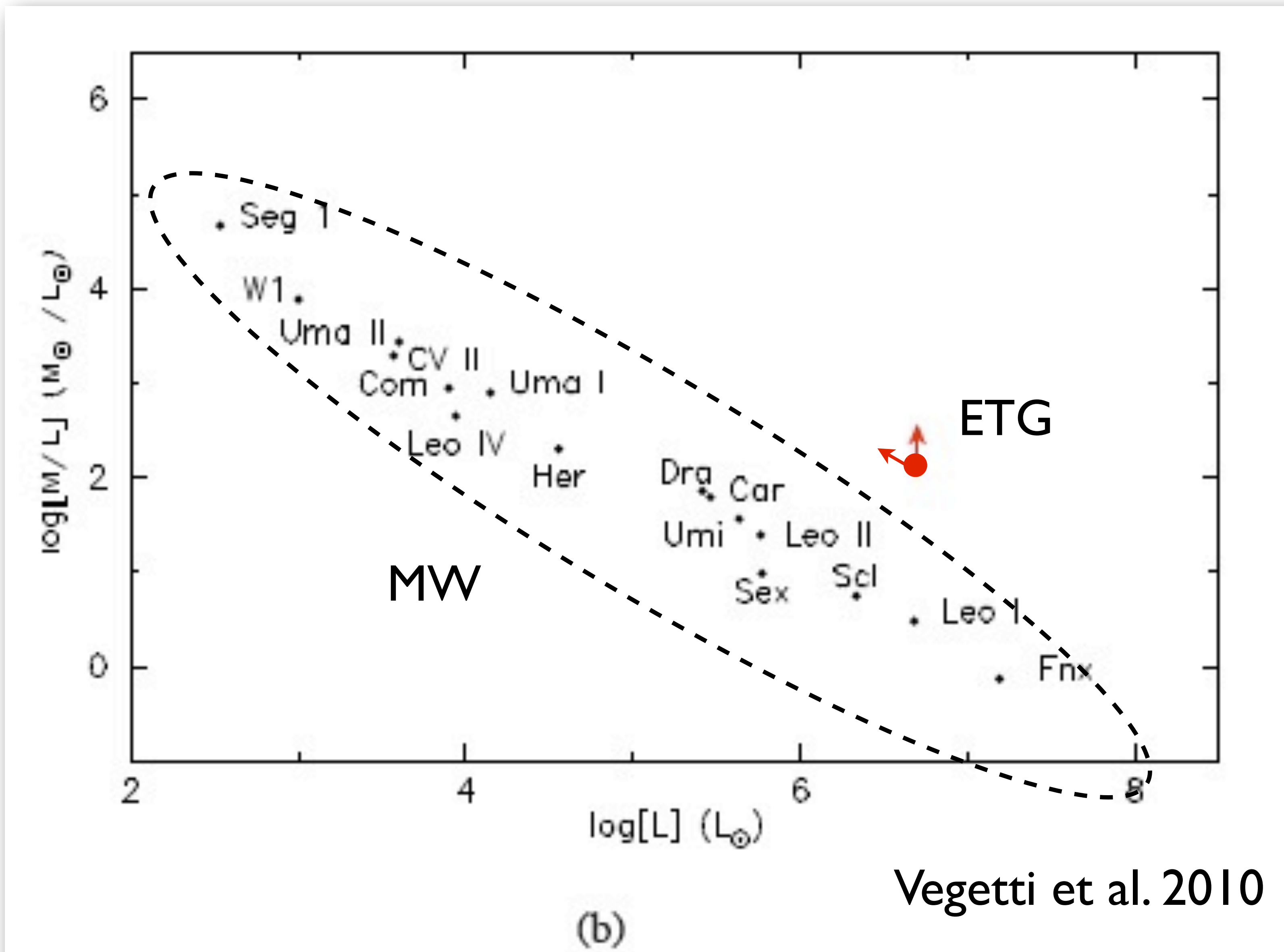

$(M/L)_V > 120\ M/L_{V,sun}$ (3-sigma) inside 0.3 kpc (r_{tidal} =1.1 kpc)

Detecting Lower-Mass Substructures

Different approaches to find even low mass substructures:

- More source structure > higher amplitude of SB anomalies - HST UV/B
- Higher S/N obervations > better measurement of the SB anomalies - HST IR
- Higher spatial resolution > more constraints on the SB anomalies - Ground-based AO

HST

AO

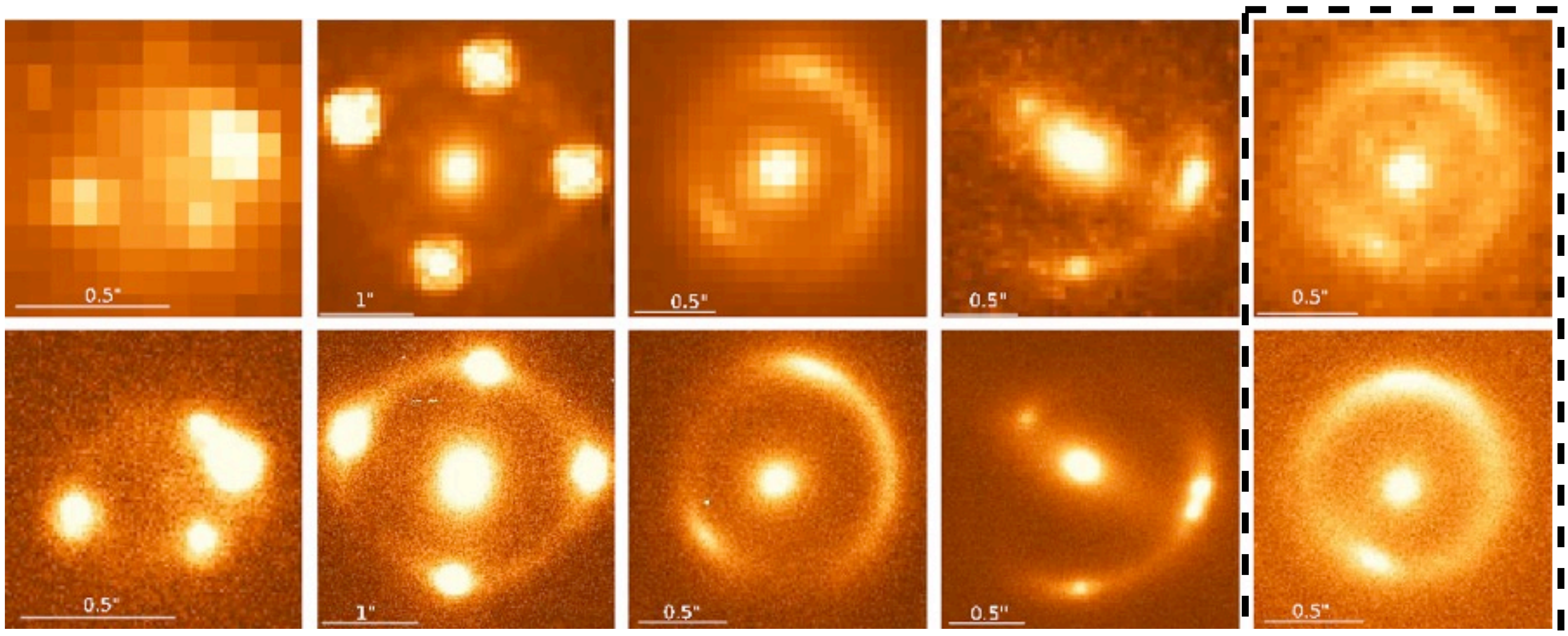

B1938+666

Nature article will appear tomorrow.

LETTER

doi:10.1038/nature10669

Gravitational detection of a low-mass dark satellite galaxy at cosmological distance

S. Vegetti[1], D. J. Lagattuta[2], J. P. McKean[3], M. W. Auger[4], C. D. Fassnacht[2] & L. V. E. Koopmans[5]

The mass function of dwarf satellite galaxies that are observed around Local Group galaxies differs substantially from simulations[1–5] based on cold dark matter: the simulations predict many more dwarf galaxies than are seen. The Local Group, however, may be anomalous in this regard[6,7]. A massive dark satellite in an early-type lens galaxy at a redshift of 0.222 was recently found[8] using a method based on gravitational lensing[9,10], suggesting that the mass fraction contained in substructure could be higher than is predicted from simulations. The lack of very low-mass detections, however, prohibited any constraint on their mass function. Here we report the presence of a $(1.9 \pm 0.1) \times 10^8 M_\odot$ dark satellite galaxy in the Einstein ring system JVAS B1938+666 (ref. 11) at a redshift of 0.881, where $M_\odot$ denotes the solar mass. This satellite galaxy has a mass similar to that of the Sagittarius[12] galaxy, which is a satellite of the Milky Way. We determine the logarithmic slope of the mass function for substructure beyond the local Universe to be $1.1^{+0.6}_{-0.4}$, with an average mass fraction of $3.3^{+3.6}_{-1.8}$ per cent, by combining data on both of these recently discovered galaxies. Our results are consistent with the predictions from cold dark matter simulations[13–15] at the 95 per cent confidence level, and therefore agree with the view that galaxies formed hierarchically in a Universe composed of cold dark matter.

The gravitational lens system JVAS B1938+666 (ref. 11) has a bright infrared background galaxy at redshift $z = 2.059$ (ref. 16), which is gravitationally lensed into an almost complete Einstein ring of diameter radius, r. The best-fitting model was then fixed and further refined using local potential corrections defined on a regular grid, which are translated into surface density corrections using the Laplace operator. We found for both the 1.6- and the 2.2-μm adaptive optics data sets that there was a significant positive density correction, which indicated the presence of a mass substructure (Fig. 1 and Supplementary Information). Directly from the pixelated potential correction, we measured a substructure mass of $\sim 1.7 \times 10^8 M_\odot$ inside a projected radius of 600 pc around the density peak.

As an independent test, we repeated the analysis of the 2.2-μm data set, which had the highest-significance positive density correction, with different models of the point spread function, different data reduction techniques, different rotations of the lensed images, different models for the lens galaxy surface brightness subtraction and different resolutions for the reconstructed source. We also analysed an independent data set taken at 1.6 μm with the Near Infrared Camera and Multi-Object Spectrograph on board NASA's Hubble Space Telescope. In total, we tested fourteen different models and three different data sets that all independently led to the detection of a positive density correction at the same spatial position, although with varying levels of significance (Supplementary Information). Differential extinction across the gravitational arc could also produce a surface brightness anomaly. However, the colour of the arc was found to be consistent around and at the location of substructure, ruling out the possibly that dust affected our results.

Detecting Lower-Mass Substructures

A smooth mass model shows residuals at a significant level in the AO data; the HST data is of too low quality to assess this effect.

Keck-AO

HST

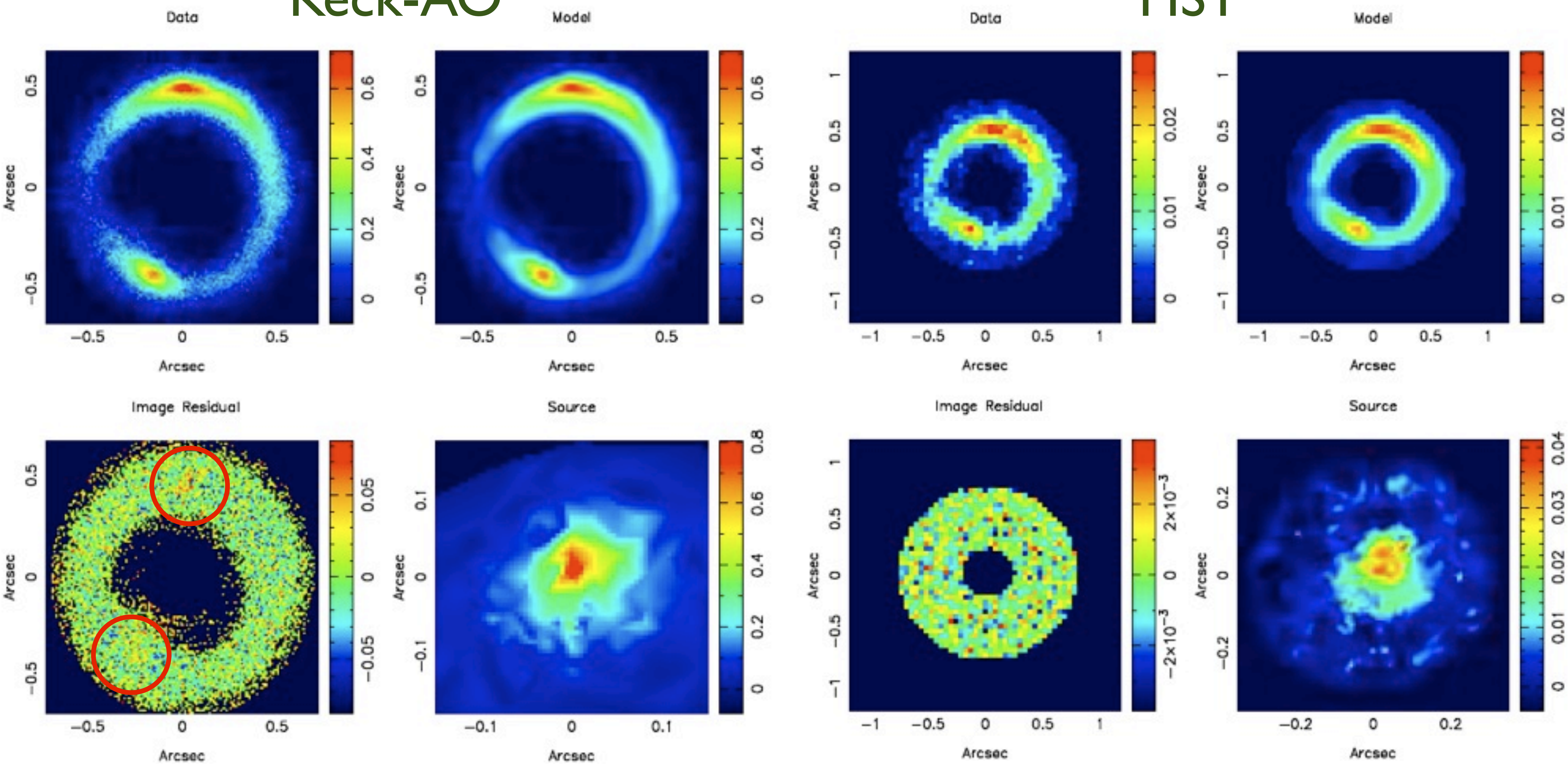

Lagattuta et al. 2012

Detection Lower-mass Substructure

A smooth mass model shows residuals at a significant level in the AO data; the HST data is of too low quality to assess this effect.

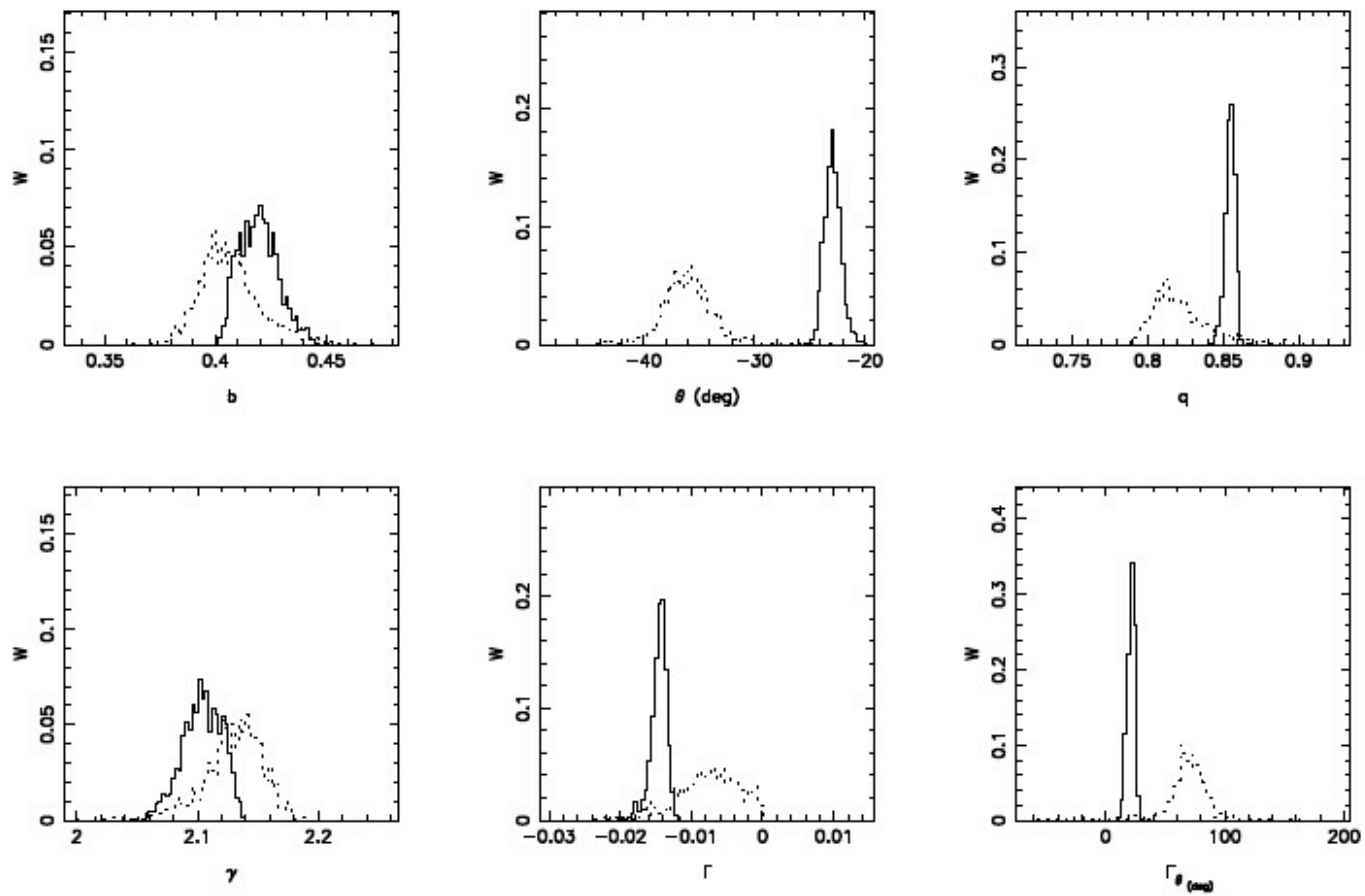

Detecting Lower-Mass Substructures

A grid-based mass model shows a significant detection of a mass substructure near the upper arc image.

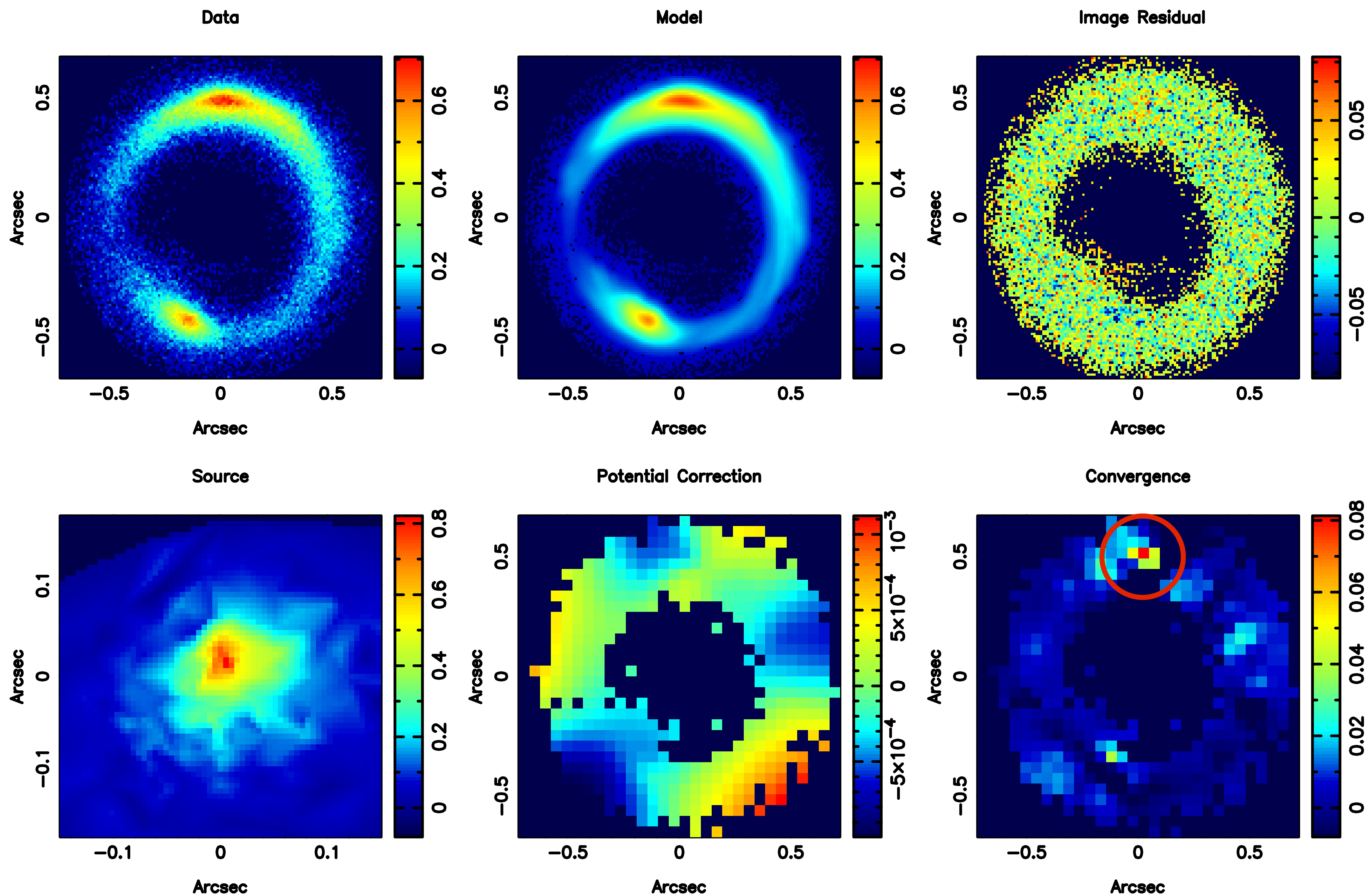

Vegetti et al. 2012, Nature

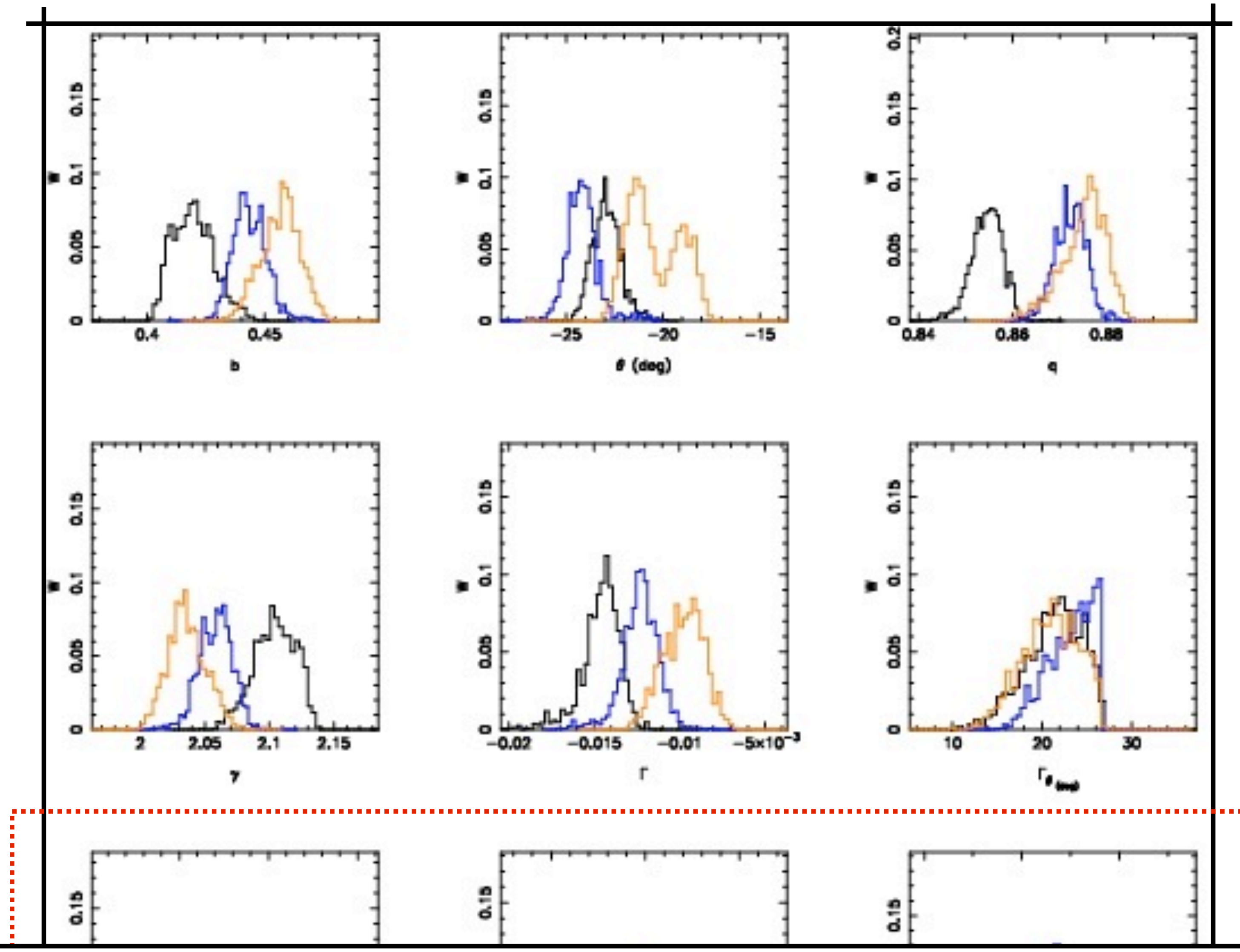

A full Bayesian analysis, using a Pseude-Jaffe mass model for the substructure shows its impact on the smooth-model parameters

$M_{0.6kpc,sub} = (1.1 \pm 0.1) \times 10^8\ M_{sun}$ (12-σ CL)
[or $\sigma_{SIS,sub} \approx 16$ km/s]

A perturbation of <0.01 on the main galaxy indicates the extreme level of sensitivity to perturbations of this strong-lensing methodology

Vegetti et al. 2012, Nature

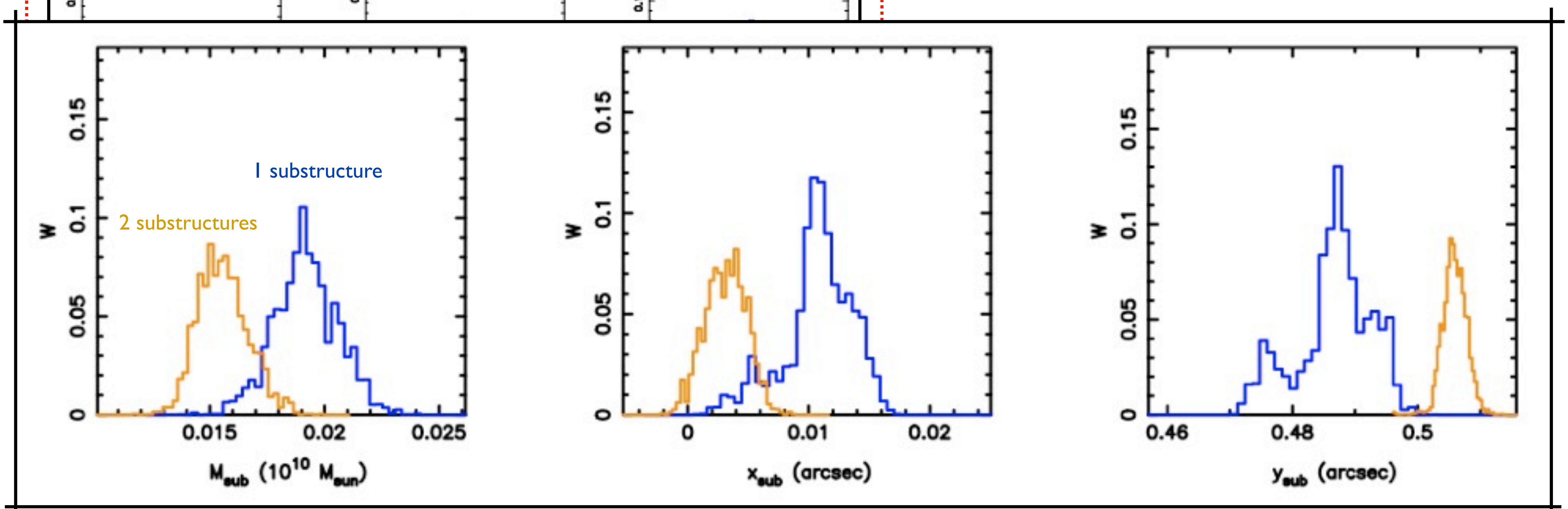

Detecting Lower-Mass Substructures

Substructure as a parametric model

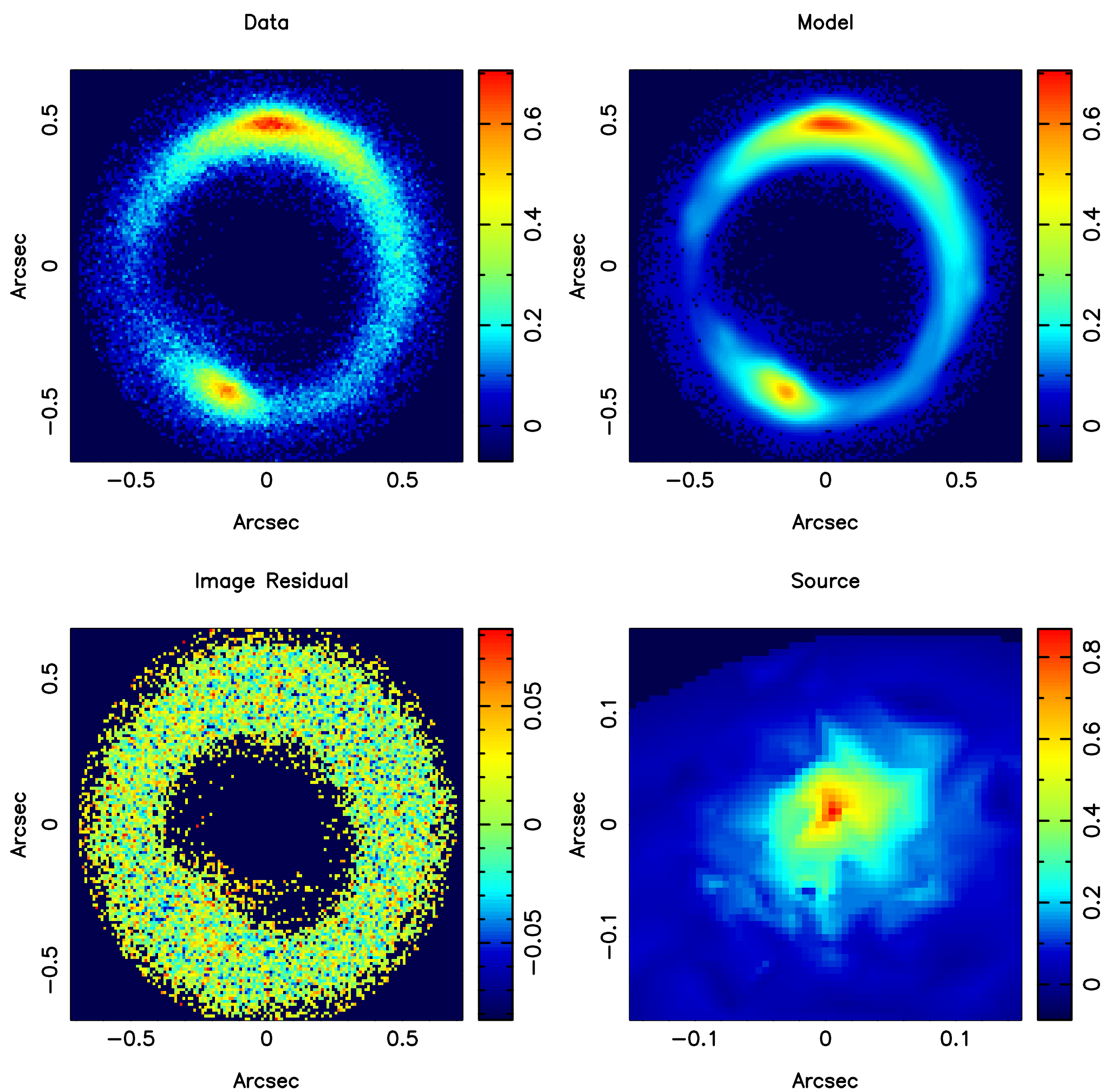

$$\Delta \log E = 65.0$$

$$M_{sub} = (1.9 \pm 0.01) \times 10^8 M_\odot$$
$$r_t = 440pc$$
$$\sigma_v \sim 16\ km\ s^{-1}$$
$$L_V \leq 5 \times 10^8 L_\odot$$

The host galaxy has an isothermal profile

Vegetti et al. 2012, Nature

Constraints on the mass-function by combining the DR & B1938+666 Results

$$P\left(\alpha, f \mid \{n_s, \mathbf{m}\}, \mathbf{p}\right) = \frac{\mathcal{L}\left(\{n_s, \mathbf{m}\} \mid \alpha, f, \mathbf{p}\right) P\left(\alpha, f \mid \mathbf{p}\right)}{P\left(\{n_s, \mathbf{m}\} \mid \mathbf{p}\right)}$$

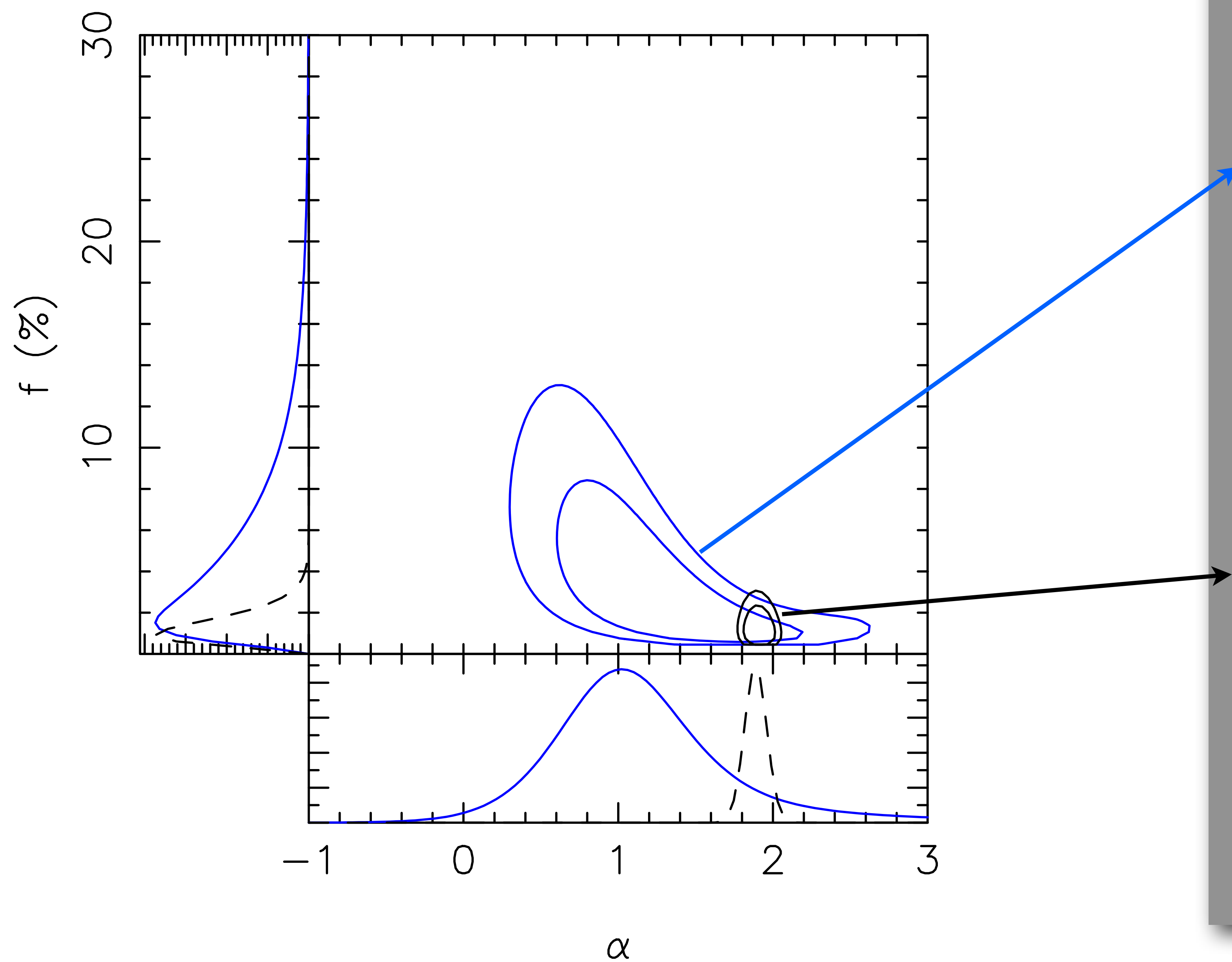

Within the inner 5 kpc

$f = 3.33^{+3.64}_{-1.81}\ \%$

$\alpha = 1.06^{+0.56}_{-0.44}$

$f = 1.21^{+0.6}_{-0.6}\ \%$

$\alpha = 1.87^{+0.08}_{-0.04}$

$f_{CDM} \sim 0.1\%$

How many lenses are needed to quantify the substructure mass function?

Several hundred (~200) lenses with extended rings/arcs are needed (comparable to the DR) to quantify f_{sub} (to <<1%) and the mass-function slope

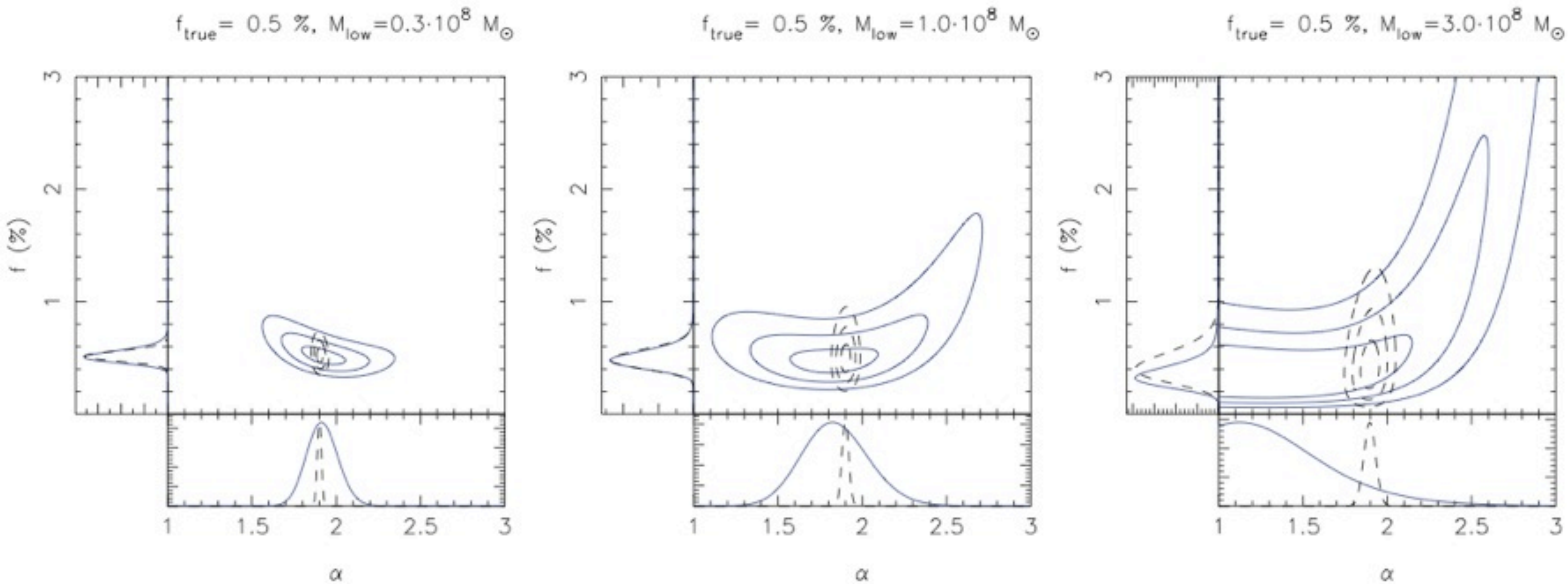

New instruments (e.g. Herschel/ALMA, Euclid/JDEM, LSST, SKA, etc) can provide these numbers of new strong galaxy-scale lenses in the next 5-10 years.

Vegetti & Koopmans 2009

Constraints on the mass-function by combining the DR & B1938+666 Results

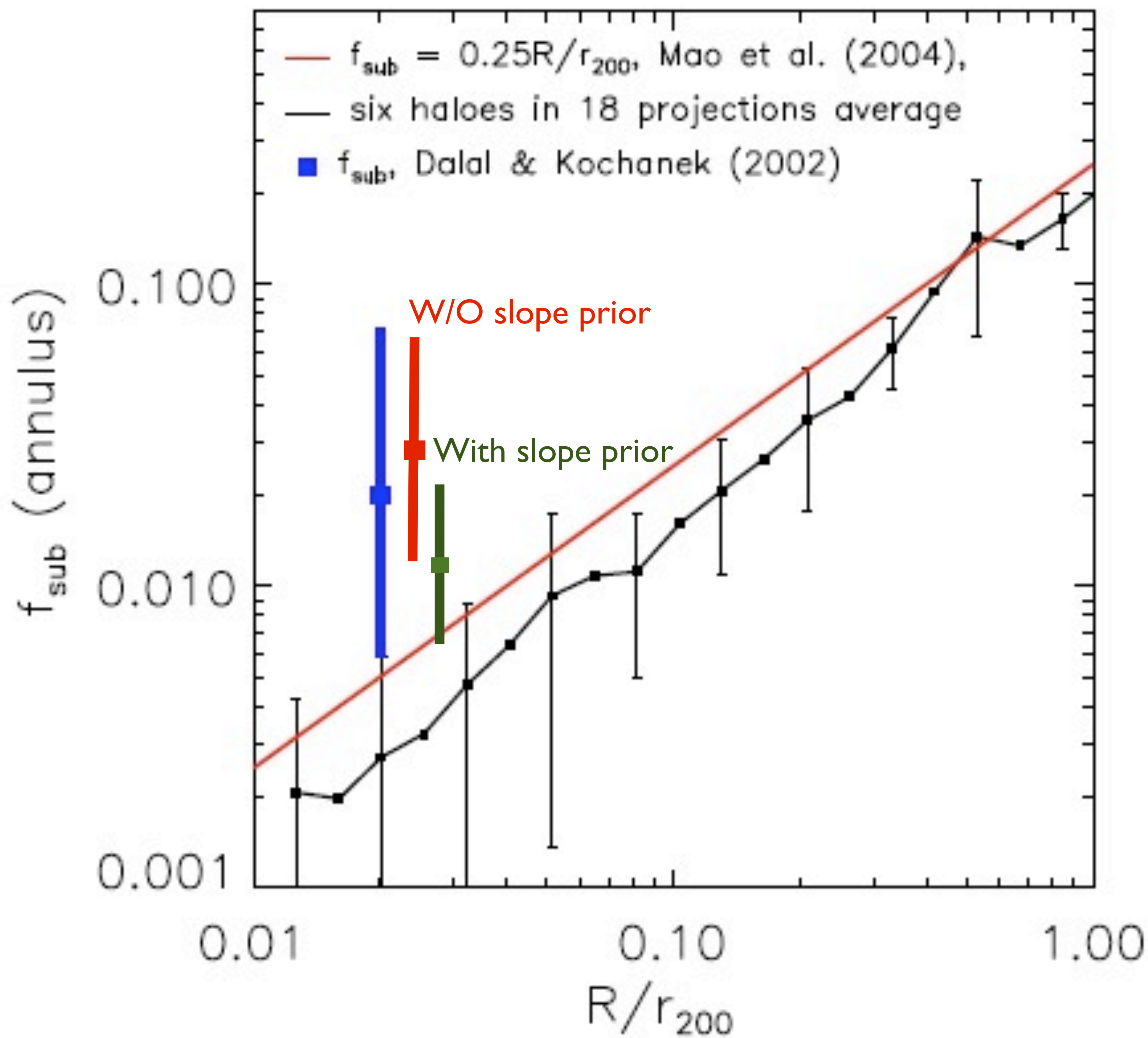

Also our results give consistently more mass substructure toward lens galaxies (as D&K02) compared to simulations.

Why?

Are CDM simulations wrong or is there something else?

Contamination by L.O.S. objects?

Contamination along
the l.o.s. could be
substantial. But
the jury is still out on this!

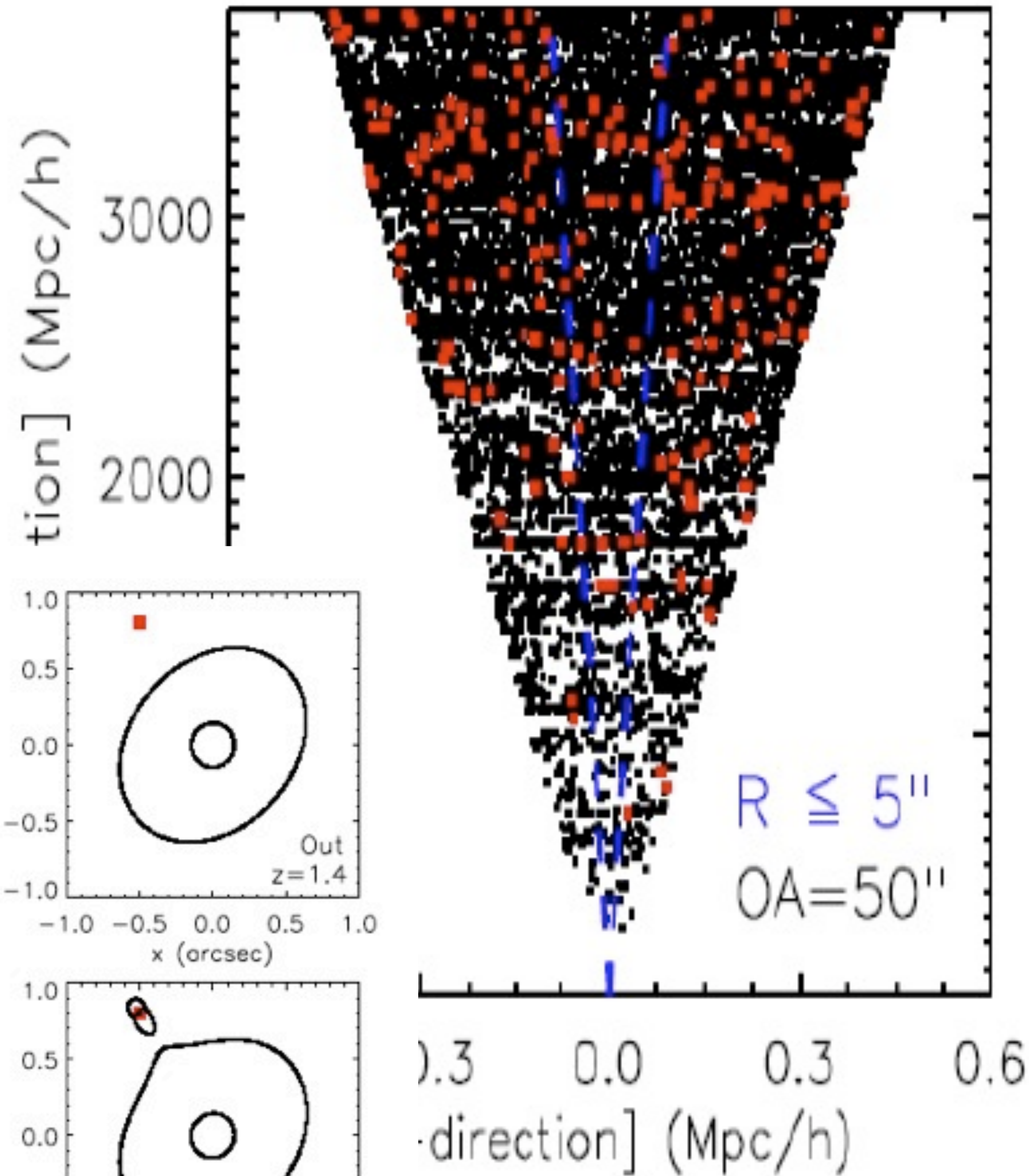

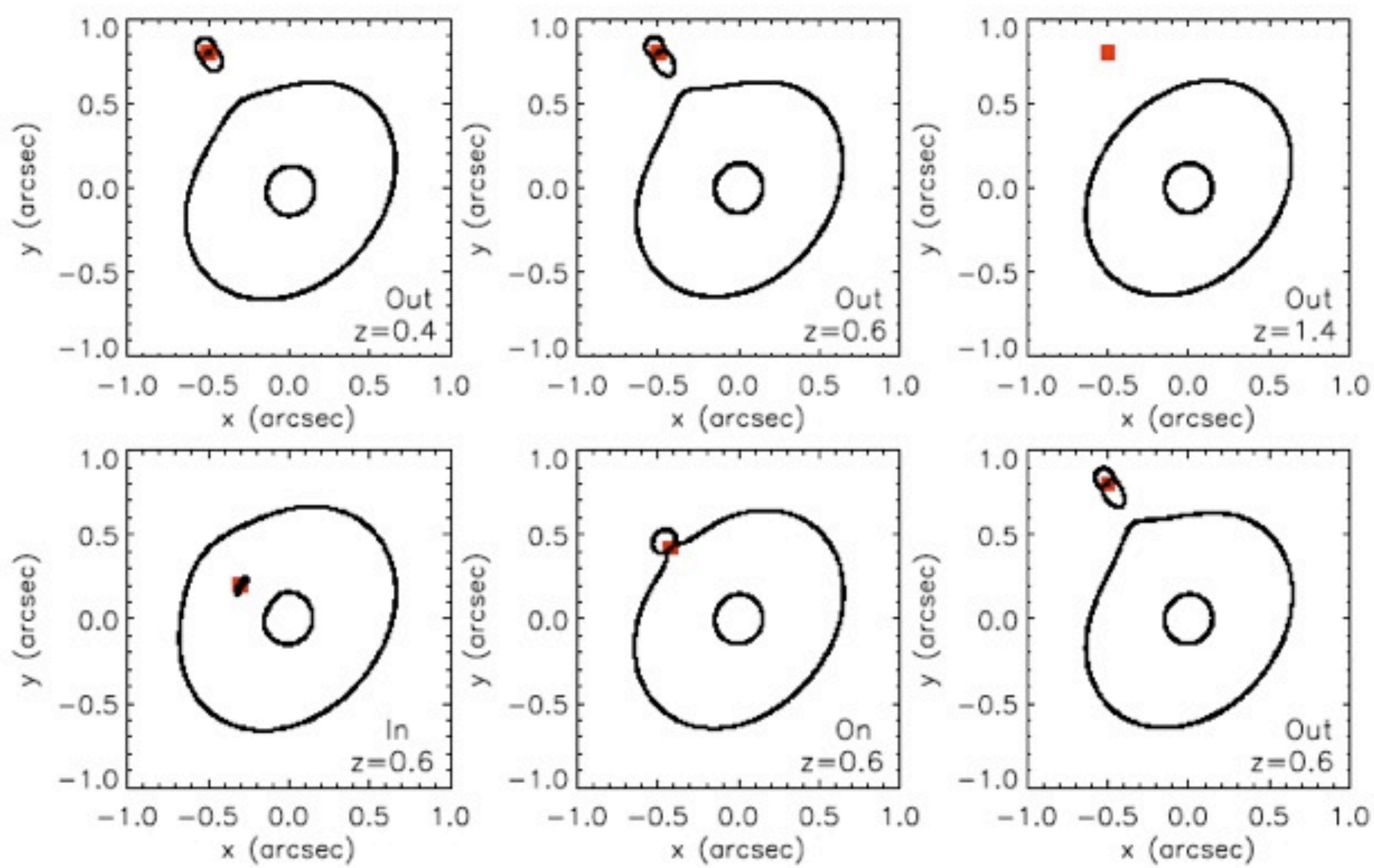

Xu et al.

Contamination if there can help!

10 lenses a la DR/B1933+666

Galaxy

Galaxy + l.o.s. ?

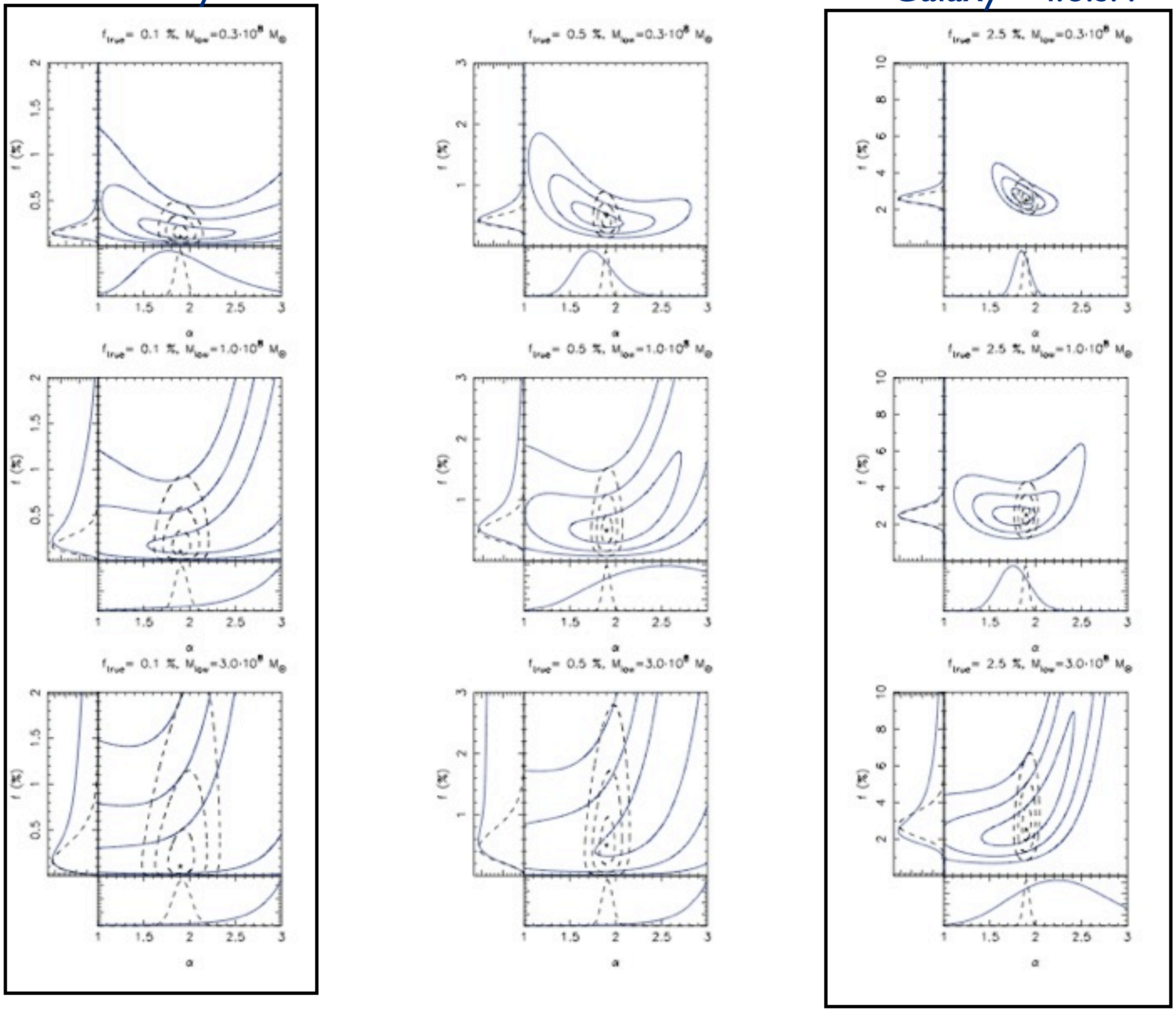

Vegetti et al. 2009

Boost of substructures!

A few (~10) lenses are enough to pin down f_{sub}!